Functional Surface-initiated Polymers: Device Applications and Polymerization Techniques

This dissertation is submitted
for the degree of Doctor of Philosophy

Paul Johan Hamelinck
Gonville and Caius college
University of Cambridge

September 2007

Declaration

This dissertation is the result of my own work and includes nothing which is the outcome of work done in collaboration except where specifically indicated in the text.

No parts of this dissertation have been submitted for any other qualification.

This dissertation does not exceed the word limit prescribed by the Degree Committee of Physics and Chemistry.

September 2007, Paul Hamelinck

Summary

Self-assembled monolayers and surface-initiated polymers, or polymer brushes, have attracted attention as they form dense layers with much higher structural order than bulk or solution polymers. Another field of research which has emerged over the last two decades is the field of organic and polymer electronics. In this field molecular order and surface modification are of major influence on the device performance, hence that both self-assembled monolayers and polymer brushes have been investigated to find applications in organic electronic devices.

After an introduction into the field self-assembled monolayers, polymer brushes and organic electronics, the first part of this thesis focusses on three examples of surface modification for applications in devices.

Alignment of the active material is crucial for high mobilities in organic electronics. Chapter 2 discusses the synthesis of a liquid crystalline surface-initiated polymer and its application to induce strong homeotropic alignment. The alignment is homogeneous over large areas and can be patterned by combining the polymerization with soft lithographic techniques.

Mobilities of organic electronic materials can also be strongly influenced by dopants in the material. In field-effect transistors the positioning of the dopant is thought to be crucial, as the conductance predominantly takes place in only a small channel near the dielectric interface. In chapter 3 dopant functionalized monolayers and polymer brushes are presented which enable the localized deposition of dopants in the channel of organic transistors. It is shown that the mobility of charges and hence the device performance is affected by the introduction of this dopant layer.

Polymer brushes have been suggested for the fabrication of highly ordered

semiconducting polymers, but the fabrication of surface grafted conjugated polymer layers that are both smooth and thick enough to be used in applications is only rarely reported. In chapter 4 the use of a thiophene functionalized polymer brush is shown, that can be used as a template for the subsequent growth of highly conjugated surface grafted polythiophene layers. Thick polythiophene layers are obtained, that are low in roughness and show photoluminescence and polychromism upon doping. These polymers are potentially useful for device applications as well.

The second part (chapter 5 and 6) of this thesis presents new techniques for surface polymerizations, which make them more versatile and attractive and better fit to meet the tailored demands of high-end applications.

It is attractive to investigate reduction of reactor volume for polymer brush growth, both considering the high wastes associated with this technique and considering the applications of brushes in micro-fluidic devices. Chapter 5 discusses a method to achieve volume reduction by back-filling the superfluous volume with beads. It is found that this influences the polymerization kinetics significantly. The combined advantages of less volume and enhanced reaction speeds enable reduction of the total amount of monomer needed by up to 90%.

Many applications demand complex device architectures with several polymers either perfectly mixed or ordered in blocks or multiple layers. Chapter 6 presents a controlled way to convert initiators for atom transfer radical polymerization into initiators for nitroxide mediated polymerization. In this way both mixed polymer brushes and block co-polymer brushes become accessible. This combination makes it an attractive tool to fabricate complex polymer architectures.

The technologies used in this thesis show that the synthesis of polymer brushes enable the fabrication of complex architectures without the wastes normally associated with surface-initiated polymers. Combined with several functionalized polymer brushes with properties that enhance order, influence mobility or serve as template for the growth of surface attached conjugated polymers this shows the high potential for the application of surface-initiated polymers in organic electronics.

Abbreviations and symbols

Δ	Stokes parameter (ellipsometry) measuring phase shift
θ_{a5cb}	Advancing contact angle of pentyl cyanobisphenyl (s5CB = static)
θ_{aw}	Advancing contact angle of water (rw = receding, sw = static)
μ	Absolute dynamic fluid viscosity
μCP	Micro-contact printing
ν	Kinematic fluid viscosity
ρ	Density
ϕ	Concentration
Ψ	Stokes parameter (ellipsometry) measuring amplitude ratio
5CB	Pentyl cyanobisphenyl
A	Area
AFM	Atomic force microscopy
AIBN	2,2'-azobis(isobutyronitrile)
ARGET	Activators regenerated by electron transfer
ATRP	Atom transfer radical polymerization
BPO	Benzoyl peroxide
BPY	Bipyridine
CRP	Controlled radical polymerization
CV	Cyclic Voltammetry
c_p	Heat capacity
$\mathcal{D}$	Diffusion coefficient

DC	Decanoyl chloride
DDQ	2,3-dichloro-5,6-dicyano-1,4-benzoquinone
DMF	*N,N'*-dimethyl formamide
EThMA	3-ethylthienyl methacrylate
FET	Field effect transistor
FF_{vol}	Space filling factor
F_4-TCNQ	Tetrafluorotetracyanoquinodimethane
FT-IR	Fourier transform infrared (spectroscopy)
GMA	Glycidyl methacrylate
GPTMS	3-Glycedoxypropyl trimethoxysilane
h	Convective heat transfer coefficient *or* height
HOMO	Highest occupied molecular orbital
IBC	Isobutyryl chloride
IR	Infrared (spectroscopy)
ITO	Indium tin oxide
k	Thermal conductivity
k_a	Activation constant
k_{da}	Deactivation constant
k_p	Propagation constant
K_c	Overal mass transfer coefficient
K_{eq}	Equilibrium constant
L	Characteristic length
LB	Langmuir Blodgett (deposition)
LC	Liquid crystal(line)
LCD	Liquid crystal display
LCP	Liquid crystalline polymer
LED	Light emitting diode
LUMO	Lowest unoccupied molecular orbital
Me_6TREN	*tris*(2-dimethyl-aminoethyl)amine
MMA	Methyl methacrylate
MTM	Methylthienyl methacrylate
NMP	Nitroxide mediated polymerization
NMR	Nuclear magnetic resonance (spectroscopy)
Nu	Nusselt number

ODS	Octadecyl trimethoxysilane
ODTS	Octadecyl trichlorosilane
OTS	Octyl trichlorosilane
P3HT	Poly(3-hexylthiophene)
P*t*BA	Poly-*tert*-butyl acrylate
PBTTT	Poly(2,5-bis(3-alkylthiophen-2-yl) thieno[3,2-b]thiophene)
PDMCS	Propyl dimethylchlorosilane
PDMA	Poly-*N,N*-dimethyl acrylamide
PDMS	Polydimethyl siloxane
PEDOT	Polyethylene dioxythiophene
PET	Polyethylene terephthalate
PGMA	Polyglycidyl methacrylate
PL	Photoluminescence (spectroscopy)
PMA	Polymethyl acrylate
PMDETA	*N,N,N',N",N"*-Pentamethyl diethylenetriamine
PMMA	Polymethyl methacrylate
Pe	Péclet number
PS	Polystyrene
PSF	Polystyrene-*co*-2,3,4,5,6-pentafluorostyrene
PSS	Polystyrene sulfonic acid
r	Radius
RAFT	Reversible addition-fragmentation chain transfer polymerization
Re	Reynolds number
RM	Reactive mesogen
RP	(Free) radical polymerization
R_p	Rate of polymerization
SAM	Self-assembled monolayer
SCE	Standard calomel electrode
S_S	Free interface tensions of a solid-air interface (L: liquid-air; SL: solid-liquid)
Sh	Sherwood number
SIP	Surface initiated polymerization
TCNQ	Tetracyanoquinodimethane

TEA	Triethyl amine
TEMPO	2,2,6,6-Tetramethyl piperidinoxy
UV	Ultraviolet
UV/Vis	Ultraviolet-visible (spectroscopy)
v	Mean fluid velocity
V	Volume
VOPc	Vanadyl phthalocyanine
x	Position
XPS	X-ray photoelectron spectroscopy
ZnPc	Zinc phtalocyanine

Contents

List of Tables

List of Figures

List of Schemes

Chapter 1

General introduction

Synopsis: The recent history of surface chemistry has seen the development of a broad range of compounds that spontaneously self-assemble on the surface to form dense monolayers. These compounds are widely applied to change the chemical and physical properties of the surface. Additionally several techniques have been developed that use monolayer forming initiators at the surface to start polymerization reactions. These techniques have drawn interest, as surface-initiated polymers are expected to have more order than bulk or solution polymers. Another field of research that has emerged in the past two decades is the field of organic and polymer electronics. In the devices developed in this field, molecular order plays an important role. The first part of this thesis will deal with surface polymerizations to form surface grafted materials that may find application in devices. The second part will present new techniques for surface polymerizations to make them more versatile and attractive and better fit to meet the tailored demands of high-end applications. This chapter deals on one hand with giving a brief introduction into the field of surface modifications by self-assembled monolayers and polymer brushes and on the other hand with giving background information about the working of some electronic devices in which self-organization of organic or polymeric materials plays a major role.

1.1 Self-assembled monolayers

Self-assembled monolayers (SAMs) are closely packed and highly ordered monomolecular films, formed by the adsorption and spontaneous ordering of a surfactant on a surface. The molecules that make up the SAM have at least one functional end group, which can form stable bonds with the surface of the substrate. Depending on the substrate these functional end-groups include thiols and disulfides (on gold),[1,2] alkoxy- and chloro-silanes (on hydroxylated silicon, glass and some metal oxides)[3–6] and carboxylic and hydroxamic acids (on silver oxide and some other metal oxides).[7,8]

The order in SAMs is a result of Vanderwaals interactions between the aliphatic tails of the molecules making up the SAM. The preparation of SAMs is simple and is carried out by immersing the substrate into a dilute solution of the surfactant[4,9,10] or by exposure of the substrate to a vapor of this reactant.[11,12] Langmuir–Blodgett (LB) techniques have been applied as well.[13–15]

Alkylchlorosilanes and alkylalkoxysilanes require hydroxylated surfaces as substrates for their formation. During their chemisorption to the surface they form polysiloxane, which is connected to the surface silanol groups by covalent Si—O—Si bonds. Water catalyzes this reaction but an excess of water results in polymerization in solution and irregular films.[5,10,16] Small differences in water content in the reaction mixture and concentration of surface hydroxyls may result in differences in monolayer quality. Nevertheless their stability makes them ideal materials for surface modification.

Thiols and disulfides form monolayers on gold that are most probably based on the formation of Au(I) thiolate (RS^-) species. This bond is not thermally stable. This reduced surface anchoring results in migration on the surface, which is essential for the healing of defects. Silanes, lacking this mobility, result in SAMs that are slightly less ordered.[1,17]

Apart from the surfactant group, the ω-position of the SAM-forming molecule also allows for functionalization. When the SAM is formed it is this side of the molecule that is at the air-monolayer interface and determines the "flavour" of the surface. Hence a variety of surfaces with control over specific chemical and physical interactions can be produced. Due to these properties, SAMs have been successfully applied in biomedical,[18] biochemical,[19] opto-

electronic[20] and electro-optic devices.[21]

Monolayers can also effectively be tuned by mixing two or more monolayer forming species in the solution. For thiols the ratio of both components in the SAM will be the same as the ratio in solution, as long as the molecules are of similar chain length.[22] Also for silanes ideal mixing in competitive adsorption has been shown.[16,23]

Modification of the chain terminus also allows for chemistry, *e.g.* changing the surface energy, creating binding sites and introducing sites that can start chain-reactions like polymerizations. These functional groups can be introduced before adsorption of the species at the surface or by surface chemistry after adsorption. Thiols and silanes with amine, alcohol, carboxylic acid, epoxide and other end groups are commercially available. The choice and successfulness of the reactions are limited as steric effects play a more important role and reactions have to avoid etchants to the substrate and conditions that might affect the stability of the monolayer.

A more complete review of SAMs has been written by Ulman[17]. Reactions at SAMs have been reviewed by Sullivan *et al.*[24]

1.1.1 Micro-contact printing

Micro-contact printing (μCP) is a patterning technique based on self-assembly that uses flexible stamps that are brought in conformal contact with the substrate to deliver a monolayer of material.[25] The material generally used for the stamps is the elastomer polydimethylsiloxane (PDMS). Stamps are fabricated by covering a master (patterned by *e.g.* photolithography) with a mixture of the pre-polymer and the curing agent, followed by curing at elevated temperature. The cured elastomer stamp has good thermal and chemical stability and the stamp is flexible and transparent.

When the stamp is 'inked' with a silane or thiol and then brought in contact with the substrate for 10-30 s, the material transfers to the silicon or gold and forms a patterned monolayer (see scheme 1.1).[26,27] To avoid migration of the thiols over the surface, patterning on gold is usually followed with backfilling the non-derivatized areas with a second thiol. In this way either the original pattern or the negative pattern of reactive SAMs can be obtained with 'dummy'

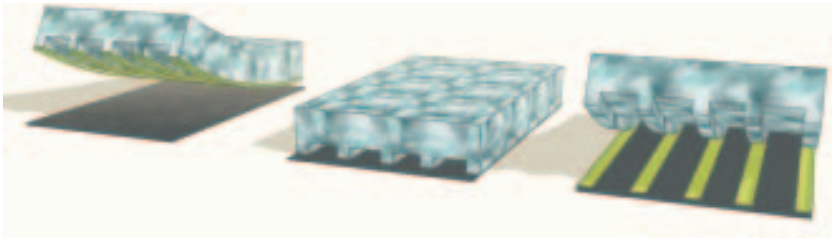

Scheme 1.1: Micro-contact printing: an inked stamp is brought in conformal contact with a substrate. Upon release a monolayer of the ink has been deposited.

molecules in the other areas.

The resolution of μCP is not diffraction-limited, so feature sizes smaller than the wavelength of light are possible (most photolithographic instruments have a cut-off of the light at $\sim$200 nm). Patterned lines of dendrimers down to only 50 nm wide have been shown.[28] However printing of features with high aspect ratios (small features spaced widely) is difficult due to stamp deformation and migration of the ink.[29] Nevertheless, the many advantages of this method, low costs, small feature sizes and wide range of materials that can be patterned, make it an attractive and versatile technique.

1.2 Controlled/living polymerizations and surface-initiated polymerizations

Free radical polymerization is by far the most widely used process for polymer synthesis.[30] It combines many advantages as a low sensitivity to impurities and a high reaction rate, but a significant drawback is the lack of structure control due to termination by recombination and disproportionation. Living or controlled radical polymerizations (CRP) decrease the concentration of active radical in solution dramatically by reversible end-capping and therefore termination plays a minor role: the polymerization becomes controlled, the reaction rate becomes linear with monomer concentration, the chain length can be tuned and the polydispersity becomes lower.[31–34]

CRP has also gained a lot of interest for the synthesis of polymers covalently bound to the surface. There are two ways to obtain polymers covalently bound to the surface of a substrate: i) by attaching a end-functionalized poly-

mer to the surface by reaction of the polymer with the surface or a surface-bound monolayer ('grafting *to*');[35–37] ii) by growing the polymer directly from the surface ('grafting *from*'). In the latter method initiator molecules have to be attached to the surface first, to initiate the polymerization from the surface, hence the term surface-initiated polymerization (SIP).

Surface-initiated polymers are often referred to as "polymer brushes". The properties of the polymer brush are greatly dependent on the grafting density of the brush. With high grafting density the chains are forced into a much more extended conformation than they would adopt in solution.[38] If the grafting density decreases, the polymers get more freedom and coiling will increase, resulting in less extended chains and a decrease in thickness. If the grafting density is even lower, a certain point the polymers will become isolated, with each polymer occupying a half sphere with a radius comparable to their radius of gyration (see scheme 1.2).[39] At this point the individual polymer chains can be distinguished with atomic force microscopy. This is called the mushroom regime. At even lower grafting density, polymers that have high affinity with the surface can spread out to form flat round discs, so-called pancakes.

Brushes that are grafted *to* the surface generally have a lower grafting density than brushes that are grafted *from* the surface as extended chains are entropically unfavourable, hence chain attachment at neighbouring sites is hindered by the coil formation of the polymers.

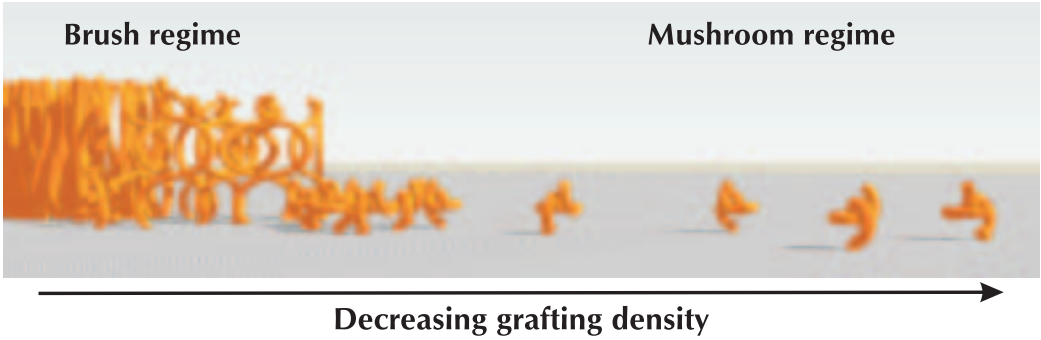

Scheme 1.2: The brush and mushroom regime for polymer brushes depending on grafting density.

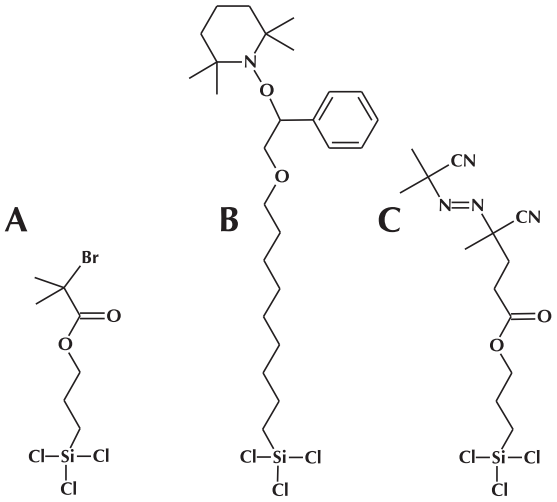

Scheme 1.3: Three commonly used initiators for surface-initiated polymerizations: A) surface initiator for ATRP; B) for NMP;[49] C) for free radical polymerization.[47]

The deposition of the initiator monolayer in grafting *from* approaches can be combined with μCP. The brushes grown from these patterned monolayers amplify the pattern into a polymer layer.[40–42] These patterned polymer layers have been used as barriers to wet chemical etchants of gold,[41] to synthesize 2D polymers[43,44] and to obtain patterned alignment of liquid crystals.[45]

Surface grafted polymers have been grown from flat surfaces, curved surface[46] and particles[47–49]. Growing polymers is not only possible on inorganic substrates like gold,[41,45,50] glass,[51,52] silicon,[43,52–57] and ITO,[58] but also on polymeric substrates like PDMS[59] and PET.[60]

The field of polymer brushes has been reviewed recently.[61] Many polymerization techniques have been applied for SIP, but recent research has focused on controlled techniques, such as nitroxide mediated polymerization (NMP) and atom transfer radical polymerization (ATRP). Scheme 1.3 shows the most common initiators for surface-initiated ATRP, NMP and free radical polymerization (RP).

Polymer brushes are potentially interesting for a wide variety of applications. The covalent bounding to the surface makes these polymer films robust: they are not removed or damaged upon solvent treatment, *e.g.* for the deposition of subsequent films. The tunable density gives them properties like enhanced order in the film, that are inaccessible by other techniques. Polymer

brushes are of interest for applications as adhesives,[62] for the fabrication of 2D-polymers,[43,44] as membranes,[63,64] as binding sites for proteins or bacteria in bioarrays,[65] as protein resistant coatings,[66] for electronic applications[51,58,67] and as stimuli responsive surfaces[37,68–70].

1.2.1 ATRP and polymer brushes

The proposed reaction scheme for ATRP is given in scheme 1.4.[71,72] The living nature of ATRP lies in the deactivation of the reactive chain by end-capping it with a halide atom. The halide at the end of the chain is removed by a copper(I) complex, turning into a copper(II) complex. After this, the radical chain can propagate by reacting with a monomer. The equilibrium however lies on the side of the inactive, 'dormant' state. To make the reaction more controllable, often deactivator is added in the form of extra copper(II) halide salt, although this slows down the overall reaction. As a ligand not only the

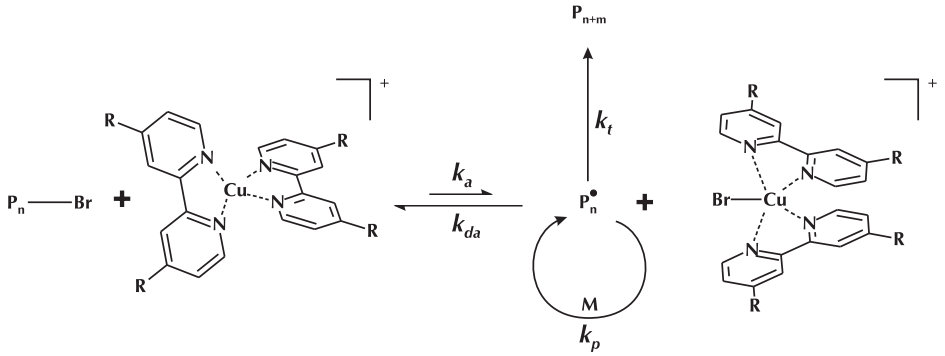

Scheme 1.4: The proposed reaction mechanism for ATRP,[71] P_n = polymer chain, M = monomer and P_{n+m} = terminated polymer; k_a is activation constant, k_{da} = deactivation constant, k_p = propagation constant, k_t = termination constant.

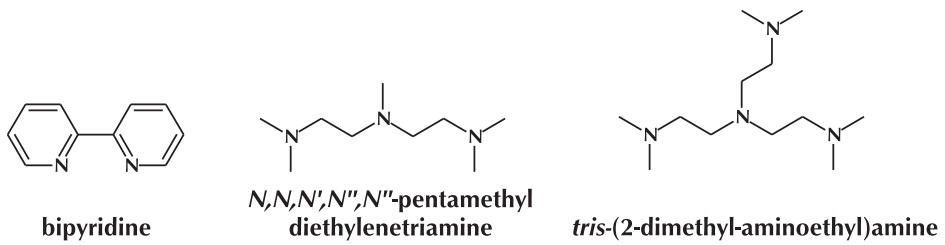

Scheme 1.5: Three commonly used ligands for ATRP.

bidentate bipyridine can be used, as shown in the reaction scheme, but also the tridentate N,N,N',N",N"-pentamethyl diethylenetriamine (PMDETA) and the tetradentate tris(2-dimethyl-aminoethyl)amine (Me6TREN) are often used. Scheme 1.5 shows these three commonly used ligands. Other metal catalysts like ruthenium(II) halides and zinc(II) halides have been applied in ATRP as well.[31] However, copper-catalyzed polymerizations are usually the systems of preference as they are compatible with a wider range of monomers.[73] The reaction kinetics can be influenced by the concentrations of copper(I), copper(II) and the nature of the ligand and halide.

Copper catalyzed ATRP has been shown to work with a broad range of monomers, like styrenic monomers,[72,74–76] acrylonitriles,[77] acrylates[75,76] and methacrylates.[75,76]

ATRP results in low polydispersities and is especially attractive since it shows rapid controlled polymer growth at room temperature when aqueous solvent mixtures are used.[78,79] This makes it compatible with thermally unstable SAMs on substrates, like thiols on gold, and suppresses undesired reactions, like thermo induced polymerization in solution and termination. Because of the living nature of the polymers, block co-polymers can easily be obtained by re-initiating the substrates with different monomer.

In the last few years ATRP has become the most popular route for the synthesis of surface-initiated polymers. This is because of the accessible reaction conditions (room temperature, no dry conditions required as in anionic and cationic polymerizations) and the compatibility with a broad range of monomers and substrates. ATRP reaction kinetics will be discussed in detail in section 1.3.

1.2.2 NMP and polymer brushes

NMP is based on the reversible end-capping of the active end-group radical by a nitroxide leaving group (see scheme 1.6). This nitroxide radical is in itself a stable radical and the success of the reaction is based on the persistent radical effect: the reluctance of the stable radicals to either undergo homocoupling or induce other radical reactions.[80] The concentration of the chain ends in the uncapped radical state is again too low to undergo homocoupling. The

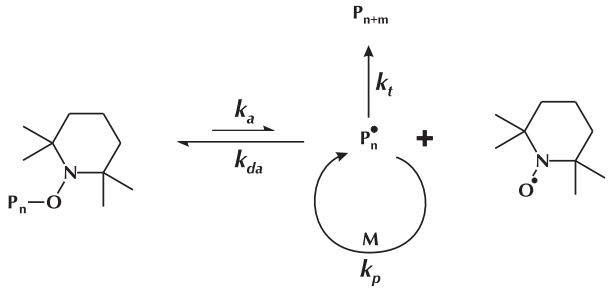

Scheme 1.6: The proposed reaction mechanism for NMP,[71] P_n= polymer chain, M = monomer and P_{n+m} = terminated polymer; k_a is activation constant, k_{da} = deactivation constant, k_p = propagation constant, k_t = termination constant.

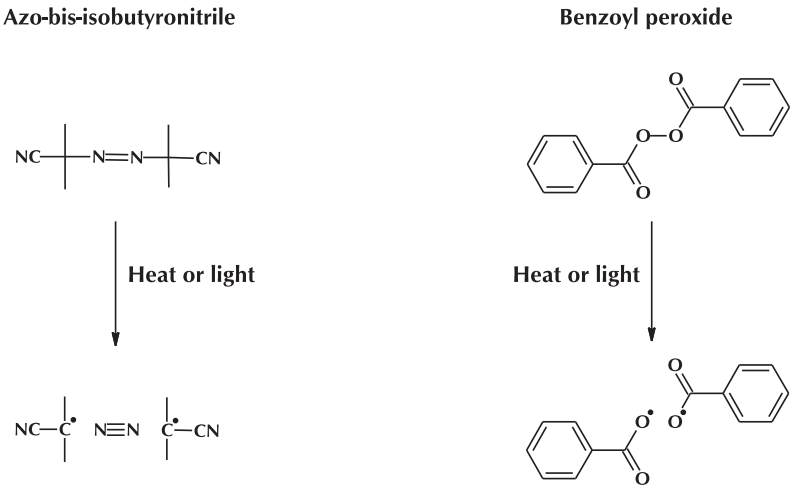

Scheme 1.7: The decomposition of two commonly used free radical initiators.

radical chain end however does induce other radical reactions (it is a so-called *transient* radical) and undergoes coupling with the monomer: the propagation step of the polymerization.

The field of NMP has been reviewed extensively by Hawker *et al.*[81] In general there are two approaches for the initiation of the reaction. Firstly it is possible to start the reaction with one of the standard initiators for radical polymerizations, *i.e.* 2,2'-azobisisobutyronitrile (AIBN) or benzoyl peroxide (BPO, scheme 1.7), secondly specific initiators for NMP have been developed, that dissociate in the mediating persistent radical and the transient radical that serves as an initiator for the polymerization. In the first approach it is necessary to add mediating nitroxide, hence the common name "bi-molecular" for

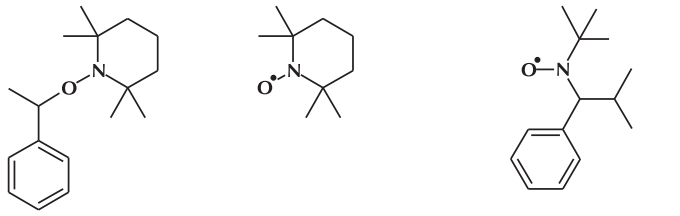

Scheme 1.8: Three compounds commonly used for NMP: the unimolecular initiator based on the structure of styrene and TEMPO, the mediator TEMPO and the "universal" mediator, which is compatible with a wider range of monomers.

this approach in contrast to the uni-molecular second approach. Scheme 1.8 shows the most commonly used mediator, 2,2,6,6-tetramethylpiperidinyloxy (TEMPO), together with the unimolecular initiator derived from its structure.

NMP has to be performed at elevated temperatures to reach an equilibrium in the dissociation reaction. NMP has been shown to work with styrenic monomers, acrylamides, 1,3-dienes, acrylonitriles and acrylates, although for most of these monomers TEMPO can not be used as the mediator. At the high dissociation temperature associated with TEMPO (typically a temperature of 125 °C is used for polymerizations mediated by TEMPO), most monomers undergo auto-polymerization at a high rate, making the polymerization difficult to control. Therefore a more universal mediator, 2,2,5-trimethyl-4-phenyl-3-azahexane-3-oxy, has been developed, which can be used at lower temperatures and with a broader range of monomer types, including acrylates, acrylamides and acrylonitrile (scheme 1.8).[82]

Surface-initiated NMP has been explored using both unimolecular nitroxide functionalized SAMs[49,83,84] and bimolecular systems.[85] With surface-initiated polymerization by NMP the concentration of the mediator in the solution is too low to control the reaction, if it is only provided by dissociation at the surface. Therefore additional mediator is often added. However, as the equilibrium is delicately controlled by the ratio of initiator and mediator concentration, addition of a bulk initiator is needed to control the reaction from the start.[49,86] This results in the formation of polymer in the solution, which has to be removed from the brush substrates. The polydispersity for polymers obtained by this method is reasonably low ~1.2[49] and the living

nature of the polymerization has been confirmed by re-initiation to form block co-polymers.

The kinetics of NMP will be discussed in section 1.3. Approaches to form initiator monolayers for NMP will be discussed in more detail in chapter 6 from page 145 onwards, together with a new approach for conversion of polymers formed by ATRP and ATRP initiator monolayers into NMP (macro-) initiators.

1.2.3 Surface-initiated polymers by other methods

Free radical polymerization is based upon the decomposition of a symmetrical molecule into two identical radicals at elevated temperature. For bulk polymers either an azo-initiator, *e.g.* AIBN, or an organic peroxide, *e.g.* BPO, is used (see scheme 1.7 on page 9). For SIP by free radical polymerization the reaction is initiated from the surface by a self-assembled monolayer of an azo-initiator. Mostly a derivative of AIBN is used (scheme 1.3C on page 6).[60,87] When the bonds to the azo group are cleaved, two radicals are created, initiating the free radical polymerization. When used for SIP, free radical polymerization yields thick polymer layers (often >200 nm) with high polydispersities.[54,88]

Ring opening polymerization (ROP) is a generic term for all addition polymerizations in which the terminal end of a polymer acts as a reactive center, where further cyclic monomers join to form a larger polymer chain through anionic or cationic propagation or polycondensation. As ROP is the polymerization of choice for the synthesis of many commercially important polymers as nylon-6 and polyethylene glycol it has also attracted attention for the use in surface-initiated polymerizations.

Husemann *et al.* used a SAM terminating in diethylene glycol moieties as initiator for the polymerization of ϵ-caprolactone catalyzed by diethyl aluminium alkoxides (see scheme 1.9A).[40] Free initiator (benzyl alcohol) was added to achieve better control. Brushes of up to 70 nm were obtained at room temperature.

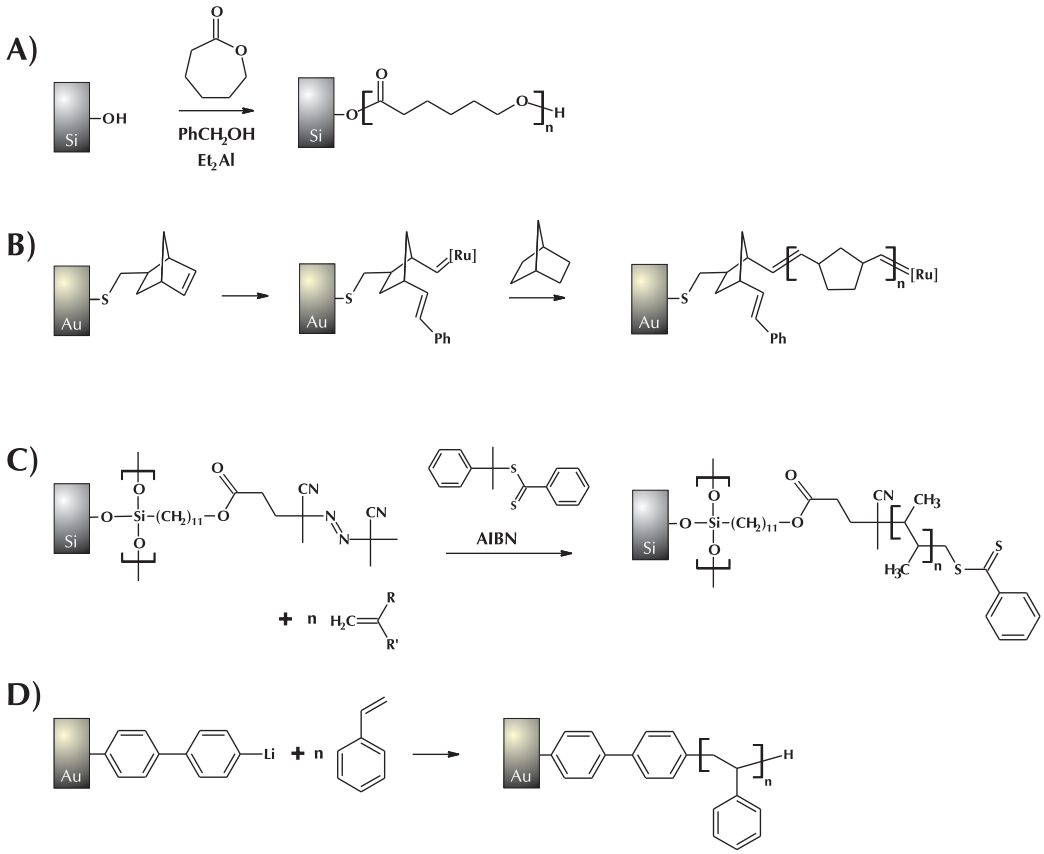

Scheme 1.9: Examples of surface-initiated polymers by A) ring opening polymerization; B) ring opening metathesis polymerization; C) reversible addition-fragmentation chain transfer polymerization; D) anionic polymerization.

Ring opening metathesis polymerization (ROMP) is a polymerization technique in which strained cyclic molecules, *e.g.* norbonenes are polymerized. This polymerization is catalyzed by metal carbenes, *e.g.* the ruthenium based catalysts developed by Grubbs and coworkers.[89] This polymerization method has particularly raised interest as it is one of the avenues for the synthesis of conjugated polymers.[90, 91]

Rutenberg *et al.* used ROMP for the synthesis of surface-initiated polymers based on norbonenes for application as dielectric layers in FETs.[67] They started with the deposition of a norbonene functionalized thiol on gold, which they then reacted with Grubbs ruthenium catalyst and exposed to a solution of

monomer as shown in scheme 1.9B. The 1.2 μm thick layers that they obtained showed good dielectric behaviour.

Reversible addition-fragmentation chain transfer (RAFT) polymerization is a controlled radical polymerization based on the stable intermediates that are formed by the reaction of a radical with dithioester chain transfer agents.[92] The chain growth is usually initiated using a conventional free radical initiator, *e.g.* AIBN.

Baum *et al.* used RAFT initiated by a surface grafted azo-initiator to grow PMMA, poly-*N,N*-dimethyl acrylamide and PS brushes of up to 28 nm (see scheme 1.9C).[93] Although this polymerization is very slow, the living character was proved by re-initiating the reaction to obtain block co-polymers.

Anionic polymerization is a living polymerization which yields well-defined polymers with low polydispersity. On the down-side, the technique is limited to only a handful of monomers and requires elaborate reaction conditions as low reaction temperatures and exclusion of moisture.

Jordan *et al.* used surface-initiated anionic polymerization to obtain polystyrene brushes on gold substrates.[94] They first prepared a SAM of 4'-bromo-4-mercaptobiphenyl which they then reacted with butyl lithium to form a monolayer of biphenyllithium. Next, this initiator was reacted with styrene to obtain 18 nm thick polystyrene brushes (see scheme 1.9D).

1.3 Reaction kinetics for ATRP and NMP

As we have seen, the essential reaction responsible for the controlled character of living radical polymerizations is the equilibrium in the activation/deactivation reaction step. For ATRP this is:

$$\mathrm{P-X + Cu(I)} \underset{k_{da}}{\overset{k_a}{\rightleftharpoons}} \mathrm{P^{\bullet} + Cu(II)X} \tag{1.1}$$

For NMP this is:

$$\mathrm{P-O-NR} \underset{k_{da}}{\overset{k_a}{\rightleftharpoons}} \mathrm{P^{\bullet} + {^{\bullet}O-NR}} \tag{1.2}$$

From this equilibrium reaction, the equilibrium constants can be derived. For ATRP, the following equation follows:

$$K_{eq} = \frac{k_a}{k_{da}} = \frac{[\mathrm{P}^\bullet][\mathrm{Cu(II)X}]}{[\mathrm{Cu(I)}][\mathrm{PX}]} \tag{1.3}$$

This means, that if one wants to influence the equilibrium between activated and dormant state, one has to change the relative concentrations between copper(I) and copper(II). Changing the absolute concentrations does not have any influence, as long as the relative concentrations remain the same. This property was utilized by Jakubowski *et al.*[95] They only used 10 ppm of copper(II) and ligand in the polymerization of styrene, but added a reducing agent, tin(II) 2-ethylhexanoate or glucose, which produces low amounts of copper(I) *in situ*. This technique based on activators regenerated by electron transfer (ARGET) has the advantage of easier purification. Also it is suggested, that the presence of a reducing agent could eliminate air or other radical traps in the system. In aqueous conditions the disproportionation between two copper(I) ions into elemental copper and a copper(II) ion also plays a role,[96] but as the exact role of elemental copper in aqueous ATRP is not fully understood, it will not be discussed here.

For solution polymerization a reasonable amount of copper(II) is created during the early stages of the polymerization by the initiation reaction. If polymer brushes are grown by controlled polymerization from flat surfaces, however, the number of radicals created at the surface is very low. Hence also the concentration of deactivator resulting from the dissociation at the surface is very low. This can result in a slow start of the reaction or in enhanced termination till the equilibrium between activation and deactivation has been established. To compensate for this, extra deactivator or extra 'sacrificial' initiator is often added to the solution.[97] The addition of solution initiator of course results in the formation of solution polymer.[49,53] Both methods have been applied for ATRP.[49,53,55,98]

For NMP, the equilibrium equation is as follows:

$$K_{eq} = \frac{k_a}{k_{da}} = \frac{[\mathrm{P}^\bullet][^\bullet\mathrm{O-NR}]}{[\mathrm{P-O-NR}]} \tag{1.4}$$

For the polymerization of styrene controlled by the nitroxide free radical

TEMPO, at 125 °C, this equilibrium was proved to be constant with a value of $K = 2.1 \cdot 10^{-11}$.[34] This means that the equilibrium is strongly to the deactivated side, with concentrations of the dormant state approximately $2 \cdot 10^5$ higher than the activated state (when a monomolecular initiator is used).

As can be seen in this equation, in NMP the equilibrium is controlled by the relative ratio between initiator and free nitroxide radical. This has major implications for surface-initiated polymerizations, where the total amount of initiator at the surface is very low. When the initiation reaction takes place, the free radical end-capping agent is diluted by the relatively large reaction volume. To gain control, adding the nitroxide free radical alone is not the solution, as it is very difficult to tune this equilibrium due to the minimal amounts of initiator. Therefore generally bulk initiator is added to the solution as well.[49]

When the polymer chain end is in the activated state, propagation can take place:

$$\mathrm{P^{\bullet}}_n + \mathrm{M} \quad \xrightarrow{k_p} \quad \mathrm{P^{\bullet}}_{n+1} \tag{1.5}$$

An equation for the rate of polymerization can now be derived:

$$R_p = \frac{\mathrm{d[M]}}{\mathrm{d}t} = k_p[\mathrm{P^{\bullet}}][\mathrm{M}] \tag{1.6}$$

For ATRP equation 1.3 can be used to substitute $[\mathrm{P^{\bullet}}]$, which yields:[73]

$$R_p = k_p K_{eq}[\mathrm{PX}]\frac{[\mathrm{Cu(I)}]}{[\mathrm{Cu(II)X}]}[\mathrm{M}] \tag{1.7}$$

As the number of activated polymer chain sides is very low, it is valid by approximation to say:

$$[\mathrm{PX}] \approx [\mathrm{I_0}] \tag{1.8}$$

with $[\mathrm{I_0}]$ as the initiator concentration at the start of the reaction. If this is substituted into equation 1.7 the following equation is obtained:[72]

$$R_p = k_{app}[\mathrm{M}] = k_p K_{eq}[\mathrm{I_0}]\frac{[\mathrm{Cu(I)}]}{[\mathrm{Cu(II)X}]}[\mathrm{M}] \tag{1.9}$$

in which the rate of polymerization is first order in [M] and k_{app}, the apparent reaction constant, is dependent on concentrations that normally should remain constant during the reaction.

For NMP the rate of polymerization is similar:

$$R_p = k_{app}[\mathrm{M}] = k_p K_{eq}[\mathrm{I}_0]\frac{1}{[^{\bullet}\mathrm{O}-\mathrm{NR}]}[\mathrm{M}] \tag{1.10}$$

The last reaction step to be discussed is the termination. In free radical polymerizations, the most important reaction responsible for termination is the recombination of two radicals:[30]

$$2 \quad \mathrm{P}^{\bullet} \quad \xrightarrow{k_t} \quad \mathrm{P}-\mathrm{P} \tag{1.11}$$

$$R_t = k_t[\mathrm{P}^{\bullet}]^2 \tag{1.12}$$

In controlled radical polymerizations, the concentration of $[P^{\bullet}]$ is very small and the rate of termination is negligibly small, if the equilibrium conditions have been chosen well.[73]

In the case of surface-initiated polymerizations, the concentration of initiators is very low relative to all the other concentrations. This means, that as the reaction proceeds, the concentration of monomer [M] stays nearly constant. With neglegible termination this means that the number average chain length M_n of the polymers increases almost linear in time.[55]

It has to be noted, that for surface-initiated polymerizations the linearity with monomer concentration as given in equation 1.9 is not always valid. At low monomer concentration propagation is slowed down, but the reaction rate for most side reactions does not depend on monomer concentration.[33] This results in a certain window of concentrations of monomer, where the polymerization is well controlled.

It has been shown in literature that for surface-initiated polymers in the brush regime, the number average chain length is linear with the thickness of the polymer layer on the surface.[49,55,99] This means that for a well controlled surface-initiated polymerization, the thickness of the polymer brush layer increases linear with time.[55,100]

1.4 Devices

Until the 1970s polymeric materials were considered to be electrically non-conducting materials. In 1977 it was discovered that polyacetylene becomes electrically conducting when it is oxidized.[101] This discovery had great influence on academic and industrial research as it started a totally new field of scientific research,[102] both with the synthesis of new semiconductive materials[91] as with the development of organo-electronic devices.[103] Semiconducting devices play an important role in electronic circuits and displays and organic and polymeric conductors offer advantages as low cost, solution processibility and the possibility of patterning by soft lithographic and digital printing techniques. Organic LEDs are already applied in displays for cameras, MP3 players and mobile phones.

The performance of organo-electronic devices is highly dependent on order in the active layer. In this section we will discuss three classes of devices, in which the self organization of polymeric and organic materials plays an important role: Field effect transistors, photovoltaic cells and liquid crystalline displays. Polymer or organic LEDs, a fourth class of organo-electronic devices, will not be discussed as order is not required for optimal device performance here. Readers interested in organic LED are referred to excellent reviews in the literature.[104–106] At the end of this section some applications of polymer brushes in polymer electronic devices are discussed.

1.4.1 Field effect transistors

The field effect transistor (FET) is a transistor that makes use of the electric field, created by a voltage on one of its electrodes, to switch the device on and off. Like all transistors, FETs have three electrodes that are known as source (S), drain (D), and gate (G). These names refer to their functions: electrons flow from the source to the drain through a "channel", which width is determined by the gate potential. The gate is separated from the active layer by a non-conductive, dielectric, layer. The channel is a conductive pathway through the semiconductive layer of the device, at the interface of dielectric and semiconductive layer. The charges of this pathway can be either positive

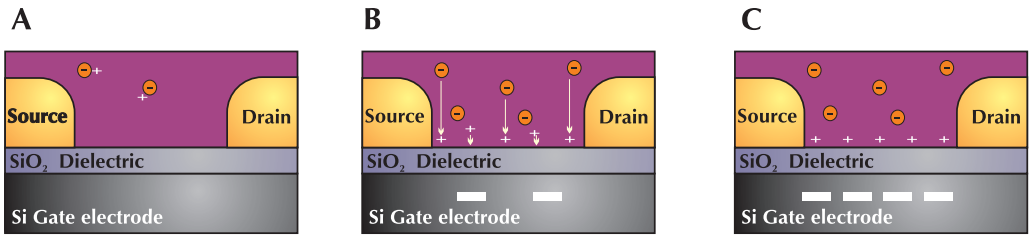

Scheme 1.10: The working of a organic p-type field effect transistor: A) when not operated, charges do exist in the polymer semiconductor layer, but occur in pairs, so-called polarons, and have limited mobility; B) when a negative gate bias is applied, the charges are separated by the electric field and the holes are drawn toward the interface between semiconductor and dielectric. Also new polarons are separated, as soon as they occur; C) at even higher gate bias, the positive charges form a conductive channel at the semiconductor/dielectric interface.

(p-type) or negative (n-type devices), dependent on whether the material of the active layer is acting as an electron donor or acceptor respectively. Both n- and p-type silicon devices do exist. In the case of organic or polymer active layers, p-type devices, with positive charges in the channel, are the most common, although n-type[107] and even ambi-polar devices exist.[108,109]

The working of a p-type FET is schematically pictured in scheme 1.10. When the device is not operated, or when a positive voltage is applied to the gate, there is no conductive pathway. Charges are still present in the active layer, but the concentration is very low. When new charges are created by charge transfer, they are not separated by an electric field and recombination can occur. When the device is switched on, *i.e.*, a negative potential is applied to the gate electrode, positive charges are attracted by the electric field between source and gate to the interface between semiconductor and dielectric. At this interface they form a layer with a high concentration of charges and this layer becomes conductive: a channel of conducting charges is created and the device is switched on. The ratio between current flowing in the on-state and in the off-state is called the on/off ratio.

The switching of the device does not always occur at 0V exactly. Sometimes the concentration of charges throughout the device (and thus in the channel) is high enough to cause conductivity at 0 V. Only a positive gate bias can then drive the charges away from the channel to switch off the device. In other

cases charges are trapped at the surface and the device only switches on at gate voltages well below 0 V. The voltage at which the device switches is called the threshold voltage, sometimes also called the turn-on voltage.

At source-drain voltages much lower than the source-gate voltage, varying the gate voltage will alter the concentration of charges in the entire channel and the FET operates as a variable resistor. In this regime, the source-drain current is almost linear with the source-drain voltage and hence, this mode of operation is called the linear regime.

When the source-drain voltage is increased well above the source-gate voltage, the electric field in the channel becomes highly asymmetric: near the drain the field inverses and the channel no longer connects source and drain. However: charges still can flow from source to drain, as from this inversion point they are driven toward the drain by the electric field. In this situation the source-drain current becomes relatively independent of the source-drain voltage. This regime is called the saturation regime.

The fabrication of organic FETs became a popular research topic short after the development of processable conjugated polymers.[110] One of the interesting feature of polymer FETs is the fact that theoretically all the elements — substrate, insulator, semiconductor and even the electrodes — could be made of polymeric material.[111,112] However, the success of organic or polymer FETs was limited till recently due to the relatively low field effect mobilities (a measure for how quick the charge carriers can move). Nowadays mobilities of μ_{FET}> 0.7 $cm^2V^{-1}s^{-1}$ and on/off ratios >10^7 can be achieved.[113–115] The mobility is highly dependent on the order of the molecules in the channel and many research has been performed to improve this order and hence the mobility of charges in FETs.[116–120] Liquid crystalline materials, known for their enhanced order in the processable liquid phase, are often used for the fabrication of transistors for the same reason.[121–124]

Another way to increase the mobility is the addition of dopants,[125–130] although the application in polymer FETs is limited. The addition of dopant generally not only increases the on-current, but also the off-current. The doping of organic active layers in FETs will be discussed in more detail in chapter 3 on page 56.

Other research in the field of organic and polymer FETs includes the in-

fluence of molecular design on the order of processed layers and hence the performance of devices,[131–134] structuring and layer deposition techniques in device fabrication[112,135] and new device lay-outs.[113]

FETs play an important role in electronic circuits and in displays.[136] As organic and polymer FETs are cheap to produce, they are expected to play an important future role in low-cost disposable electronics.[103]

1.4.2 Photovoltaic cells

Photovoltaic (PV) cells are devices that transform the energy of light into electrical energy. For this these devices have to absorb the light inducing an electron to go into a state of higher energy (excitation) and then transfer the (potential) energy of this short lived state into kinetic energy of the electrons to create a current. In this way, solar cells can be compared to a trampoline (excitation) connected to a slide. Silicon solar cells were already developed in the early fifties of the previous century by forming a layer of *p*-doped layer on top of an *n*-doped silicon layer.[137]

In organic electronics the same concept was initially followed by depositing a *n*-type material on top of a *p*-type polymer coated ITO-electrode (the substrate being transparent). This bilayer PV cell had an efficiency of 0.3%, though the performance was severely limited by the limited diffusion length of the excitons: After excitation by a photon, the exciton has to travel to the *p*-*n*-interface where charge transfer can take place, before the exitation energy is lost via radiative and non-radiative decay. This excitaton diffusion length is typically limited to 5-20 nm.[138] In polymer solar cells with donor and acceptor material in two separate layers on top of each other, the performance is severely limited by this process, as the layer thickness is in the order of 50 nm, to absorb sufficient light.

This problem was overcome by the so-called bulk-heterojunction cell developed by the group of Heeger,[139] in which the donor and acceptor are mixed to reduce the required diffusion length. The working of this cell is depicted in scheme 1.11: Incoming light excites an electron. This exciton can than travel a short distance to the interface between donor and acceptor material, where the electron is accepted in the lowest unoccupied molecular orbital (LUMO)

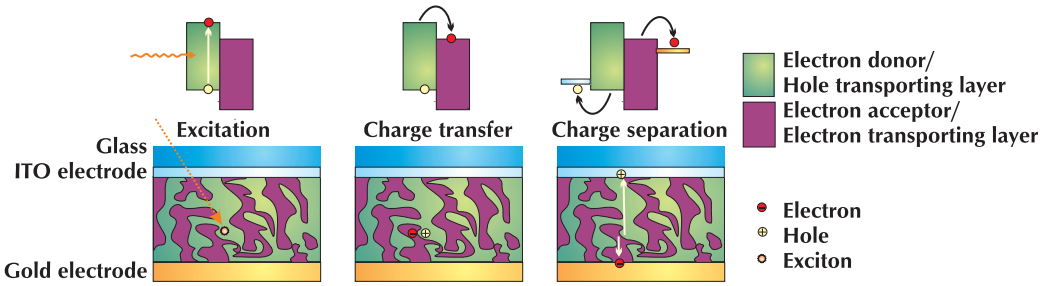

Scheme 1.11: Schematic working principle of bulk heterojunction solar cell. Upon illumination excitation takes place. If the excitation takes place close to a interface between electron donor and acceptor, charge transfer can occur. The charges are then separated by the difference in work function between the two electrodes.

of the acceptor molecule. This charge transfer creates a positive charge (an electron deficiency or hole) and a negative charge (electron). The hole and electron are transported to the opposite electrodes via the donor and acceptor material respectively. This charge separation is driven by the difference in work function between both electrodes.

For a good performance of the PV cell, all processes of light absorption, charge transfer, charge separation and charge transport have to be efficient. The light absorption is addressed in research on the development of low band-gap conjugated polymers, that can absorb a bigger share of the solar spectrum.[140,141] For improvement of charge transfer and separation the morphology and blending of the two components is studied[142,143] and materials that combine donor and acceptor functionalities have been developed.[144,145] For efficient charge transport order perpendicular to the substrate plays an enormous role and, again, LC materials find applications because of their intrinsic molecular order.[146–148] Top performing polymer solar cells have efficiencies up to 2.5%.[149]

N-type materials that are often used in polymer solar cells are fullerene derivatives[139,141,149] and perylenes.[150,151] *P*-type materials include polyphenylene vinylene derivatives[139,144,149,151] and polythiophene derivatives[141,152] and many other conjugated polymers. Chapter 4 (page 87 onwards) discusses the synthesis of polythiophenes in more detail and presents a new method to grow polythiophene from the surface.

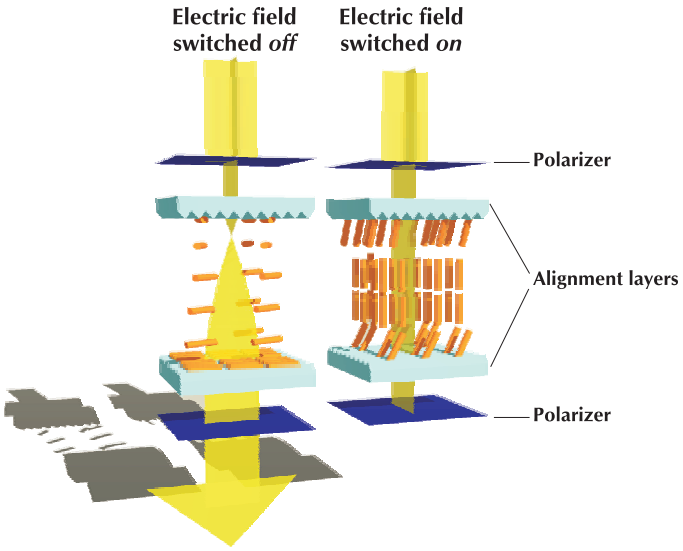

Scheme 1.12: Schematic working principle of an LCD. When the electric field across the cell is switched off, the liquid crystal molecules describe a twist over 90° which guides the polarized light, so it can pass the second polarizer at the bottom of the cell. When an electric field is applied, the molecules orient themselves perpendicular to the alignment layers: the light passes the cell unaltered and is blocked by the second polarizer.

1.4.3 Liquid crystal displays

The last device that will be discussed in this chapter is the liquid crystal display (LCD). LCDs proceeded from early applications as the pocket calculator and the digital watch to full colour flat-panel displays and now find applications in many portable electronic devices as well as computer and television screens.[153] LCDs are not organic electronic devices, in which the organic layer plays a role in creating or conducting charges, like the applications discussed above. However, it is useful to look into these devices, as a lot of research on alignment and molecular engineering originally developed for the LCD field is of interest for polymer and organic electronic devices as well.[122, 124, 146, 154, 155]

The working principle behind LCDs revolves around alignment layers. These layers strongly influence the orientation of the liquid crystal material in the LCD cell. The most basic LCD that is used for everyday items is called the twisted nematic (TN) display.[136] This device consists of a nematic liquid crystal sandwiched between two alignment layers. The alignment layers have such anisotropy that the molecules align planar yet the director at the top of

the sample is perpendicular to the director at the bottom. This configuration sets up a 90° twist in the bulk. Sometimes a small amount of a chiral material is added to ensure a uniform twist.

As can be seen in scheme 1.12, apart from the alignment layers, two polarizers are applied in twisted nematic displays. If the input polarizer is set parallel to the alignment of the liquid crystal molecules at the top plate, the plane of polarization of the light passing through the liquid crystal will be rotated by 90° because of the gradual twist of the liquid-crystal molecules. This light will then pass through the second polarizer adjacent to the lower plate whose orientation is set perpendicular to the first polarizer.

In LCDs, the molecules applied are designed to have a strong dipole moment in the axial direction. If now an AC voltage is applied across the cell, the molecules (except those held by surface forces at the alignment layers) will to a large degree orient themselves perpendicular to the alignment layers as shown in the right part of scheme 1.12. In this orientation the LC layer can no longer produce a rotation in the polarization plane of the light, causing it to be blocked by the bottom polarizer.

Chapter 2 will discuss the application of polymer brushes as alignment layers.

1.4.4 Polymer brushes in polymer electronic devices

As most organo-electronic applications benefit from enhanced order, polymer brushes have attracted attention for these applications. Mulfort *et al.* report the fabrication of surface-initiated polymer films of polystyrene sulfonic acid (PSS) doped with polyethylene dioxythiophene (PEDOT).[51] PEDOT:PSS is known to form highly conductive films and is used in many organic electronic devices. Polystyrene brushes were prepared from a living polymerization using benzoyl peroxide (BPO) as an initiator and 2,2,6,6-tetramethyl-1-piperidinyloxy (TEMPO) as a scavenger and subsequently sulfonated. Ethylene dioxythiophene (EDOT) was diffused into the films and polymerized. The resulting films had low density due to poor initiator density. The conductivity of the films obtained by this method were lower than spin coated films from commercially available PEDOT:PSS.

Whiting and Huck have recently fabricated photovoltaic devices by spin casting CdSe nanocrystals on brushes of the hole conductor polytriphenylamine acrylate (PTPAA).[58] The brush device was compared to an optimized blend device and had a peak external quantum efficiency three times higher than that of the blend. This higher efficiency was attributed to enhanced order in the hole conducting layer.

The use of surface-initiated polymers as a dielectric layer was demonstrated by Rutenberg and coworkers.[67] This application is based on the high achievable density with this class of polymers. They grew 1.2 μm thick polynorbornene by ring opening metathesis polymerization. Although films of this thickness result in high switching voltages and low on/off ratios, the use of the dense properties of surface-initiated polymers for dielectric layers is a promising application.

1.5 Aim and outline of this thesis

As shown in this introduction, the field of polymer electronics has developed from the discovery of polymer conductance to commercial applications in less than thirty years. The performance of polymer FETs and PV cells however are highly dependent on the order of the molecules in the active layer and polymer brushes have attracted attention for potential application in this field. The aim of this thesis is on one hand to explore new avenues in the application of surface-initiated polymers in polymer electronic devices and on the other, to develop surface-initiated polymerizations into more versatile and economical technologies, so they become more attractive for the fabrication of devices.

The remainder of this thesis is split in two parts, of which the first part will deal with surface polymerizations to form surface grafted materials that may find application in devices. This part contains three chapters with three different applications.

The first chapter of this section (chapter 2 on page 35) discusses the synthesis of side chain liquid crystalline polymer brushes for application as homeotropic alignment layer. Alignment has become an important part of the research in organic electronics and these brushes could potentially play a role in enhancing the order in the active layer of devices to improve device perfor-

mance. Brush layers with liquid crystalline functionality could be an advantage over conventional alignment layers as they provide stronger liquid crystalline interaction with the bulk as opposed to aliphatic interactions. Also the covalent bond with the surface provides resistance of this alignment layer against solvent treatments, which could be an additional advantage.

The following chapter (page 56) discusses the synthesis and the application of dopant functionalized monolayers and polymer brushes to locally dope the active layer of a FET. The surface attached layer enables exact positioning of the dopant in the channel of the device.

Chapter 4 (page 87) explores the use of thiophene functionalized polymer brushes as a template to grow the conjugated polymer polythiophenes from the surface by oxidative polymerization. As has been discussed above, conductive pathways perpendicular to the substrate could be of interest for solar cells. Additionally, polythiophenes without side-chains can not be solution processed to obtain surface coatings, so growing them by polymerization from the surface would provide a potentially useful technique to fabricate these layers.

In the second part of this thesis the focus is on new technologies, that could make SIP more versatile and attractive and better fit to meet the tailored demands of high-end applications. This part has two chapters.

The first chapter of this section (chapter 5 on page 118) introduces a technique to reduce the reactor volume during surface-initiated polymerizations. In this way the waste of monomer and other chemicals can be reduced considerably, which can be of importance for many device applications, as the monomers used are often expensive or laborious to synthesize. The effects of reduction of reactor volume on reaction kinetics will be studied in detail in this chapter.

The last chapter (page 145) explores the conversion of ATRP initiator sites into NMP initiators to obtain mixed brushes and block co-polymer brushes. The synthesis of mixed brushes will be of use for the fabrication of devices that require a combination of two interpenetrating polymers. The potential to obtain both mixed and block co-polymer brushes will enable complex polymer architectures.

References

[1] M. D. Porter, B. Bright, Thomas, D. L. Allara, and C. E. D. Chidsey, *J. Am. Chem. Soc.* **109**, 3559 (1987).

[2] T. P. Sullivan, M. L. van Poll, P. Y. W. Dankers, and W. T. S. Huck, *Angew. Chem., Int. Ed.* **43**, 4190 (2004).

[3] R. Banga, J. Yarwood, A. M. Morgan, B. Evans, and J. Kells, *Langmuir* **11**, 4393 (1995).

[4] J. Sagiv, *J. Am. Chem. Soc.* **102**, 92 (1980).

[5] J. J. Cras, C. A. Rowe-Taitt, D. A. Nivens, and F. S. Ligler, *Biosensors and Bioelectronics* **14**, 683 (1999).

[6] H. Hillebrandt and M. Tanaka, *J. Phys. Chem. B* **105**, 4270 (2001).

[7] J. P. Folkers, C. B. Gorman, P. E. Laibinis, S. Buchholz, and G. M. Whitesides, *Langmuir* **11**, 813 (1995).

[8] C. Yan, M. Zharnikov, A. Golzhauser, and M. Grunze, *Langmuir* **16**, 6208 (2000).

[9] J. Duchet, B. Chaber, J. P. Chapel, J. F. Gérard, J. M. Chovelon, and N. Jaffrezic-Renault, *Langmuir* **13**, 2271 (1997).

[10] B. C. Bunker, R. W. Carpick, R. A. Assink, M. L. Thomas, M. G. Hankins, J. A. Voigt, D. Sipola, M. P. de Boer, and G. L. Gulley, *Langmuir* **16**, 7742 (2000).

[11] H. Sugimura, K. Ushiyama, A. Hozumi, and O. Takai, *Langmuir* **16**, 885 (2000).

[12] T. M. Mayer, M. P. de Boer, N. D. Shinn, P. J. Clews, and M. T. A., *J. Vac. Sci. Technol., B* **18**, 2433 (2000).

[13] P. Fontaine, M. Goldmann, and F. Rondelez, *Langmuir* **15**, 1348 (1999).

[14] K. Kojio, A. Takahara, and T. Kajiyama, *Langmuir* **16**, 9314 (2000).

[15] S. R. Carino, H. Tostmann, R. S. Underhill, J. Logan, G. Weerasekera, J. Culp, M. Davidson, and R. S. Duran, *J. Am. Chem. Soc.* **123**, 767 (2001).

[16] J. D. Le Grange, J. L. Markham, and C. R. Kurkjian, *Langmuir* **9**, 1749 (1993).

[17] A. Ulman, *Chem. Rev.* **96**, 1533 (1996).

[18] M. Mrksich and G. M. Whitesides, *Annu. Rev. Biophys. Biomol. Struct.* **25**, 55 (1996).

[19] T. Wink, S. J. van Zuilen, A. Bult, and W. P. van Bennekom, *The Analyst* **122**, 43R (1997).

[20] I. Campbell, J. D. Kress, R. L. Martin, D. L. Smith, N. N. Barashkov, and J. P. Ferraris, *Appl. Phys. Lett.* **71**, 3528 (1997).

[21] J. H. Fendler, *Chem. Mater.* **13**, 3196 (2001).

[22] M. W. Tsao, C. L. Hoffmann, J. F. Rabolt, H. E. Johnson, D. G. Castner, C. Erdelen, and H. Ringsdorf, *Langmuir* **13**, 4317 (1997).

[23] S. R. Wasserman, Y. T. Tao, and G. M. Whitesides, *Langmuir* **5**, 1074 (1989).

[24] T. P. Sullivan and W. T. S. Huck, *Eur. J. Org. Chem.* , 17 (2003).

[25] Y. N. Xia and G. M. Whitesides, *Angew. Chem., Int. Ed.* **37**, 551 (1998).

[26] Y. Xia, X.-M. Zhao, and G. M. Whitesides, *Microelectron. Eng.* **32**, 255 (1996).

[27] N. B. Larsen, H. Biebuyck, E. Delamarche, and B. Michel, *J. Am. Chem. Soc.* **119**, 3017 (1997).

[28] H.-W. Li, B. Muir, G. Fichet, and W. Huck, *Langmuir* **19**, 1963 (2003).

[29] Y. Xia and G. M. Whitesides, *Langmuir* **13**, 2059 (1997).

[30] A. Rudin, *The elements of polymer science and engineering, Second Edition*, Academic Press, San Diego, 1999.

[31] T. Ando, M. Kato, M. Kamigaito, and M. Sawamoto, *Macromolecules* **29**, 1070 (1996).

[32] B. Zhao and W. J. Brittain, *Prog. Polym. Sci.* **25**, 677 (2000).

[33] K. Matyjaszewski, *Curr. Org. Chem.* **6**, 67 (2002).

[34] A. Goto and T. Fukuda, *Prog. Polym. Sci.* **29**, 329 (2004).

[35] I. Luzinov, D. Julthongpiput, H. Malz, J. Pionteck, and V. V. Tsukruk, *Macromolecules* **33**, 1043 (2000).

[36] M. LeMieux, D. Usov, S. Minko, M. Stamm, H. Shulha, and V. V. Tsukruk, *Macromolecules* **36**, 7244 (2003).

[37] M. C. LeMieux, D. Julthongpiput, K. N. Bergman, P. D. Cuong, H. S. Ahn, Y. H. Lin, and V. V. Tsukruk, *Langmuir* **20**, 10046 (2004).

[38] S. Yamamoto, M. Ejaz, Y. Tsujii, and T. Fukuda, *Macromolecules* **33**, 5608 (2000).

[39] P. G. DeGennes, *Macromolecules* **13**, 1069 (1980).

[40] M. Husemann, D. Mecerreyes, C. Hawker, J. Hedrick, R. Shah, and N. Abbott, *Angew. Chem., Int. Ed.* **38**, 647 (1999).

[41] R. R. Shah, D. Merreceyes, M. Husemann, I. Rees, N. L. Abbott, C. J. Hawker, and J. L. Hedrick, *Macromolecules* **33**, 597 (2000).

[42] Y. Harada, G. S. Girolami, and R. G. Nuzzo, *Langmuir* **19**, 5104 (2003).

[43] S. Edmondson and W. T. S. Huck, *Adv. Mater.* **16**, 1327 (2004).

[44] S. Edmondson, K. Frieda, J. E. Comrie, P. R. Onck, and W. T. S. Huck, *Adv. Mater.* **18**, 724 (2006).

[45] Y. D. Gu, F. Nederberg, R. Kånge, R. R. Shah, C. J. Hawker, M. Möller, J. L. Hedrick, and N. L. Abbott, *ChemPhysChem* **3**, 448 (2002).

[46] M. D. Miller, G. L. Baker, and M. L. Bruening, *J. Chromatogr. A* **1044**, 323 (2004).

[47] O. Prucker and J. Rühe, *Macromolecules* **31**, 592 (1998).

[48] O. Prucker and J. Rühe, *Macromolecules* **31**, 602 (1998).

[49] M. Husemann, E. E. Malmström, M. McNamara, M. Mate, D. Mecerreyes, D. G. Benoit, J. L. Hedrick, P. Mansky, E. Huang, T. P. Russell, and C. J. Hawker, *Macromolecules* **32**, 1424 (1999).

[50] D. M. Jones, A. A. Brown, and W. T. S. Huck, *Langmuir* **18**, 1265 (2002).

[51] K. L. Mulfort, J. Ryu, and Q. Y. Zhou, *Polymer* **44**, 3185 (2003).

[52] P. J. Hamelinck and W. T. S. Huck, *J. Mater. Chem.* **15**, 381 (2005).

[53] M. Ejaz, S. Yamamoto, K. Ohno, Y. Tsujii, and T. Fukuda, *Macromolecules* **31**, 5934 (1998).

[54] B. Peng, D. Johannsmann, and J. Rühe, *Macromolecules* **32**, 6759 (1999).

[55] K. Matyjaszewski, P. J. Miller, N. Shukla, B. Immaraporn, A. Gelman, B. B. Luokala, T. M. Siclovan, G. Kickelbick, T. Vallant, H. Hoffmann, and T. Pakula, *Macromolecules* **32**, 8716 (1999).

[56] W. X. Huang, G. L. Baker, and M. L. Bruening, *Angew. Chem., Int. Ed.* **40**, 1510 (2001).

[57] S. Yamamoto, Y. Tsujii, and T. Fukuda, *Macromolecules* **35**, 6077 (2002).

[58] G. L. Whiting, H. J. Snaith, S. Khodabakhsh, J. W. Andreasen, D. Breiby, M. M. Nielsen, N. C. Greenham, P. H. Friend, and W. T. S. Huck, *Nano Lett.* **6**, 573 (2006).

[59] T. Wu, K. Efimenko, P. Vlček, V. Šubr, and J. Genzer, *Macromolecules* **36**, 2448 (2003).

[60] S. Roux and S. Demoustier-Champagne, *J. Polym. Sci., Part A: Polym. Chem.* **41**, 1347 (2003).

[61] S. Edmondson, V. L. Osborne, and W. T. S. Huck, *Chem. Soc. Rev.* **33**, 14 (2004).

[62] C. F. Sun, F. Zhou, L. Shi, B. Yu, P. Gao, J. Y. Zhang, and W. M. Liu, *Appl. Surf. Sci.* **253**, 1729 (2006).

[63] Y. Ito and Y. Park, *Polym. Adv. Technol.* **11**, 136 (2000).

[64] L. Sun, G. Baker, and M. Bruening, *Macromolecules* **38**, 2307 (2005).

[65] C. D. H. de las Heras Alarcón, T. Farhan, V. L. Osborne, W. T. S. Huck, and C. Alexander, *J. Mater. Chem.* **15**, 2089 (2005).

[66] A. A. Brown, N. S. Khan, L. Steinbock, and W. T. S. Huck, *Eur. Polym. J.* **41**, 1757 (2005).

[67] I. M. Rutenberg, O. A. Scherman, R. H. Grubbs, W. R. Jiang, E. Garfunkel, and Z. Bao, *J. Am. Chem. Soc.* **126**, 4062 (2004).

[68] W. J. Brittain, S. G. Boyes, A. M. Granville, M. Baum, B. K. Mirous, B. Akgun, B. Zhao, C. Blickle, and M. D. Foster, *Adv. Polym. Sci.* **198**, 125 (2006).

[69] P. Uhlmann, N. Houbenov, N. Brenner, K. Grundke, S. Burkert, and M. Stamm, *Langmuir* **23**, 57 (2007).

[70] O. Azzaroni, A. A. Brown, and W. T. S. Huck, *Adv. Mater.* **19**, 151 (2007).

[71] J. Pyun and K. Matyjaszewski, *Chem. Mater.* **13**, 3436 (2001).

[72] K. Matyjaszewski, T. E. Patten, and J. H. Xia, *J. Am. Chem. Soc.* **119**, 674 (1997).

[73] T. Patten and K. Matyjaszewski, *Adv. Mater.* **10**, 901 (1998).

[74] J.-S. Wang and K. Matyjaszewski, *J. Am. Chem. Soc.* **117**, 5614 (1995).

[75] J.-S. Wang and K. Mayjaszewski, *Macromolecules* **28**, 7901 (1995).

[76] T. E. Patten, J. Xia, T. Abernathy, and K. Matyjaszewski, *Science* **272**, 866 (1996).

[77] K. Matyjaszewski, S. M. Jo, H.-j. Paik, and D. A. Shipp, *Macromolecules* **32**, 6431 (1999).

[78] X. Wang, F. Malet, S. Armes, D. Haddleton, and S. Perrier, *Macromolecules* **34**, 162 (2001).

[79] V. Percec, A. V. Popov, E. Ramirez-Castillo, and O. Weichold, *J. Polym. Sci., Part A: Polym. Chem.* **41**, 3283 (2003).

[80] A. Studer, *Chem. Soc. Rev.* **33**, 267 (2004).

[81] C. J. Hawker, A. W. Bosman, and E. Harth, *Chem. Rev.* **101**, 3661 (2001).

[82] D. G. Benoit, V. Chaplinski, R. Braslau, and C. J. Hawker, *J. Am. Chem. Soc.* **121**, 3904 (1999).

[83] F. J. Xu, Y. Song, Z. P. Cheng, X. L. Zhu, C. X. Zhu, E. T. Kang, and K. G. Neoh, *Macromolecules* **38**, 6254 (2005).

[84] C. Devaux, J. P. Chapel, E. Beyou, and P. Chaumont, *Eur. Phys. J. E* **7**, 345 (2002).

[85] J. Parvole, J. P. Montfort, and L. Billon, *Macromol. Chem. Phys.* **205**, 1369 (2004).

[86] R. A. Sedjo, B. K. Mirous, and W. J. Brittain, *Macromolecules* **33**, 1492 (2000).

[87] O. Prucker and J. Rühe, *Langmuir* **14**, 6893 (1998).

[88] R. Konradi and J. Rühe, *Langmuir* **22**, 8571 (2006).

[89] T. Trnka and R. Grubbs, *Acc. Chem. Res.* **34**, 18 (2001).

[90] C. B. Gorman, E. J. Ginsburg, and R. H. Grubbs, *J. Am. Chem. Soc.* **115**, 1397 (1993).

[91] W. J. Feast, J. Tsibouklis, K. L. Pouwer, L. Groenendaal, and E. W. Meijer, *Polymer* **37**, 5017 (1996).

[92] R. T. A. Mayadunne, E. Rizzardo, J. Chiefari, Y. K. Chong, G. Moad, and S. H. Thang, *Macromolecules* **32**, 6977 (1999).

[93] M. Baum and W. J. Brittain, *Macromolecules* **35**, 610 (2002).

[94] R. Jordan, A. Ulman, J. Kang, M. Rafailovich, and J. Sokolov, *J. Am. Chem. Soc.* **121**, 1016 (1999).

[95] W. Jakubowski, K. Min, and K. Matyjaszewski, *Macromolecules* **39**, 39 (2006).

[96] N. V. Tsarevsky, W. A. Braunecker, and K. Matyjaszewski, *J. Organomet. Chem.* **692**, 3212 (2007).

[97] J. Pyun, T. Kowalewski, and K. Matyjaszewski, *Macromol. Rapid Commun.* **24**, 1043 (2003).

[98] J. B. Kim, W. X. Huang, M. D. Miller, G. L. Baker, and M. L. Bruening, *J. Polym. Sci., Part A: Polym. Chem.* **41**, 386 (2003).

[99] S. Yamamoto, M. Ejaz, Y. Tsujii, M. Matsumoto, and T. Fukuda, *Macromolecules* **33**, 5602 (2000).

[100] D. M. Jones and W. T. S. Huck, *Adv. Mater.* **13**, 1256 (2001).

[101] H. Shirakawa, E. Louis, A. MacDiarmid, C. K. Chiang, and A. Heeger, *Physical Review Letters* **39**, 1098 (1977).

[102] A. G. MacDiarmid, *Angew. Chem., Int. Ed.* **40**, 2581 (2001).

[103] S. R. Forrest, *Nature* **428**, 911 (2004).

[104] A. Kraft, A. C. Grimsdale, and A. B. Holmes, *Angew. Chem., Int. Ed.* **37**, 402 (1998).

[105] R. H. Friend, R. W. Gymer, A. B. Holmes, J. H. Burroughes, R. N. Marks, C. Taliani, D. D. C. Bradley, D. A. Dos Santos, J. L. Bredas, M. Logdlund, and W. R. Salaneck, *Nature* **397**, 121 (1999).

[106] U. Mitschke and P. Bäuerle, *J. Mater. Chem.* **10**, 1471 (2000).

[107] L.-L. Chua, J. Zaumseil, J.-F. Chang, E.-W. Ou, P. K.-H. Ho, H. Sirringhaus, and R. H. Friend, *Nature* **434**, 194 (2005).

[108] E. J. Meijer, D. De Leeuw, S. Setayesh, E. Van Veenendaal, B.-H. Huisman, P. W. M. Blom, J. C. Hummelen, U. Scherf, and T. M. Klapwijk, *Nat. Mater.* **2**, 678 (2003).

[109] H. Sirringhaus, *Nat. Mater.* **2**, 641 (2003).

[110] J. H. Burroughes, C. A. Jones, and R. H. Friend, *Nature* **335**, 137 (1988).

[111] F. Garnier, R. Hajlaoui, A. Yassar, and P. Srivastava, *Science* **265**, 1684 (1994).

[112] H. Sirringhaus, T. Kawase, R. H. Friend, T. Shimoda, M. Inbasekaran, W. Wu, and E. P. Woo, *Science* **290**, 2123 (2000).

[113] H. Sirringhaus, N. Tessler, and R. H. Friend, *Science* **280**, 1741 (1998).

[114] I. McCulloch, M. Heeney, C. Bailey, K. Genevicius, I. Macdonald, M. Shkunov, D. Sparrowe, S. Tierney, R. Wagner, W. Zhang, M. Chabinyc, R. Kline, M. M.D., and M. Toney, *Nat. Mater.* **5**, 328 (2006).

[115] J. R. Kline, D. M. DeLongchamp, D. A. Fischer, E. K. Lin, M. Heeney, I. McCulloch, and M. F. Toney, *Appl. Phys. Lett.* **90**, 062117 (2007).

[116] H. Sirringhaus, P. J. Brown, R. H. Friend, M. M. Nielsen, K. Bechgaard, B. M. W. Langeveld-Voss, A. J. H. Spiering, R. A. J. Janssen, E. W. Meijer, P. Herwig, and D. M. de Leeuw, *Nature* **401**, 685 (1999).

[117] Y. Wu, P. Liu, B. Ong, T. Srikumar, N. Zhao, G. Botton, and S. Zhu, *Appl. Phys. Lett.* **86**, 142102 (2005).

[118] H. Sirringhaus, R. J. Wilson, R. H. Friend, M. Inbasekaran, W. Wu, E. P. Woo, M. Grell, and D. D. C. Bradley, *Appl. Phys. Lett.* **77**, 406 (2000).

[119] X. Z. Wang, D. J. Zhou, T. Rayment, and C. Abell, *Chem. Commun.* , 474 (2003).

[120] D. Kim, Y. Park, Y. Jang, H. Yang, Y. Kim, J. Han, D. Moon, S. Park, T. Chang, C. Chang, M. Joo, C. Ryu, and K. Cho, *Adv. Funct. Mater.* **15**, 77 (2005).

[121] M. Funahashi and J. Hanna, *Appl. Phys. Lett.* **73**, 3733 (1998).

[122] N. Yoshimoto and J. Hanna, *J. Mater. Chem.* **13**, 1004 (2003).

[123] I. McCulloch, W. M. Zhang, M. Heeney, C. Bailey, M. Giles, D. Graham, M. Shkunov, D. Sparrowe, and S. Tierney, *J. Mater. Chem.* **13**, 2436 (2003).

[124] C. D. Simpson, J. S. Wu, M. D. Watson, and K. Müllen, *J. Mater. Chem.* **14**, 494 (2004).

[125] C. Jarrett, R. H. Friend, A. Brown, and D. De Leeuw, *J. Appl. Phys.* **77**, 6289 (1995).

[126] J. Blochwitz, M. Pfeiffer, T. Fritz, and K. Leo, *Appl. Phys. Lett.* **73**, 729 (1998).

[127] J. Blochwitz, T. Fritz, M. Pfeiffer, K. Leo, D. Alloway, P. Lee, and N. Armstrong, *Organic Electronics* **2**, 97 (2001).

[128] X. Zhou, M. Pfeiffer, J. Blochwitz, A. Werner, A. Nollau, T. Fritz, and K. Leo, *Appl. Phys. Lett.* **78**, 410 (2001).

[129] W. Y. Gao and A. Kahn, *Appl. Phys. Lett.* **79**, 4040 (2001).

[130] W. Y. Gao and A. Kahn, *Appl. Phys. Lett.* **82**, 4815 (2003).

[131] T. Q. Nguyen and B. J. Schwartz, *J. Chem. Phys.* **116**, 8198 (2002).

[132] R. J. Kline, M. D. McGehee, E. N. Kadnikova, J. S. Liu, and J. M. J. Fréchet, *Adv. Mater.* **15**, 1519 (2003).

[133] R. J. Kline and M. D. McGehee, *Polymer Reviews* **46**, 27 (2006).

[134] R. J. Kline, M. D. McGehee, and M. F. Toney, *Nature Materials* **5**, 222 (2006).

[135] N. Stutzmann, R. H. Friend, and H. Sirringhaus, *Science* **299**, 1881 (2003).

[136] B. Kazan, *Science* **208**, 927 (1980).

[137] D. M. Chapin, C. Fuller, and G. Pearson, *J. Appl. Phys.* **25**, 676 (1954).

[138] G. Dellepiane, C. Cuniberti, D. Comoretto, G. Musso, G. Figari, A. Piaggi, and A. Borghesi, *Phys. Rev. B* **48**, 7850 (1993).

[139] G. Yu, J. Gao, J. C. Hummelen, F. Wudl, and A. J. Heeger, *Science* **270**, 1789 (1995).

[140] C. Winder and N. Sariciftci, *J. Mater. Chem.* **14**, 1077 (2004).

[141] M. M. Wienk, M. G. Turbies, M. P. Struijk, M. Fonrodona, and R. A. J. Janssen, *Appl. Phys. Lett.* **88**, 153511 (2006).

[142] J. Van Duren, X. Yang, J. Loos, C. Bulle-Lieuwma, A. Sieval, and R. Janssen, *Adv. Funct. Mater.* **14**, 425 (2004).

[143] H. Hoppe and N. S. Sariciftci, *J. Mater. Chem.* **16**, 45 (2006).

[144] A. Marcos Ramos, M. T. Rispens, J. K. J. Van Duren, J. C. Hummelen, and R. A. J. Janssen, *J. Am. Chem. Soc.* **123**, 6714 (2001).

[145] A. Cravino and N. Sariciftci, *J. Mater. Chem.* **12**, 1931 (2002).

[146] L. Schmidt-Mende, A. Fechtenkötter, K. Müllen, E. Moons, R. H. Friend, and J. D. MacKenzie, *Science* **293**, 1119 (2001).

[147] L. Schmidt-Mende, A. Fechtenkötter, K. Müllen, R. H. Friend, and J. D. MacKenzie, *Physica E* **14**, 263 (2002).

[148] P. Samori, X. M. Yin, N. Tchebotareva, Z. H. Wang, T. Pakula, F. Jackel, M. D. Watson, A. Venturini, K. Mullen, and J. P. Rabe, *J. Am. Chem. Soc.* **126**, 3567 (2004).

[149] S. E. Shaheen, C. J. Brabec, N. S. Sariciftci, F. Padinger, T. Fromherz, and J. C. Hummelen, *Appl. Phys. Lett.* **78**, 841 (2001).

[150] A. J. Breeze, A. Salomon, D. S. Ginley, B. A. Gregg, H. Tillmann, and H.-H. Hörhold, *Appl. Phys. Lett.* **81**, 3085 (2002).

[151] E. E. Neuteboom, S. C. J. Meskers, P. A. van Hal, J. K. J. van Duren, E. W. Meijer, R. A. J. Janssen, H. Dupin, G. Pourtois, J. Corni, R. Lazzaroni, J.-L. Brédas, and D. Beljonne, *Journal of the American Chemical Society* **125**, 8625 (2003).

[152] K. M. Coakley and M. D. McGehee, *Chem. Mater.* **16**, 4533 (2004).

[153] H. Kawamoto, *Proc. IEEE* **90**, 460 (2002).

[154] A. M. van de Craats, J. M. Warman, A. Fechtenkötter, J. D. Brand, M. A. Harbison, and K. Müllen, *Adv. Mater.* **11**, 1469 (1999).

[155] M. Grell and D. D. C. Bradley, *Adv. Mater.* **11**, 895 (1999).

Part I

Surface-initiated Polymers for Device Applications

Chapter 2

Homeotropic Alignment on Surface-initiated Liquid Crystalline Polymer Brushes *

Synopsis: With the development of new types of liquid crystal displays and the use of liquid crystals as organic semiconductors, homeotropic alignment layers have become more and more important. Liquid crystalline polymer brushes have been suggested as an alignment layer and are expected to have more interaction with the liquid crystal phase than other homeotropic alignment layers. In this chapter the synthesis of side chain liquid crystalline polymer brushes by surface-initiated atom transfer radical polymerization is reported. The brushes with thicknesses in the nanometer regime are succesfully used as homeotropic alignment layers.

2.1 Introduction

2.1.1 Liquid crystals and alignment

A liquid crystal (LC) is generally defined as an intermediate phase (a mesophase) between solid and liquid which has liquid-like properties in at least one direction, and possesses a degree of anisotropy, which is characteristic of some

*part of this work has been published: P.J. HAMELINCK, W.T.S. HUCK, *J. Mater. Chem.* **15**, 381 (2005)

sort of order.[1] Therefore all molecules that make up LC are anisotropic, either rod-like (two or more aromatic rings connected by rigid bonds) or disc-like (flat polycyclic aromatic compounds). An LC material goes through different phases when heated up from the crystalline phase, the most common are the smectic phase, in which the molecules are organized in layers, and nematic, in which the molecules only have their axis aligned along a director (common orientation of the axis of the molecules). Above a certain temperature, the clearing point, all order in the material dissappears and the material is in the isotropic phase.

2.1.2 Alignment

When no alignment layer is used, liquid crystalline materials form small separate domains with alignment, but without a common director. For applications, however, where LC materials are used because of their order, long range homogeneous alignment is required. This can be induced by using alignment layers. There are generally two forms of alignment: homeotropic (perpendicular to the surface) and planar or azimuthal (parallel to the surface). There are several techniques available such as rubbing of a polymer layer,[2–4] photoalignment of a layer containing azo dyes,[5,6] friction transfer[7] and oblique evaporation[8,9] to realize this alignment.

Alignment has been the key topic of research in the field of liquid crystal displays (LCDs, see for instance the review by Kawamoto[10]) but since liquid crystalline materials are more and more used as semiconducting materials, alignment has become an important part of the research in organic electronics as well.[11–15] Alignment of molecules on surfaces is one of the most important ways to improve device performance.[16] For display applications generally a planar alignment of molecules is needed. These alignment layers can be obtained by rubbing or photoalignment.

More recent display technologies however, like reverse mode LCD, require homeotropic alignment and tilted alignment.[17,18] In electronic devices with a liquid crystalline active phase, homeotropic alignment has been used for fabricating field effect transistors (FETs).[19–21] Homeotropic alignment generally occurs when the anchoring energy is low;[22] these alignment layers

are normally hydrophobic in nature, with the aliphatic tails of the LC molecules driven to the interface.

2.1.3 Alignment on monolayers

Alignment of LC on Langmuir Blodgett monolayers

Langmuir-Blodgett (LB) monolayers are organized molecular films deposited on solid substrates by transferring a monolayer at the air-water interface to a solid support. LB is a non-contact technique and both homeotropic and planar alignment is accessible with this technique. The field was recently reviewed by Lu *et al.*[23] Planar alignment occurs usually on LB materials that orient parallel to the dipping direction. Homeotropic alignment occurs on LB films of materials with a large dipole moment, like surfactants. The molecules of these materials orient perpendicular to the surface and have interaction with the aliphatic chains on the LC molecules.

By mixing a homeotropically directing LB material with a planar directing LB material, a pre-tilt angle can be obtained which varies with composition of the LB-layer. The anchoring energy is also highly dependant of the composition of the LB layer, which could be of importance for *e.g.* switching of a display device.[24]

Collins *et al.* include liquid crystals while depositing a LB monolayer of arachidic acid and show that the homeotropic alignment of these monolayer moieties is succesfully transferred into the bulk LC material.[25]

Alignment of LC on Self-Assembled Monolayers

Abbott and co-workers report alignment on SAMs on obliquely deposited gold.[8,9] Gold which is deposited obliquely under a fixed angle has enough anisotropy to align LC materials. In this method, the gold is deposited under an angle of 50° by electron beam evaporation followed by chemisorption of an alkanethiol to form a self-assembled monolayer (SAM). The orientation of liquid crystalline material injected into cells, with a top and bottom plate coated with a SAM, is nematic and the director is dependant on the direction of the deposition and the number of repeat units in the alkanethiol used for the formation of the SAM.[26] When alkanethiols with an even number of carbon atoms are used, the nematic LC has its director parallel to the direction of the

deposition of the gold. When the number of carbon atoms is odd, however, the LC is still planar, but aligned perpendicular to the direction of the deposition of the gold. When a mixture of alkanethiols with odd and even numbers of repeating units are used, the director of the LC alignment is perpendicular to the substrate.

Reznikov *et al.* found in experiments on quartz substrates that when these substrates are immersed in a dilute solution of 4'-pentyl-4-biphenyl-carbonitrile (pentyl cyano-bisphenyl, 5CB) a self-assembled monolayer is formed, which is oriented perpendicular to the substrate, but that when these substrates are used for LC cells, the bulk alignment in the cell is planar with respect to the substrate.[27] This alignment is explained by the alignment of dimers of 5CB (without net dipole) on the bed of hydrophobic chains at the bulk/SAM interface. When compared with the mixed monolayers in the study of Collins, apparently interactions between the liquid crystals at the surface and the bulk liquid crystals are needed to result in a homeotropic alignment. These interactions are not available in the closely packed monolayer of 5CB, but are provided in the mixed monolayer of arachidic acid and LC.

2.1.4 Alignment on polymer brushes

Surface-initiated polymers are a class of polymers known to possess a high degree of order.[28] A theoretical study by Halperin and Williams in 1994 suggests that liquid-crystalline polymer (LCP) brushes can be used as alignment layers.[29] Polymer brushes are expected to have more interaction with the liquid crystal phase than other alignment layers, and the alignment is assumed to be dependent on grafting density. Dense main chain LC polymers would result in homeotropic alignment because the polymer chains are more stretched. When the grafting density is low, planar alignment is expected. These polymers would thus provide a means of tuning both the pretilt angle and the surface anchoring energy via grafting density. Monte Carlo simulations were consistent with this theory and show that these predictions also hold for short chains of four monomers.[30]

Peng *et al.* synthesize and study side chain liquid crystalline surface-initiated polymers by free radical polymerization for use as an alignment

layer.[31,32] Because of the orientation of side chains with respect to the main chain, the brushes are expected to induce planar alignment, so that the combination of brushes and *e.g.* substrate would allow for tuning of the pre-tilt angle. Growing polymers from untreated surfaces however does not result in a preferred alignment.[31] Polymers grown from rubbed surfaces result in an anisotropy in the 230 nm thick brushes observable by polarising microscopy.[32] Liquid crystalline material shows planar alignment in the rubbing direction when injected into a capillary cell of these substrates, the same alignment as on pre-treated substrates without brush layer.

In this chapter the synthesis of side chain liquid crystalline polymer brushes from anisotropic substrates and their application as a homeotropic alignment layer is discussed.

2.2 Synthesis of side chain liquid crystalline polymer brushes

For the growth of LC polymer brushes, the acrylate functionalized liquid crystal 4-(4-propylphenyl)ethynylphenyl-4-5-(acryloyloxy)pentyloxy-benzoate (reactive mesogen RM488) was used. Surface-initiated polymers were grown on

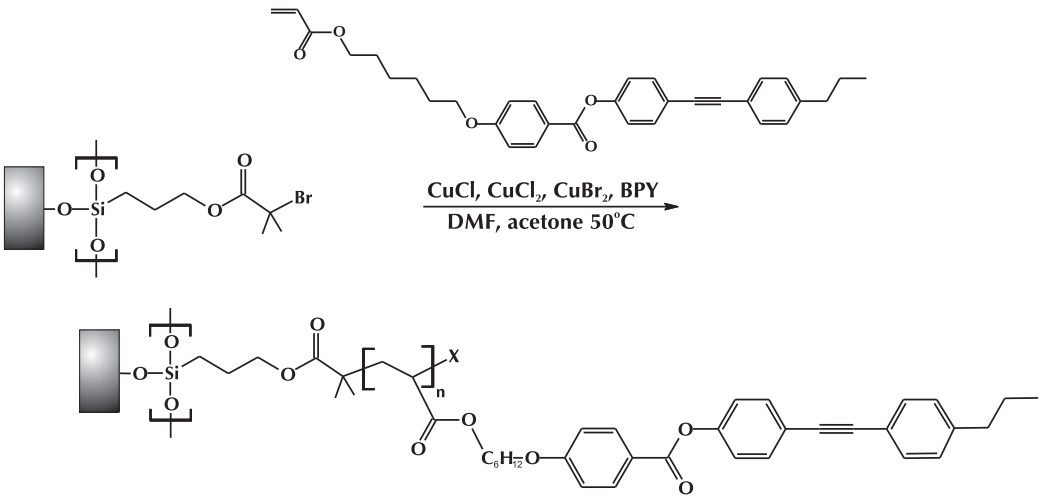

Scheme 2.1

Table 2.1: Reaction conditions used in optimization of the surface-initiated polymerization of RM488.

Conditions			Reaction time	Brush thickness (nm)
Toluene 90 °C (1 g monomer/2 ml)				
$CuBr : CuBr_2 : PMDETA : monomer$	=	1 : 0.3 : 5 : 300	3 days	5
$CuBr : CuBr_2 : PMDETA : monomer$	=	1 : 0.3 : 5 : 500	3 days	5
$CuBr : CuBr_2 : PMDETA : monomer$	=	1 : 0.3 : 5 : 700	3 days	5
Toluene / DMF 1:1 (v/v) 100 °C (1g monomer / 2ml)				
$CuCl : CuCl_2 : CuBr_2 : BPY : monomer$	=	1 : 0.2 : 0.3 : 5 : 300	23 h	6
$CuCl : CuCl_2 : CuBr_2 : BPY : monomer$	=	1 : 0.4 : 0.3 : 5 : 300	21 h	6
$CuCl : CuCl_2 : CuBr_2 : BPY : monomer$	=	1 : 0 : 0.3 : 5 : 3000	21 h	7
$CuCl : CuCl_2 : CuBr_2 : BPY : monomer$	=	1 : 0.2 : 0.3 : 5 : 3000	21 h	7
$CuCl : CuCl_2 : CuBr_2 : BPY : monomer$	=	1 : 0.4 : 0.3 : 5 : 3000	21 h	6
DMF				
1 g monomer / 3 ml – 90 °C				
$CuBr : CuBr_2 : PMDETA : monomer$	=	1 : 0.3 : 5 : 200	23 h	1
$CuBr : CuBr_2 : PMDETA : monomer$	=	1 : 0.3 : 5 : 300	23 h	7
$CuBr : CuBr_2 : PMDETA : monomer$	=	1 : 0.3 : 5 : 2000	23 h	9
1 g monomer / 2 ml – 90 °C				
$CuBr : CuBr_2 : PMDETA : monomer$	=	1 : 0.3 : 5 : 300	3 days	10
$CuBr : CuBr_2 : PMDETA : monomer$	=	1 : 0.3 : 5 : 500	3 days	9
$CuBr : CuBr_2 : PMDETA : monomer$	=	1 : 0.3 : 5 : 700	3 days	10
1 g monomer / 1 ml				
90 °C				
$CuCl : CuBr_2 : BPY : monomer$	=	1 : 0.3 : 5 : 300	23 h	11
50 °C				
$CuCl : CuCl_2 : CuBr_2 : BPY : monomer$	=	1 : 0.2 : 0.3 : 5 : 300	3 days	12
$CuCl : CuCl_2 : CuBr_2 : BPY : monomer$	=	1 : 0.2 : 0.3 : 5 : 1000	3 days	15
Acetone 50 °C (1 g monomer / 3 ml)				
$CuCl : CuCl_2 : CuBr_2 : BPY : monomer$	=	1 : 0.2 : 0.3 : 5 : 300	3 days	12
$CuCl : CuCl_2 : CuBr_2 : BPY : monomer$	=	1 : 0.2 : 0.3 : 5 : 1000	3 days	14
DMF / Acetone 2:1 (v/v) 50 °C				
1 g monomer / 2 ml				
$CuCl : CuBr_2 : BPY : monomer$	=	1 : 0.5 : 5 : 3000	25 h	5
1 g monomer / 1.5 ml				
$CuCl : CuCl_2 : CuBr_2 : BPY : monomer$	=	1 : 0.7 : 0.3 : 5 : 1000	24 h	20
DMF / Acetone 1:1 (v/v) 50°C				
1g monomer / 4 ml				
$CuCl : CuBr_2 : BPY : monomer$	=	1 : 0.5 : 5 : 300	23 h	8
$CuCl : CuBr_2 : BPY : monomer$	=	1 : 0.5 : 5 : 600	23 h	8
$CuCl : CuBr_2 : BPY : monomer$	=	1 : 0.5 : 5 : 1000	23 h	8
$CuCl : CuBr_2 : BPY : monomer$	=	1 : 0.5 : 5 : 1500	23 h	9
1 g monomer / 2 ml				
$CuCl : CuCl_2 : CuBr_2 : BPY : monomer$	=	1 : 0.7 : 0.3 : 5 : 1000	24 h	20

glass and silicon, which resulted in polymer brushes with liquid crystalline side chains (see scheme 2.1). Different reaction conditions were investigated by varying the copper(I) halide and copper(II) halide concentrations, with bromide and chloride used as halides, and by varying the temperature and solvents. An overview of reaction conditions and resulting brush thicknesses can be found in table 2.1.

The reaction conditions used eventually were 50 °C, copper(I) chloride as the catalyst, 2,2'-bipyridyl as the ligand, copper(II) bromide and copper(II) chloride added for more living character in a molar ratio of 1:0.7:0.3:5:1000 CuCl:$CuCl_2$:$CuBr_2$:BPY:RM488. By changing the halide from bromide to chloride the living character is enhanced as the C—Cl bond is stronger than the C—Br bond, thus favouring the dormant state. A mixed halide system, in which both chloride and bromide are present, was used to balance the advantages of fast brush growth with enhanced living character.[33]

The solvent mixture used was a 2:1 (v/v) DMF:acetone mixture at a concentration of 1 g monomer per 1.5 mL of this mixture. Although the solubility of the monomer in toluene is higher than in the DMF:acetone mixture, the use of the latter mixture results in thicker brushes. Faster brush-growth in solvents with higher dielectric constants is common for ATRP.[34]

The time-resolved growth of surface-initiated polymers grown from silicon is shown in figure 2.1 for different reaction conditions and the graph clearly shows the enhancement of the living character upon adding copper(II) halide and upon changing to a mixed halide system. Brush thicknesses of up to 20 nm are achieved in 24 hours following the procedure mentioned above. The film remains stable during intensive cleaning steps including two minutes rinsing in dichloromethane and toluene in an ultrasonic bath.

At temperatures higher than 60 °C polymer formation in the reaction solution is also observed, independent of solvent used (toluene or DMF). This is either a result of radical transfer from chains growing on the surface or from auto-initiation in the polymerization solution.

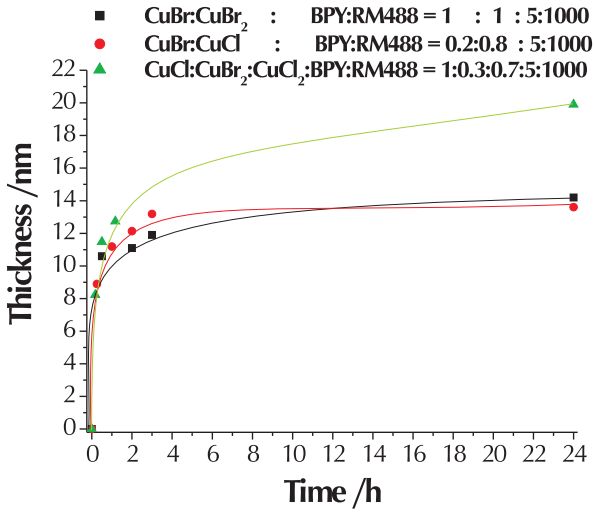

Figure 2.1: Time resolved surface-initiated polymerization of RM488 on silicon. The lines are given as a guide for the eye. The solvent was a DMF/acetone mixture in all three experiments.

2.2.1 Contact angles of water and 5CB

Contact angles of water and 5CB were measured on bare glass substrates, substrates coated with octadecyl trichlorosilane (ODTS) and substrate coated with polymer brushes of RM488 and are shown in table 2.2 and 2.3. As the contact angle of 5CB is strongly dependent on temperature,[35,36] care was taken to keep the temperature constant during measurement.

It is remarkable that even though the bare and ODTS coated substrates differ considerably in hydrophilicity, the affinity of 5CB to either substrate is similar. This is because 5CB has a hydrophilic cyano group at one end and a

Table 2.2: Advancing (θ_{aw}), static (θ_{sw}) and receding (θ_{rw}) contact angles of water on bare glass, ODTS coated glass and pRM488 coated glass at 25 °C.

	θ_{aw}	θ_{sw}	θ_{rw}
Glass	35	32	9
ODTS	91	107	79
RM488 Brush	82	74	54

Table 2.3: Advancing (θ_{a5CB}) and static (θ_{s5CB}) contact angles of the nematic liquid crystal 5CB on bare glass, ODTS coated glass and pRM488 coated glass at 25 °C.

	θ_{a5CB}	θ_{s5CB}
Glass	10	8
ODTS	12	12
RM488 Brush	0	0

hydrophobic alkyl chain at the other.

Polymer brushes of RM488 are slightly more hydrophilic than ODTS monolayers. When a drop of 5CB is syringed onto these substrates, the wetting is complete, in contrast to the wetting of the bare sample or the sample with an ODTS monolayer. This shows that there is enhanced interaction between the LC and the brush, which is expected to be the result of partial penetration of the LC into the brush layer and interactions of the molecules with the LC polymer side chains.

2.2.2 Clearing point of the polymer brush

There are various reports in which the glass transition point of polymer brushes is measured by temperature dependent ellipsometry.[37–39] This technique was used here to measure the clearing point of the LC polymer brush. The clearing point in a side chain liquid crystalline polymer is the point at which the LC interactions between the side chains are overcome by the thermal motion of the polymer coil. Above this point the polymer behaves as a normal (non-LC) polymer.

Using a hot stage, the temperature was varied in time and Δ and Ψ were measured (see figure 2.2). It can be seen that there is a sudden increase in both Δ and Ψ at 77.5 °C, which is associated with the clearing point of the polymer. This change is different from changes associated with glass transition points which are identified by a change in the slope of Ψ or the ellipsometric thickness *vs.* temperature.

The clearing point of the polymer formed in the bulk solution was also measured with polarized microscopy and was observed at 52 °C. The difference between clearing point in bulk polymer and in the brush may be

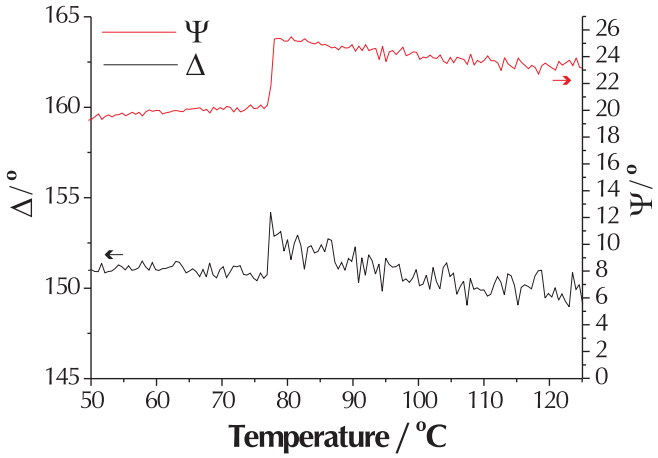

Figure 2.2: Δ and Ψ as a function of temperature in temperature dependent ellipsometry on polymer brushes of RM488.

explained by the higher density associated with brushes. Due to this higher density LC units are forced together even at elevated temperatures. Also the contribution of entropy in the 2D system in the case of polymer brushes is totally different to a 3D system in the case of bulk polymer, which will have a considerable impact on phase transitions.

2.3 Alignment of liquid crystals on surface-initiated polymers

Glass substrates with surface-initiated polymers were used to construct LC cells. Two substrates were glued together, separated by a spacer of

Scheme 2.2: Schematic structure of a capillary LC cell. The liquid crystal is injected in the space between the two substrates and spreads as a result of capillary forces.

approximately 10 μm (scheme 2.2). The nematic liquid crystal 5CB was injected in the capillary space between the substrates and alignment was studied with polarized light microscopy with the substrate between two crossed polarizers.

Samples with 5 nm and 8 nm thick brushes show homogeneous homeotropic alignment over the entire area of the cells (several cm^2, see figure 2.3 B). When studied between crossed polarizers, homeotropic alignment in a substrate can be identified in two different ways: as the axis of homeotropically aligned LC molecules is perpendicular to the substrate, rotation of the sample in the plane of the stage will not result in change in extinction (so the alignment is not planar), the transition to isotropic is still observed upon heating. Apart from that, a characteristic interference pattern – a Maltese cross – can be observed under illumination with convergent light in the homeotropic phase.

Alignment is not observed in LC cells of plain glass or in LC cells of initiator-coated glass substrates without a brush layer or with a PMMA brush layer (figure 2.3 A).

To study the influence of brush thickness on the alignment, LC cells with 20 nm thick brush samples were also fabricated. In these samples there are still large areas of homeotropic alignment, but interspersed with areas where the extinction changes upon rotation of the cells in the plane of the viewing stage (figure 2.3 C). In these areas the observed interference pattern is a tilted cross. This indicates that the alignment is somewhat between planar and homeotropic, *i.e.* tilted. No clear phase boundaries can be distinguished between the areas of homeotropic and tilted alignment.

As was shown in figure 2.1 (page 42), at the reaction time for 20 nm thick brushes, the reaction rate is no longer in the linear regime, which indicates the polymerization is not controlled and many chains have terminated. This results in higher conformational freedom of the chains at the surface which could explain the decreased alignment of the nematic phase.

In their theoretical study Halperin and Williams suggested that LC align homeotropically on densely grafted main chain LC polymers.[29] If it is assumed that side chain LC polymers would result in an alignment perpendicular to that on main chain LC polymers, alignment on side chain

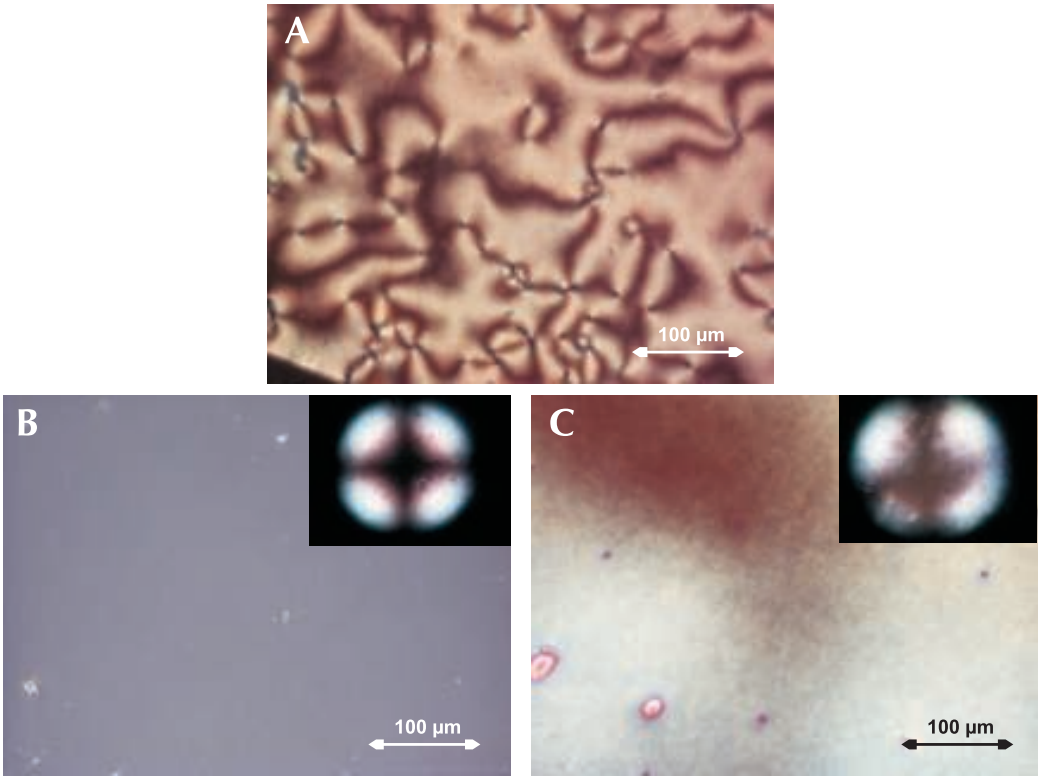

Figure 2.3: Optical micrographs of LC cells of substrates with polymer brush coatings, studied between crossed polarizers: A) No preferential alignment on 18 nm thick PMMA brushes (the observed texture is a Schlieren texture); B) Homeotropic alignment over large areas on 5 nm thick brushes of RM488; C) Alignment on 20 nm thick brushes of RM488 is homeotropic in some areas (top left corner) and tilted in others (rest of the micrograph) without clear phase bounderies. The insets in B and C show the interference pattern observed with convergent illumination.

liquid crystalline polymer brushes is expected to be planar. However in this study homeotropic alignment on brushes is observed. This difference can be explained by either rejecting the assumption that the bulky side chains have an orientation perpendicular to the main chain or by rejecting the idea that the brush backbones are predominantly perpendicular to the substrate.

The side chains could have another orientation because of steric interactions or because of solvation effects, when the LC molecules penetrate the brush layer. The polymer backbones in brushes are not completely stretched out but still have a certain amount of coiling dependent on the grafting density.[40,41] This coiling could be responsible for a homeotropic

orientation of the side chains, thus inducing homeotropic alignment in the liquid crystal layer. The effect of grafting density of the brushes on liquid crystal alignment was investigated. However, initial results indicate that even diluting the brushes by a factor of ten (using a mixed monolayer of initiator and propyl trichlorosilane in a 1:9 ratio) does not lead to an appreciable decrease in the ability to align the liquid crystalline layer on top. This does indeed suggest that disordered brushes with side chains perpendicular to the surface are responsible for the observed alignment.

A model study by Lange and Schmid suggests that LC molecules penetrate the brush and solvate it.[30] As a result LC interactions perpendicular to the substrate are preferred, as only that results in one director for all LC units. This means the alignment will be homeotropic. Their model is valid for short, stiff chains and they predict that if the chains get more conformational freedom, the alignment changes to a tilted alignment.

Peng *et al.* did not observe homeotropic alignment in their experimental studies.[31,32] There are, however, two important differences between their experiments and the experiments described here. Firstly much thicker brushes of over 200 nm were grown. Secondly, a different polymerization technique to the one described here was used, namely free radical polymerization. The latter results in higher polydispersities compared to the controlled radical polymerization we use. Higher polydispersities and longer polymer chains result in a higher conformational freedom of the chains and their side groups, especially at the brush/nematic interface. This could explain why homeotropic alignment is not observed in their experiments.

In the introduction to this chapter it was discussed that liquid crystalline interactions between the liquid crystals at the surface and the bulk liquid crystals are needed to result in homeotropic alignment. In the case of polymer brushes, penetration of LC molecules into the less dense top layer of the brush will provide these interactions.

2.3.1 Patterned alignment

Micro-contact printing (μCP) was used to deposit a patterned self-assembled monolayer of the initiator before growing brushes. Brushes were grown from

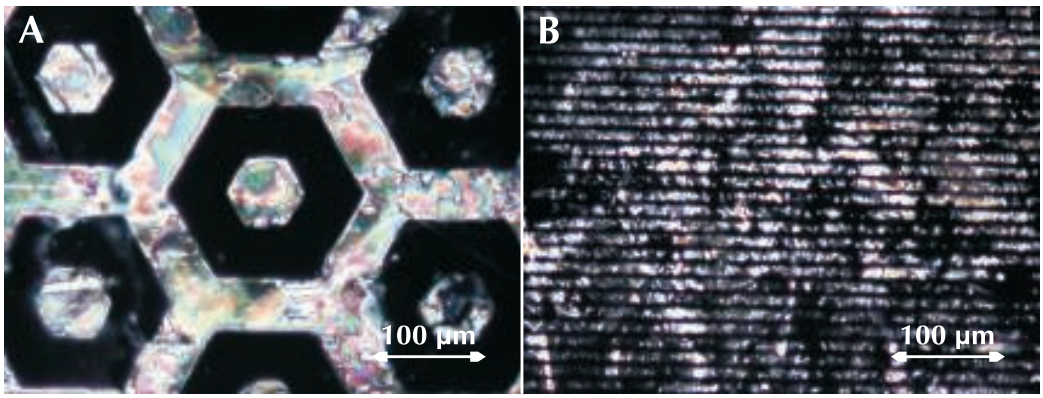

Figure 2.4: Patterned alignment on brushes grown from initiator immobilized by μCP. A) 200 μm wide hexagons; B) 5 μm wide lines in a 15 μm periodicity. The dark areas are the areas with pRM488 brushes on one of the substrates and show homeotropic alignment; the light areas have no preferential orientation.

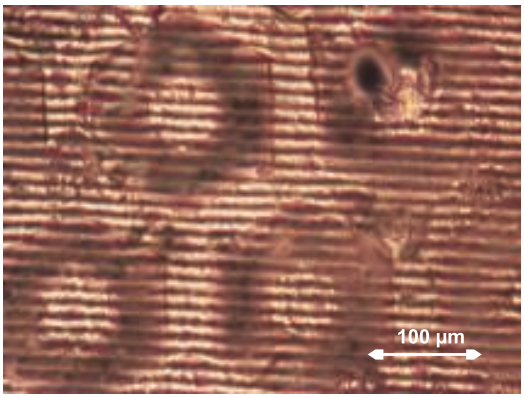

Figure 2.5: Patterned alignment in LC cells with a hexagon patterned top substrate and a line patterned bottom substrate. The hometropic alignment shows features of both patterns and is strongest in the areas where brushes are present on both substrates.

these substrates to study whether patterned alignment could be obtained. Figure 2.4 shows the alignment of the liquid crystalline phase on these patterned brushes for a pattern of 200 μm wide hexagons and for 5 μm wide lines (in a periodicity of 15 μm). For the fabrication of these LC cells we used one substrate with patterned brushes and one plain glass substrate to be able to study the alignment on one of the substrates only. It can clearly be seen that the liquid crystal aligns only on the brushes and not on the background regions. This is strong evidence for the role of the brush in

inducing homeotropic alignment.

When two substrates with different patterns are used to form an LC cell, the observed pattern shows features of both patterns (figure 2.5). The homeotropic alignment is strongest in those regions where brushes are present on both the top and bottom substrate.

The use of μCP in combination with polymer brush growth to obtain patterned alignment makes it a potentially attractive technique in device fabrication for display technologies and semiconductors.

2.4 Conclusions

In this study strong homeotropic alignment over large areas on surface-initiated polymers with liquid crystalline side chains is shown. The alignment is the result of interactions between the liquid crystalline side chains of the polymer and the molecules in the liquid crystalline phase and does not occur on substrates without a polymer layer or with polymer brushes of PMMA. Alignment occurs on brushes from 5 nm upwards and is more homeotropic on thin brushes than on thicker brushes. Using μCP to print down a pattern of the initiator before brush growth results in patterned alignment of the LC material. The homeotropic alignment over large areas and the ability to obtain patterned alignment by depositing the initiator with soft lithographic techniques make this procedure a promising tool for display and organic electronic applications.

2.5 Materials and Methods

General procedures

Ellipsometric measurements were carried out using a EL X-02C ellipsometer from Dr Riss Ellipsometerbau GmbH with a 632.8 nm laser at 70° angle of incidence. Refractive indices of 1.50 and 1.45 were used for polymer and initiator layers respectively.
FT-IR spectra were taken using a Bio-Rad FTS 6000 spectrometer. Spectra of surface-initiated polymers and spin coated monomers were taken in transmission mode using a background of the same initiator coated wafer that was used for polymer growth.
Plasma oxidation of substrates was performed in air in an Emitech K1050X plasma oxidizer for 10 minutes at 100 W.
Polarized light microscopy was performed on a Nikon Eclipse ME600 microscope equipped with a Nikon DN100 digital net camera.
Phase transitions were studied using a Linkam TMS91 hot stage in combination with the microscope or the ellipsometer mentioned above.
Contact Angle Goniometry was performed using a home-built combination of a kdScientific syringe controller and pump, a micro-syringe, a paper background screen illuminated by a KL1500LCD lamp and a Cohu CCD camera connected to a computer. Infusion and withdrawal rates of $4\,\mu\mathrm{L\,min^{-1}}$ were used. To keep the temperature constant at 25° a Linkam TMS91 hot stage was used.

Materials

Reactive mesogen RM488 was donated by Merck Chemicals Ltd, Chilworth Southampton. Dow Corning Sylgard 184 Base silicon elastomer and Sylgard 184 Silicon curing agent were purchased from VWR. All other chemicals were purchased from Aldrich, Lancaster or Fisher and used as received unless otherwize indicated. Triethylamine was distilled from and stored over potassium hydroxide. Toluene was distilled from sodium and stored over molecular sieves. Copper(I) chloride and copper(I) bromide were 99+ % and 99.999 % purity respectively and were stored in a glove box.

Dichloromethane, ethyl acetate, acetone, toluene and hexane were distilled prior to use. Methanol and ethanol were Analytical Reagent grade and used as received. The trichlorosilane ATRP initiator (2-bromo-2-methylpropionic acid 3-trichlorosilanylpropyl ester) was synthesized in the lab[†] following a reported procedure,[42] however using sallyl alcohol instead of 5-hexene-1-ol. PDMS stamps were fabricated following reported procedures.[43] Silicon wafers were obtained from Compart Technology Ltd. (100 mm diameter, phosphorous-doped, <1 0 0> orientation, polished one side).

Immobilization of the initiator monolayer on the substrate Silicon wafers were plasma oxidized before functionalization. Glass samples were sonicated for 2 minutes in a soap solution, subsequently for 2 minutes in demineralized water and finally for 2 minutes in ethanol and dried in a nitrogen stream. After this physical cleaning step they were oxidized in the plasma oxidizer. For initiation of the entire surface, the silicon and/or glass substrates were placed in a crystallising dish and 30 mL of dry toluene, 50 μL of triethylamine and 10 μL of the trichlorosilane initiator was added. The dish was covered with foil and left overnight at room temperature. Substrates were then washed sequentially with toluene, distilled acetone and absolute ethanol and dried under a nitrogen stream. For a patterned immobilization of the initiator monolayer on glass substrates by micro-contact printing (μCP), a flat piece of PDMS was used as an "ink pad". This piece was soaked in a solution of 5 μL of the trichlorosilane initator in 20 mL of hexane and blown dry in a nitrogen stream for 60 s. A patterned PDMS stamp was inked by putting it on the flat piece of PDMS and leaving it for 30 s without applying additional pressure. The stamp was than transferred to the glass substrate and left there for 30 s without applying additional pressure. The substrate with the pattern of trichlorisilane initiator was then rinsed with subsequently hexane, dichloromethane and ethanol and dried in a stream of nitrogen.

Synthesis of polymer brushes of RM 488 on silicon (typical procedure) The reaction mixture was prepared in a glove box. A solution of RM488 (4 g, 7.83 mmol) in a mixture of DMF (5 mL) and acetone (2 mL) was heated to 50 °C and transferred to a petridish containing initiated silicon and or glass samples.

[†]This synthesis was performed by Andy Brown and Ron Oren, Melville Laboratory for Polymer synthesis

Copper(I) chloride (0.80 mg, 7.7 μmol), copper(II) bromide (0.52 g, 2.3 μmol), copper(II)chloride (0.53mg, 5.4μmol) and 2,2'-bipyridyl (BPY, 6.1mg, 38μmol) were added. The petri dish was covered and sealed with parafilm to avoid evaporation of the solvents. Surface-initiated polymerization was performed at 50 °C in the glove box for 24 h. After the reaction, the substrates were removed from the glove box and subsequently washed in dichloromethane for 2 minutes under sonication, in toluene, in water and in ethanol and then dried in a stream of nitrogen. The substrates were then stored under nitrogen until further characterization and use. Ellipsometric thickness: 20 nm. IR: ν_{max}/cm^{-1}: 2958 (alkyl C–H stretch, s), 2108 (C=C stretch, w), 1735 (C=O stretch, s), 1605 (phenyl, m), 1502 (phenyl, m).

Fabrication of capillary LC cells Two thin plastic spacers (thickness approx. 10 μm, cling film) were placed 3 mm from the edges of an upward facing substrate. A second substrate was glued facing down on top of the first substrate, using two drops of cyanoacrylate glue between the edges and the spacers. Both the nematic liquid crystal 4'-pentyl-4-biphenylcarbonitrile (5CB) and the capillary cell were heated to 40 °C on a heating plate. At this temperature 5CB is an isotropic liquid. 5CB was then injected into the capillarity of the cell. The cell was cooled down to room temperature before further characterization.

References

[1] S. Kumar (Ed.), J. Brock, D. Finotello, M. Fish, C. Garland, J. Ho, M. Neubert, B. Padulka, P. Photinos, S. Sinha, and P. Ukleja, *Liquid Crystals - Experimental Study of Physical Properties and Phase Transitions*, Cambridge University Press, 2001.

[2] H. Yokoyama, S. Kobayashi, and H. Kamei, *Appl. Phys. Lett.* **41**, 438 (1982).

[3] K. Sakamoto, R. Arafune, N. Ito, S. Ushioda, Y. Suzuki, and S. Morokawa, *J. Appl. Phys.* **80**, 431 (1996).

[4] J. H. Kim, M. Yoneya, J. Yamamoto, and H. Yokoyama, *Nanotechnology* **13**, 133 (2002).

[5] M. O'Neill and S. M. Kelly, *J. Phys. D: Appl. Phys.* **33**, R67 (2000).

[6] L. T. Thieghi, J. J. Bonvent, E. A. Oliveira, J. A. Giacometti, and D. T. Balogh, *Appl. Phys. A: Mater. Sci. Process.* **77**, 911 (2003).

[7] X. L. Chen, Z. N. Bao, B. J. Sapjeta, A. J. Lovinger, and B. Crone, *Adv. Mater.* **12**, 344 (2000).

[8] J. J. Skaife and N. L. Abbott, *Chem. Mater.* **11**, 612 (1999).

[9] Y. D. Gu, F. Nederberg, R. Kånge, R. R. Shah, C. J. Hawker, M. Möller, J. L. Hedrick, and N. L. Abbott, *ChemPhysChem* **3**, 448 (2002).

[10] H. Kawamoto, *Proc. IEEE* **90**, 460 (2002).

[11] A. M. van de Craats, J. M. Warman, A. Fechtenkötter, J. D. Brand, M. A. Harbison, and K. Müllen, *Adv. Mater.* **11**, 1469 (1999).

[12] M. Grell and D. D. C. Bradley, *Adv. Mater.* **11**, 895 (1999).

[13] L. Schmidt-Mende, A. Fechtenkötter, K. Müllen, E. Moons, R. H. Friend, and J. D. MacKenzie, *Science* **293**, 1119 (2001).

[14] N. Yoshimoto and J. Hanna, *J. Mater. Chem.* **13**, 1004 (2003).

[15] C. D. Simpson, J. S. Wu, M. D. Watson, and K. Müllen, *J. Mater. Chem.* **14**, 494 (2004).

[16] H. Sirringhaus, P. J. Brown, R. H. Friend, M. M. Nielsen, K. Bechgaard, B. M. W. Langeveld-Voss, A. J. H. Spiering, R. A. J. Janssen, E. W. Meijer, P. Herwig, and D. M. de Leeuw, *Nature* **401**, 685 (1999).

[17] H. Murai, T. Gotoh, T. Nakata, and E. Hasegawa, *J. Appl. Phys.* **81**, 1962 (1997).

[18] Y. Suzuki, N. Mizoshita, K. Hanabusa, and T. Kato, *J. Mater. Chem.* **13**, 2870 (2003).

[19] A. M. van de Craats, N. Stutzmann, O. Bunk, M. M. Nielsen, M. Watson, K. Müllen, H. D. Chanzy, H. Sirringhaus, and R. H. Friend, *Adv. Mater.* **15**, 495 (2003).

[20] I. McCulloch, W. M. Zhang, M. Heeney, C. Bailey, M. Giles, D. Graham, M. Shkunov, D. Sparrowe, and S. Tierney, *J. Mater. Chem.* **13**, 2436 (2003).

[21] H. Sirringhaus, R. J. Wilson, R. H. Friend, M. Inbasekaran, W. Wu, E. P. Woo, M. Grell, and D. D. C. Bradley, *Appl. Phys. Lett.* **77**, 406 (2000).

[22] B. Alkhairalla, N. Boden, E. Cheadle, S. Evans, J. R. Henderson, H. Fukushima, S. Miyashita, H. Schönherr, G. J. Vancso, R. Colorado jr, M. Graupe, O. E. Shmakova, and T. R. Lee, *Europhys. Lett.* **59**, 410 (2002).

[23] Z. H. Lu, H. H. Deng, and Y. Wei, *Supramol. Sci.* **5**, 649 (1998).

[24] V. S. U. Fazio, L. Komitov, and S. T. Lagerwall, *Thin Solid Films* **329**, 681 (1998).

[25] J. Collins, D. Funfschilling, and M. Dennin, *Thin Solid Films* **496**, 601 (2006).

[26] V. K. Gupta and N. L. Abbott, *Science* **276**, 1533 (1997).

[27] Y. Reznikov, O. Ostroverkhova, K. D. Singer, J. H. Kim, S. Kumar, O. Lavrentovich, B. Wang, and J. L. West, *Phys. Rev. Lett.* **84**, 1930 (2000).

[28] S. Edmondson, V. L. Osborne, and W. T. S. Huck, *Chem. Soc. Rev.* **33**, 14 (2004).

[29] A. Halperin and D. R. M. Williams, *J. Phys.: Condens. Matter* **6**, A297 (1994).

[30] H. Lange and F. Schmid, *J. Chem. Phys.* **117**, 362 (2002).

[31] B. Peng, D. Johannsmann, and J. Rühe, *Macromolecules* **32**, 6759 (1999).

[32] B. Peng, J. Rühe, and D. Johannsmann, *Adv. Mater.* **12**, 821 (2000).

[33] W. X. Huang, G. L. Baker, and M. L. Bruening, *Angew. Chem., Int. Ed.* **40**, 1510 (2001).

[34] D. M. Jones and W. T. S. Huck, *Adv. Mater.* **13**, 1256 (2001).

[35] F. Vandenbrouck, S. Bardon, M. P. Valignat, and A. M. Cazabat, *Phys. Rev. Lett.* **81**, 610 (1998).

[36] M. Zaki Ewiss, G. Nabil, S. Schlagowski, and S. Herminghaus, *Liq. Cryst.* **31**, 1 (2004).

[37] J. L. Keddie, R. A. L. Jones, and R. A. Cory, *Faraday Discuss.* , 219 (1994).

[38] D. S. Fryer, R. D. Peters, E. J. Kim, J. E. Tomaszewski, J. J. de Pablo, P. F. Nealey, C. C. White, and W. L. Wu, *Macromolecules* **34**, 5627 (2001).

[39] S. Yamamoto, Y. Tsujii, and T. Fukuda, *Macromolecules* **35**, 6077 (2002).

[40] T. Wu, K. Efimenko, P. Vlček, V. Šubr, and J. Genzer, *Macromolecules* **36**, 2448 (2003).

[41] D. M. Jones, A. A. Brown, and W. T. S. Huck, *Langmuir* **18**, 1265 (2002).

[42] M. Husemann, E. E. Malmström, M. McNamara, M. Mate, D. Mecerreyes, D. G. Benoit, J. L. Hedrick, P. Mansky, E. Huang, T. P. Russell, and C. J. Hawker, *Macromolecules* **32**, 1424 (1999).

[43] Y. N. Xia and G. M. Whitesides, *Angew. Chem., Int. Ed.* **37**, 551 (1998).

Chapter 3

TCNQ monolayers and polymer brushes as dopant in field effect transistors

Synopsis: Application of monolayers to improve the performance of organic and polymer field effect transistors has recently attracted much attention in research. Dopants can be introduced in transistors to increase the amount of charges and hence the mobility. Positioning of the dopant within the device could have important effects on charge creation and mobility as the conductance in a field effect transistor only takes place in a very thin channel. This chapter discusses the synthesis of very thin dopant layers in the channels of field effect transistors, the control of the amount of dopant deposited and the effect of this dopant layer on the performance of these devices.

3.1 Introduction

In field effect transistors (FETs), applying a potential at the gate electrode induces charges in the active layer, thus making it conductive (see section 1.4.1 on page 17). In organic and polymer electronics often charge separation is inefficient and charge trapping is high resulting in low on/off ratios and/or high turn-on voltages for FETs. In these devices the conductance appears in a very thin film (around 5 nm thick) of semiconducting material (the "channel")

at the interface of dielectric and semiconducting polymer.[1]

In inorganic semiconductors it is practice to introduce dopants into the semiconducting material, to increase the amount of charges in the material. In organic semiconductors the generally hole-conducting active layer can be doped actively by adding an electron acceptor or by electrochemical anodic oxidation.[2] In many applications however no counter dopant ion is involved and doping is obtained by either photo-doping or charge injection.[3] Also dopants can be introduced unintentionally if the active material undergoes redox charge transfer with oxygen or water.[4] Generally this has a negative effect on device performance as it affects the band gap and increases the off-current in FETs (thus reducing the on/off ratio).

3.1.1 Monolayers in the channel of field effect transistors

There are numerous reports on the application of monolayers in FETs to improve device performance. The application of monolayers to improve FET performance is aimed at the improvement of molecular order in the channel,[5,6] the control of surface potential[7–9] and the endcapping of hydroxyls, which are suspected of trapping charges.[10]

Order is very important for charge transport in organic electronic devices[11] and enhancement of the order in the semiconducting channel leads to enhanced device performance.[12,13] Kline *et al.* showed that when an alkyl terminated silane is used to form a monolayer on FET substrates, the resulting order in the semiconductive poly-(3-hexylthiophene) (P3HT) layer close to the surface is enhanced.[5] The conjugated polymer has enhanced alignment with the backbone parallel to the substrate and the alkyl sidechains directed perpendicular to the substrate enhancing the formation of crystallites.

In a study of the influence of the alkyl chain length Pernstich noted that the longer the chain length of the monolayers the higher the mobilities of the devices.[6]

Monolayers with endgroups different to simple alkyles can act as a dipole layer and hence influence the surface potential. The dipole layer thus influences the electric field experienced by the polarons in the active layer. Pernstich *et al.* investigated the influence of nine different silanes, six of which

are halide functionalized and have a strong dipole.[9] The monolayers with a dipole pointing into the substrate resulted in a strong shift of the treshold to a positive gate voltage.

Kobayashi *et al.* showed that the opposite is true for an amine functionalized silane, which has an opposite dipole.[8] Sugimura *et al.* investigated the relation between measured surface potential differences between functionalized SAMs and monolayers of octadecyl trimethoxysilane (ODS) on one hand and calculated dipole moments and found that the surface potential indeed increased with increasing dipole moment pointing out of the substrate.[7]

3.1.2 Chemical doping in organic electronics

As has been discussed in the introduction to this chapter, in organic electronics the hole conducting layer can be doped either unintentionally or intentionally.

Intentional doping of the organic semiconductor zinc phthalocyanine (ZnPc) with the electronegative tetrafluorotetracyanoquinodimethane (F_4-TCNQ) has been shown by Gao *et al.* for applications in light emitting diodes (LEDs).[15,18] There is a very good match between the ionization energy ($E_{vac}-E_{HOMO}$) of ZnPc and the electron affinity ($E_{vac}-E_{LUMO}$) of F_4-TCNQ.

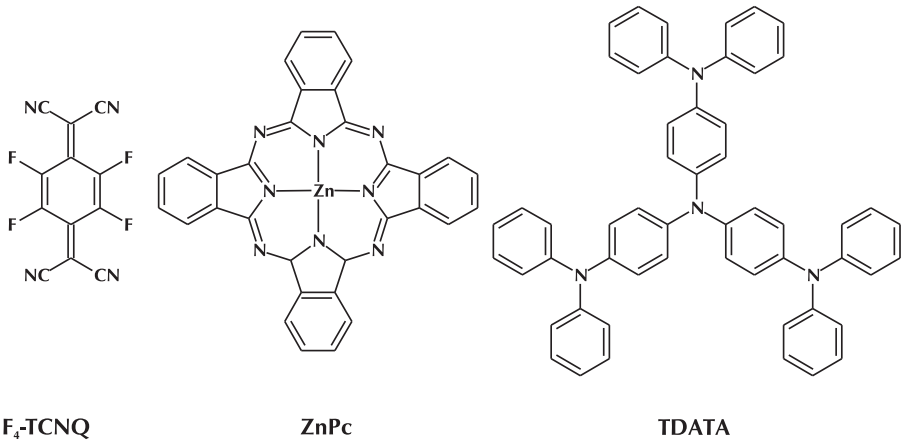

Scheme 3.1: Materials used in studies by Zhou, Gao, Blochwitz and others into the effects of doping in organic semiconductors:[14–17] the dopant F_4-TCNQ and the p-type conductors ZnPc and TDATA.

This results in very efficient charge transfer between donor and acceptor. Reduced electron transfer to the gold electrode results in a lower interfacial dipole and thus a lower hole injection barrier.

Doping of other p-type materials, like vanadyl phthalocyanine (VOPc) and 4,4',4"-tris(N,N-diphenylamino)triphenylamine (TDATA),[14,16,19] by F_4-TCNQ was shown in studies by the group of Leo together with applications in photovoltaic cells.[20] Structures of some of these dopants and electron donors are drawn in scheme 3.1. In all these studies the results were similar: a higher conductivity caused by enhanced hole injection.

Normally, in a FET without dopant, polarons (electron-hole pairs) do exist and can be separated by an electric field. This is what happens when the device is switched on by applying a negative gate bias: the positive charges are drawn towards the interface. When this occurs, a conductive channel of positive charges is formed and the source-drain current increases (for a more detailed explanation see section 1.4.1).

Leo and coworkers also studied the application of dopant in the active layer of FETs, again with ZnPc and F_4-TCNQ as donor and acceptor respectively.[21] They noted an increased mobility as a result of additional charge formation by charge transfer between dopant and donor. However the effect of dopant on other device characteristics as turn-on voltage, on/off ratio *et cetera* were not reported in this study.

Doping of the active layer of FETs with other acceptor materials than fluorinated TCNQ was studied by Rawcliffe[22] In this study the electron acceptor 2,3-dichloro-5,6-dicyano-1,4-benzoquinone (DDQ) was introduced in the bulk of P3HT. In the doped case the charge transfer is responsible for the creation of extra charges and, as expected, the on- and off-currents increase. Rawcliffe also found that the turn-on voltage is shifted to a more positive value, which can be explained again with the extra (positive) charges that have to be removed from the channel by a positive bias on the gate. Both effects are illustrated in scheme 3.2. Thirdly, the stability of the device in air was enhanced by this dopant as irreversible oxidation by oxygen was impossible as the active material was already in a (reversible) oxidized state when not operated.

It has been shown by Gao *et al.* that if small molecules are used as a dopant, diffusion of this dopant can occur.[15] This can cause problems for

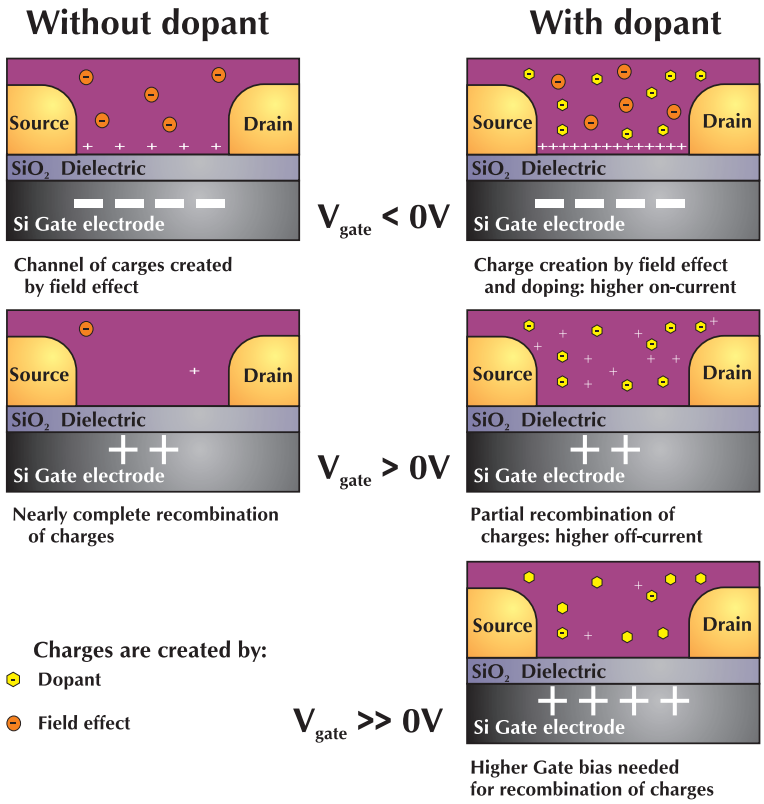

Scheme 3.2: Schematic working of doped and non-doped FETs. The extra charges created by charge separation with the dopant result in a higher on-current. However, also the off-current is increased and the turn-on voltage shifts to a more positive bias.

device engineering if localized dopants are required.

To summarize, there are many reports of the application of monolayers to affect the performance of organic electronic devices. Also there are several investigations into the intentional chemical doping of the organic active layer of organic LEDs, photovoltaic cells and FETs. The studies on intentional doping of *polymer* active layers however are rare. The positioning of dopant in FETs has not been investigated to date (to the authors knowledge).

It is expected, that dopants are most effective if they are located close to the semiconductor dielectric interface as it is there, that the charges form a conductive channel. The principle behind this is that when the device is switched on, charges are created directly in the channel, to form a conductive pathway. This is schematicly depicted in scheme 3.3. When the device

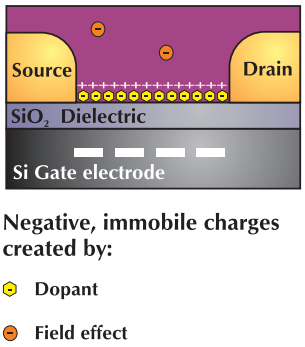

Scheme 3.3: Schematic working of a FET with dopant in the channel. Charges are created directly in the channel, leading to higher on-currents.

is switched off, the charges will diffuse, breaking up the pathway. As the concentration of dopant needed is thought to be much smaller in the case of channel doping, the effect of a higher off-current by bulk conductance, as observed in the case of bulk dopant, is expected to be much lower.

Therefore in this chapter the effect of the positioning of the dopant will be investigated by fabricating and characterising devices with nanometer thick dopant layers in the semiconductive channel. Monolayers and polymer brushes are ideal to obtain thin layers at the bottom of the channel. By using both monolayers and brushes, it will be possible to vary the total amount of dopant. As dopant moiety for the research in this chapter a TCNQ derivative was chosen, as its electron affinity of ~4.7 eV matches the ionization potential of commonly used conductive polymers like P3HT (~4.8 eV) very well.

3.2 Synthesis of dopant monolayers and surface-initiated polymers

In this study a derivative of tetracyanoquinodimethane (TCNQ) was chosen as a dopant moiety. SAMs of TCNQ have been reported in literature, but only on gold.[23–25] In this study SAMs in the channel, i.e. on silicon are required. Also polymers of TCNQ have been reported in literature,[26] but this method does not provide opportunities for dense surface grafted polymers. Therefore an approach based on a reaction of epoxy functionalized monolayers and brushes with an alcohol functionalized TCNQ derivative was followed to obtain dopant functionalized monolayers and polymer brushes.

For the formation of monolayers, first 3-glycedoxypropyl trimethoxysilane (GPTMS) was deposited by self-assembly. It has been shown for GPTMS monolayers that homogeneous SAMs are formed with the terminal epoxy groups mainly located at the SAM surface.[27]

For polymer brushes polyglycidyl methacrylate (PGMA) was synthesized by surface-initiated polymerization following a procedure by Edmondson *et al.*[28] The monomer GMA, the catalyst copper(I) chloride, the deactivator cop-

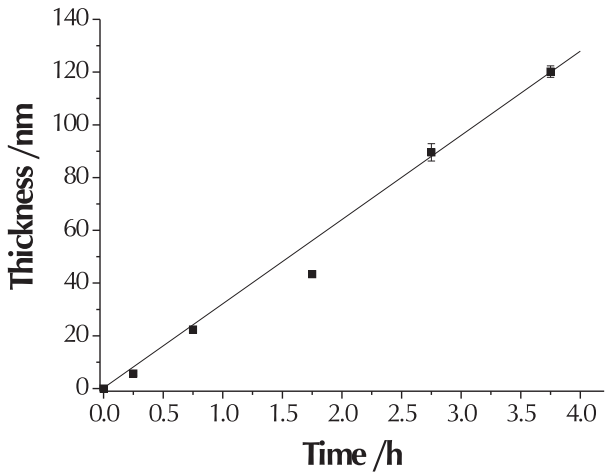

Figure 3.1: Time resolved PGMA brush growth.

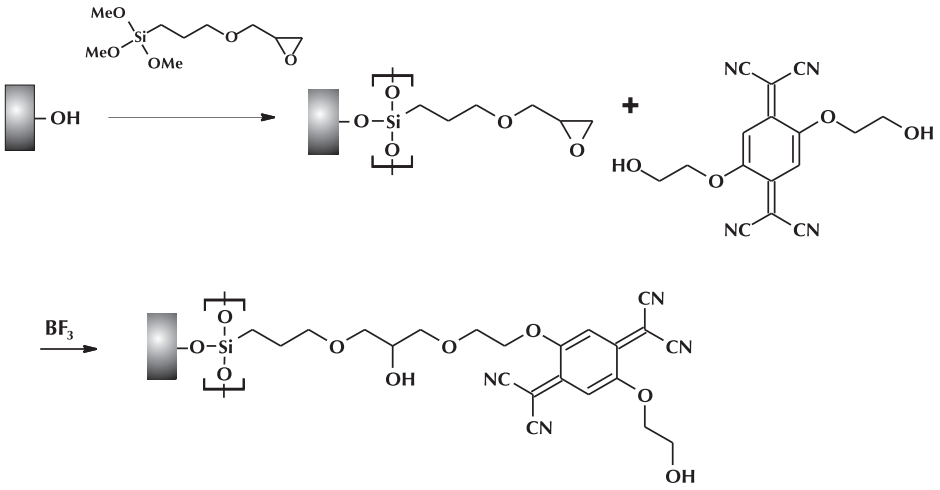

Scheme 3.4

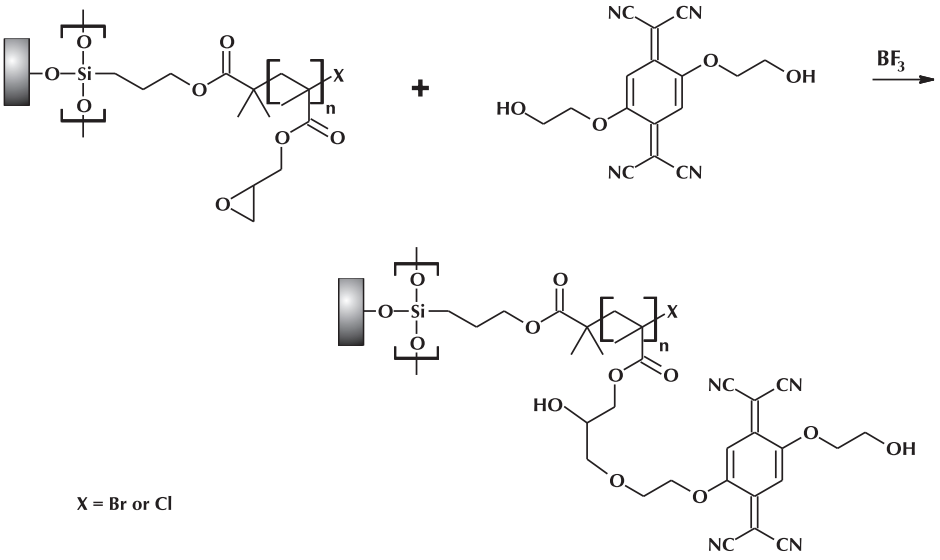

Scheme 3.5

per(II) bromide and the ligand 2,2'-dipyridyl were used in a 200:2:1:5 ratio, using a solvent mixture of methanol and water (4:1). The reaction was run for different time periods between 0.25 hour and 4 hours stopping the reaction in one of the tubes at a time. The increase in thickness of the polymer layer was linear over time and was 120 nm after 4 hours of reaction as can be seen from figure 3.1

Epoxide functionalized monolayers (see scheme 3.4) and surface grafted polymers (see scheme 3.5) were then treated with the lewis acid boron triflu-

orate to react with dioxydiethanol TCNQ in a ring opening reaction. Similar ring opening reactions at glycedoxy monolayers have been performed by Luzinov *et al.* to graft polystyrene to the surface, forming polymer layers of up to 9 nm thick.[29] However, in that study the reaction occured with a carboxylic acid functionalized polymer at elevated temperature. The advantage of using a Lewis acid is that the reaction normally proceeds with high yields at room temperature.[30]

Upon reaction with the TCNQ derivative the thickness of the monolayers increase from 0.8nm to 1.1nm as measured with ellipsometry. For the brushes the average increase in thickness was ~10%.

It has to be noted that the di-functionalized TCNQ is not the ideal compound. Reaction at both sides is improbable considering the bulkyness of the TCNQ compound. A mono-alcohol-functionalized derivative would have been a better choice as reaction at only one side is required. However, asymmetric TCNQ compounds are rarely reported as their synthesis is very elaborate.[23,31] As the symmetric di-functionalized TCNQ derivative was readily available, this compound was chosen in combination with post-functionalization of the unreacted alcohol as will be described in section 3.2.4.

3.2.1 Characterization by FT-IR spectroscopy

The IR spectrum of the monolayer before and after reaction with the TCNQ derivative is shown in figure 3.2. It can be seen that the intensities arising from the epoxy-related signals (at 2800-2700 cm^{-1} and 873 cm^{-1}) become lower and a strong aromatic (2800-3000 cm^{-1} and 880-950 cm^{-1}) absorbance and a weak nitrile (2125 cm^{-1}) band appear. The intensity of the nitrile peaks is very low which can partly be explained by the connection of another electron withdrawing nitrile to the same carbon. The conjugation slightly lowers the frequency from 2260 cm^{-1} reported for nitriles in the literature to 2125 cm^{-1} observed here.[32]

Although the epoxy signals are obscured by the aromatic bands, it can be seen that the disappearance of the epoxy bands is not complete. It can thus be concluded that the reaction of the epoxy ring with the alcohol functionalized dopant moiety does not take place with full conversion.

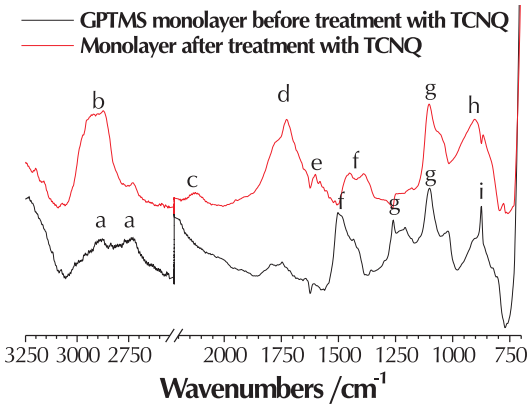

Figure 3.2: FT-IR spectrum of a 3-glycedoxypropyl trimethoxysilane before and after reaction with dioxydiethanol TCNQ. The compound specific absorption bands and regions are indicated: a: epoxy C—H stretch; b: aromatic C—H stretch; c: nitrile C≡N stretch; d: carbonyl C=O stretch; e: conjugated C=C stretch; f: alkyl C—C stretch g: O—C—C and C—O—C (asymmetric) stretches; h: aromatic isolated C—H; i: epoxy asymetric ring stretch.

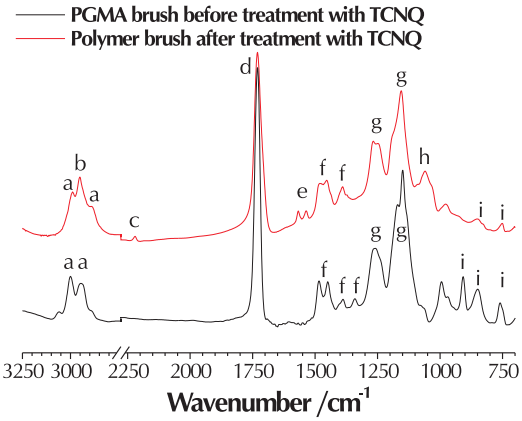

Figure 3.3: FT-IR spectrum of surface-initiated PGMA before and after reaction with dioxydiethanol TCNQ. The compound specific absorption bands and regions are indicated: a: epoxy C—H stretch; b: aromatic C—H stretch; c: nitrile C≡N stretch; d: carbonyl C=O stretch; e: conjugated C=C stretch; f: alkyl C—C stretch g: O—C—C and C—C(=O)—O (asymmetric) stretches; h: primary alcohol C—OH stretch; i: epoxy asymetric ring stretch.

The IR spectra of a 120 nm thick polymer brush before and after treatment shows similar characteristic bands to the spectra of the monolayers (see figure 3.3). Also here, the epoxy peaks do not disappear completely.

3.2.2 Characterization by UV/Vis spectroscopy

The TCNQ moiety shows a strong absorption from 370-470 nm in the violet-blue region of the spectrum. The UV/Vis spectrum for the TCNQ functionalized monolayers and the functionalized polymer brushes are shown in figures 3.4 and 3.5 respectively.

The number of TCNQ units in the monolayer was diluted by co-reacting the GPTMS monolayer with a mixture of the TCNQ derivative and a dummy phenyl ethanol at different concentration ratios. From the spectrum it can be observed that increasing the ratio TCNQ:dummy results in a stronger absorption. Therefore it can be concluded that these two reagents are in competition and that the incomplete reaction of the epoxy monolayer as observed by IR is not caused by a too low reactivity of the TCNQ alcohol derivative.

For the TCNQ functionalized polymer brushes the UV absorbance increases with brush thickness. This increase is linear as can be observed in the

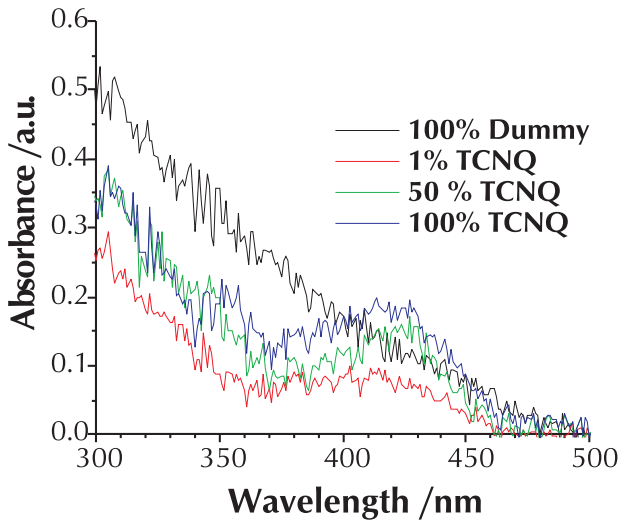

Figure 3.4: UV/Vis absorption of glycedoxy monolayers after reaction with alcohol functionalized dummy and TCNQ compounds. The percentage of TCNQ in the feed was varied.

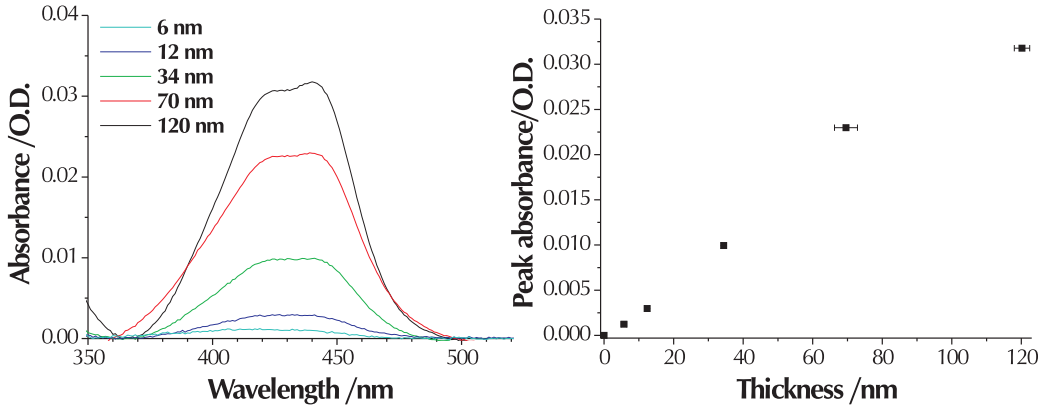

Figure 3.5: UV/Vis Absorption of PGMA polymer brushes of varying thickness after reaction with alcohol functionalized TCNQ: the absorption spectrum (left) and the peak absorbance at 440 nm as a function of thickness of the polymer brush layer (right).

right part of figure 3.5. This shows that the the TCNQ derivative can penetrate deep into the brush and that the reactivity is equal across the brush layer.

3.2.3 X-ray photoelectron spectroscopy*

X-ray photoelectron spectroscopy (XPS) was performed on samples with TCNQ monolayers to measure the ratio between elements at the surface and showed that about 1 nitrogen atom is present per 40 carbon atoms at the surface. This equals to only one in about 24 epoxide groups at the surface reacting with a TCNQ unit, which confirms the limited conversion as measured with IR.

On the other hand a fluoride absorbance is observed as well. This means that the activation of the epoxy ring by the BF_3 does take place, but that the subsequent attack by the alcohol occurs only partially. In the previous section it was concluded that the reactivity of the alcohol is not limiting the reaction, as dummy and TCNQ are reacting in competition. The low conversion of the epoxide is probably caused by steric effects: if a TCNQ derivative has succesfully reacted with an epoxy group at the surface the bulky moiety blocks access to neighbouring sites.

*XPS was performed by Wojciech Osikowicz at the Department of Physics, Linköping University, Sweden.

Table 3.1: Advancing (θ_{aw}), static (θ_{sw}) and receding (θ_{rw}) contact angles of water on substrates with 6 nm thick TCNQ functionalized polymer brushes before and after treatment with IBC, DC, PDMCS or ODTS.

	θ_{aw}	θ_{sw}	θ_{rw}
Before treatment	68 ° ± 5 °	62 ° ± 17 °	17 ° ± 14 °
Treated with IBC	105 °± 6 °	103 ° ± 7 °	53 ° ± 9 °
Treated with DC	101 ° ± 6°	100 ° ± 8 °	50 ° ± 9 °
Treated with PDMCS	105 ° ± 7 °	102° ± 8 °	54 ° ± 6 °
Treated with ODTS	103 ° ± 8 °	102 ° ± 6 °	55 ° ± 7 °

3.2.4 Endcapping of hydroxy groups

Hydroxyls in the channel of a semiconductor are suspected to trap charges.[33] Therefore it was decided to endcap the hydroxy groups on the functionalized monolayer and brushes. Two different approaches for protecting the alcohol were investigated: a condensation with either isobutyryl chloride (IBC) or decanoyl chloride (DC) and a silylation with either octadecyl trichlorosilane (ODTS) or propyl dimethylchlorosilane (PDMCS). These reactions are shown in scheme 3.6

Both these approaches increase the contact angle considerably (see table 3.1). The static contact angles increase from 62 ° to over 100 ° In the reactions with the acyl chloride however, the IR-absorptions associated with the cyanide and with the conjugated carbon double bond disappear in the spectra of the brushes (figure 3.6). In the UV/Vis-spectrum of a brush treated with decanoyl chloride, the shape of the characteristich absorbance around 440 nm almost disappears (figure 3.7). A possible side-reaction could be that the nitrile groups present in the TCNQ moiety undergo hydrolysis in presence of pyridine, the base that is needed to activate the hydroxy group. This is a known reaction for nitriles in presence of bases.[34]

The reaction with silanes was performed without addition of triethyl amine (TEA) to avoid basic hydrolysis of the nitrile. IR and UV/Vis show no reduction in absorbance for the characteristic signals and this procedure was followed for the preparation of FET substrates.

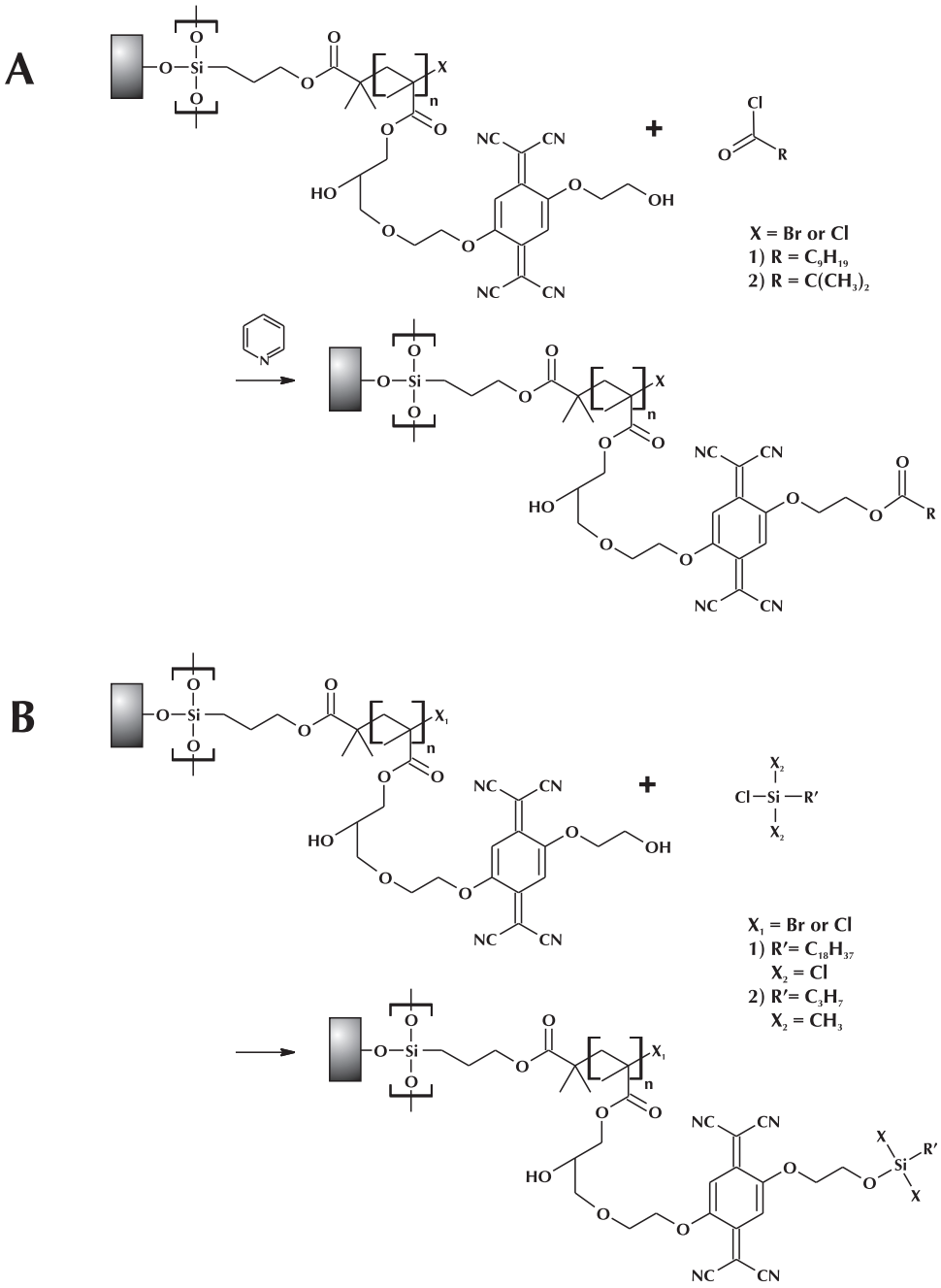

Scheme 3.6: Reactions performed to passivate the hydroxyl group: A1) with DC; A2) with IBC; B1) with ODTS; B2) with PDMCS.

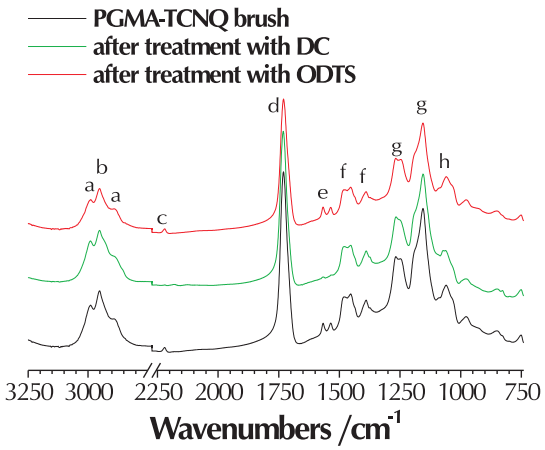

Figure 3.6: FT-IR spectrum of TCNQ functionalized brushes before and after treatment with either ODTS or DC. The compound specific absorption bands and regions are indicated: a: epoxy C—H stretch; b: aromatic C—H stretch; c: nitrile C≡N stretch; d: carbonyl C=O stretch; e: conjugated C=C stretch; f: alkyl C—C stretch g: O—C—C and C—C(=O)—O (asymmetric) stretches; h: primary alcohol C—OH stretch.

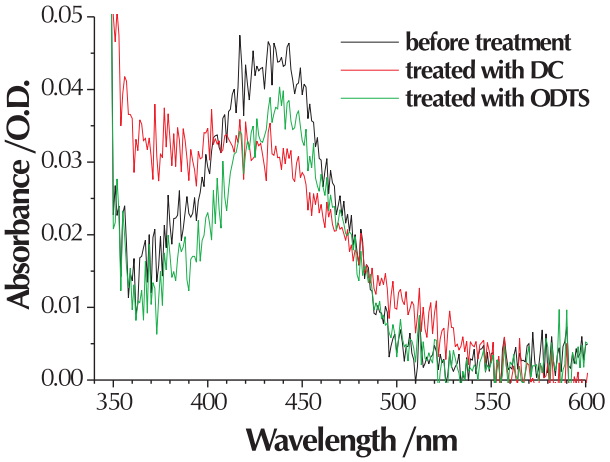

Figure 3.7: UV/Vis absorption spectrum of 6 nm thick TCNQ functionalized polymer brushes before and after treatment with DC or ODTS.

3.3 Electrochemical characterization by ultraviolet photoelectron spectroscopy[†]

Ultraviolet photoelectron spectroscopy (UPS) is a technique similar to XPS, but uses high energy ultraviolet light in stead of X-rays to induce photo-ionization of the sample. The ultraviolet photons interact with the valence levels of the molecule or solid, leading to ionization by removal of one of these valence electrons. UPS gives information about the binding energy of the electrons emitted and is used as a technique to study the electronic structure of materials. UPS can also be used to calculate the work function of a material as the relationship between largest binding energy (LBE), source emission ($h\nu$) and work function (W) is given by:[35]

$$W = h\nu - \mathrm{LBE} \tag{3.1}$$

UPS was performed on bare Si/SiO_2 substrates, on substrates with a TCNQ functionalized monolayer and on bare and monolayer substrates with a layer of P3HT spincoated on top. Using a HeI (21.2 eV) discharge emission as exitation source, the largest binding energy measured for the TCNQ functionalized monolayers was 17 eV. Hence the work function is 4.2 eV.

For substrates with P3HT on top of the TCNQ monolayer, the workfunction was 4.55eV. Following from the difference between these two values, these interfaces exhibit an interfacial dipole of 0.35 eV with positive charges stored on the side of P3HT. This is in contrast to P3HT spun on substrates with native silicon oxide, which did not show this dipole. This strongly indicates that the TCNQ monolayers can act as dopants for P3HT.

It has to be noted that the values derived for the working function are much lower than the literature values of 7.2 eV and 4.8 eV for TCNQ[36] and P3HT[‡] respectively. The huge discrepancy for TCNQ can be partly explained that in this case a derivative and not the pure compound was used and that the TCNQ content in the monolayers was very low, hence the value for the working function comes closer to that of silicon oxide, which was recorded at 3.2 eV.

[†]UPS was performed by Wojciech Osikowicz at the Department of Physics, Linköping University, Sweden.

[‡]Data provided by Merck Chemicals Ltd.

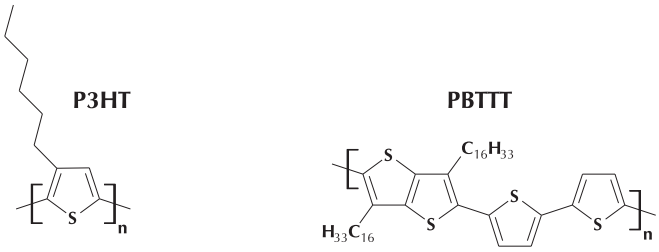

Scheme 3.7

3.4 Field Effect Transistors with TCNQ dopant layers[§§]

Devices were fabricated by synthesising TCNQ monolayers or brushes on prepatterned FET substrates followed by deposition of the semiconducting polymer by spin coating. The semiconducting polymers that were used were poly(2,5-bis(3-alkylthiophen-2-yl) thieno[3,2-b]thiophene) (PBTTT)[37] and P3HT (both shown in scheme 3.7). The devices were fabricated using prepatterned FET-grade silicon substrates with 230 nm thick SiO_2 dielectric. Devices were made on substrates with TCNQ functionalized monolayers and brushes with and without additional hydroxyl capping by either ODTS or PDMCS. Also reference devices on untreated prepatterned substrates were included. Additionally devices on substrates with a monolayer of octyltrichlorosilane (OTS) were fabricated for comparison.

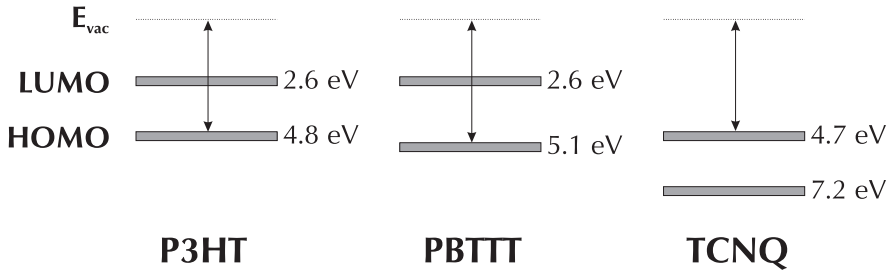

Scheme 3.8: Energy levels for both semiconductive polymers PBTTT and P3HT and for the dopant TCNQ-derivative. Ionization energy of the polymers and electron affinity of the dopant are depicted by arrows. Data for the polymers were provided by Merck Chemicals Ltd. Data for TCNQ is extracted from the optical band gap and from Inzelt *et al.*[36]

[§]Device fabrication and characterization was carried out at Merck Chemicals Ltd. Chilworth, Southampton, UK in collaboration with Dr. Maxim Shkunov

Table 3.2: On- and off-currents and on/off ratios in the saturated regime of FETs fabricated with and without TCNQ monolayers and brushes.

	PBTTT			P3HT		
	On	**Off**	**On/Off**	**On**	**Off**	**On/Off**
Bare silicon	$1.7\,10^{-4}$	$4.2\,10^{-10}$	$4.2\,10^{5}$	$1.1\,10^{-4}$	$2.4\,10^{-9}$	$4.7\,10^{4}$
SAM untreated	$3.8\,10^{-4}$	$2.7\,10^{-11}$	$1.4\,10^{7}$	$4.9\,10^{-5}$	$3.5\,10^{-10}$	$1.4\,10^{5}$
8 nm brush untreated	$5.7\,10^{-4}$	$1.7\,10^{-7}$	$3.3\,10^{3}$	$8.0\,10^{-5}$	$3.5\,10^{-8}$	$2.3\,10^{3}$
30 nm brush untreated	$6.4\,10^{-4}$	$2.1\,10^{-9}$	$3.3\,10^{5}$	$6.1\,10^{-5}$	$1.4\,10^{-8}$	$4.3\,10^{3}$
SAM + ODTS	$1.6\,10^{-4}$	$9.8\,10^{-12}$	$1.6\,10^{7}$	$5.5\,10^{-5}$	$7.5\,10^{-9}$	$7.3\,10^{3}$
8 nm brush + ODTS	$1.2\,10^{-4}$	$3.2\,10^{-10}$	$3.8\,10^{5}$	$3.8\,10^{-5}$	$3.5\,10^{-9}$	$1.1\,10^{4}$
30 nm brush + ODTS	$7.1\,10^{-6}$	$1.8\,10^{-9}$	$3.9\,10^{3}$	$2.2\,10^{-5}$	$5.8\,10^{-8}$	$3.8\,10^{2}$
SAM + PDMCS	$1.9\,10^{-4}$	$2.5\,10^{-11}$	$7.6\,10^{6}$	$5.5\,10^{-5}$	$5.5\,10^{-10}$	$1.0\,10^{5}$
8 nm brush + PDMCS	$2.5\,10^{-4}$	$6.0\,10^{-10}$	$4.2\,10^{5}$	$3.5\,10^{-5}$	$2.2\,10^{-9}$	$1.6\,10^{4}$
30 nm brush +PDMCS	$3.5\,10^{-5}$	$1.7\,10^{-9}$	$2.1\,10^{4}$	$2.0\,10^{-5}$	$7.8\,10^{-9}$	$2.6\,10^{3}$
OTS monolayer	$2.5\,10^{-3}$	$2.3\,10^{-10}$	$1.1\,10^{7}$	$7.5\,10^{-4}$	$8.0\,10^{-10}$	$9.4\,10^{5}$

Scheme 3.8 shows the energy levels of both polymers and of the dopant. It can be seen that there is a reasonably good match between the ionization energy of P3HT and the electron affinity of TCNQ. PBTTT is slightly harder to oxidize.

Table 3.2 summarizes the on- and off-currents measured for devices with different surface treatments. The wide variety of literature values for mobilities, on- and off-currents and on/off ratios makes it difficult to compare the control devices here with devices reported by other groups. In the literature,[11,38–41] mobilities in devices with P3HT on bare silicon vary between 10^{-4} and $10^{-1}\,cm^2(Vs)^{-1}$, on-currents between $5{\cdot}10^{-5}$ and $3{\cdot}10^{-4}$ A and on/off ratios between 10^2 and 10^6. The mobility in the control device on bare silicon was $3.5{\cdot}10^{-3}\,cm^2(Vs)^{-1}$, the on-current $1.1{\cdot}10^{-4}$ A and on/off ratio $4.7{\cdot}10^4$. These values are well within the range of reported values.

For devices of P3HT on OTS coated substrates, mobilities reported in the literature[5,11,42,43] range from $2{\cdot}10^{-2}$ to $2{\cdot}10^{-1}\,cm^2(Vs)^{-1}$, on-currents from 10^{-6} to 10^{-3} A and on/off ratios from 10^4 to 10^7. Again the measured values of $1{\cdot}10^{-2}\,cm^2(Vs)^{-1}$ for the mobility, $7.5{\cdot}10^{-4}$ A for the on-current and $9.4{\cdot}10^5$ for on/off ratio compare well with the reported range of values.

For non-silylated devices (without protection of the hydroxyls), it is difficult to see trends in the performance of the different devices. For both semiconducting polymers however both the on- and off-currents in devices with TCNQ monolayers are lower than in devices on bare silicon. Also for all cases, the off-currents in devices on brush substrates were higher than in devices with TCNQ monolayers. This is also true for most of the devices on substrates with silylated TCNQ monolayers and brushes.

FETs with TCNQ monolayers and brushes that have been treated with ODTS and PDMCS give more reproducible results and some additional trends

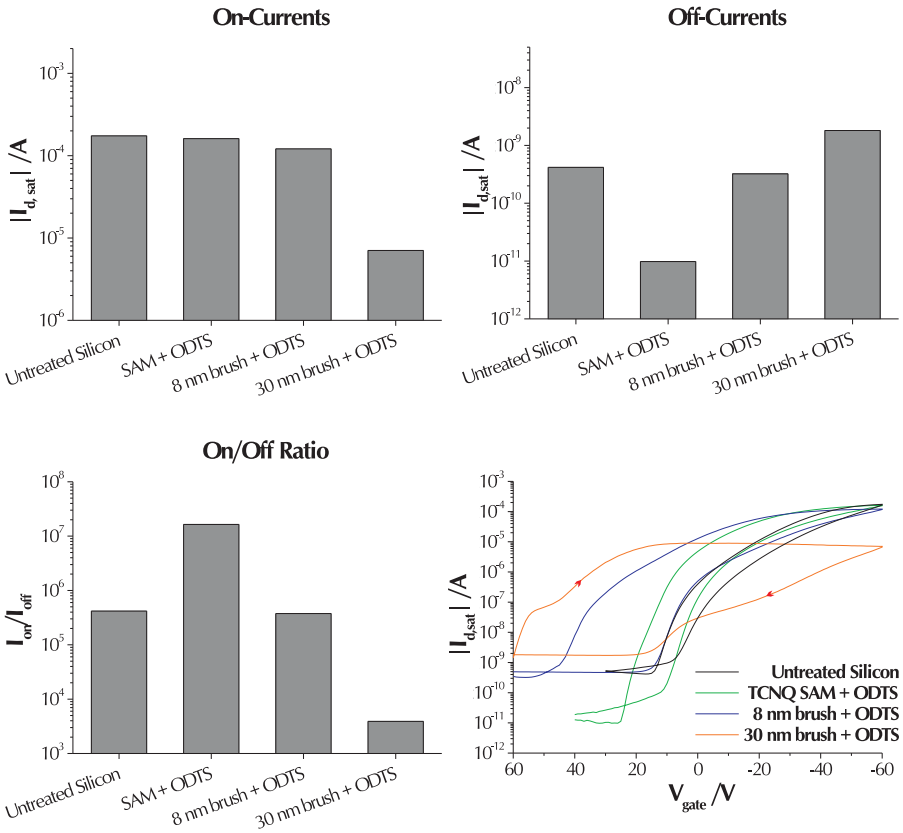

Figure 3.8: The On- and Off-currents in FETs on untreated silicon and on substrates with monolayers or polymer brushes with TCNQ moieties, measured in inert atmosphere. The monolayers and polymers were treated with ODTS before deposition of the semiconducting polymer. In all the devices in this figure the active polymer was PBTTT.

can be noted (see also figure 3.8). The effect of the dopant on the on-current is minimal. Going from untreated silicon to TCNQ monolayers to 8 nm thick to 30 nm thick TCNQ polymers, the on-currents of the FETs even decrease. On the other hand in the off-state of the devices the currents show an increasing trend with TCNQ layer thickness from monolayer to thick brush layer, although in most cases again the off-current for the device on a TCNQ monolayer is lower than on untreated silicon. Both trends together result in a decreasing on/off ratio with TCNQ layer thickness, but because of the low off-current for devices with TCNQ functionalized SAMs, the on/off ratio for these devices is higher than for FETs with untreated silicon. There are no obvious differences between the effects on FET performance of the two silanes used for passivation of the brush and monolayer hydroxyls.

These results seem to be counter-intuitive and are in contrast with expectation. As has been mentioned in the introduction to this chapter, both on- and off-current are expected to increase upon introduction of a dopant, as more charges are introduced. Apparently the positioning of the dopant at the bottom of the channel has some unforeseen effects. When the device is turned on, the positive charges that are created by charge separation with the dopant are kept near the interface with the dopant layer because of the electric field. Here they can be trapped by Coulomb interaction with their parent charge compensating counter ions[44] or can recombine with it. Therefore the effect of thin dopant layers at the bottom of the channel on the on-currents is minimal. With a thick dopant functionalized brush the on-currents even decrease which could be the result of the formation of traps by the variation in surface energy at the dielectric/polymer interface.

The lower off-currents for devices with a TCNQ monolayer can be explained by a charge trapping effect of the dopant layer: hole conduction in the channel is obstructed by recombination. However, as the dopant layer increases this is counter-acted by increasing charge separation between dopant layer and the bulk. With positive gate bias the field drives this charge separation, so bulk conductivity can occur, giving rise to higher off-currents with increasing dopant layer thickness. This could also explain why the lowering effect of the TCNQ SAM on the off-current is less predominant in the devices with P3HT than with PBTTT. P3HT is more readily doped as its oxidation

potential is lower as was shown in scheme 3.8, so doping of the bulk material already plays a major role in the case of SAMs.

It has to be noted, that although the brush is a dense layer, penetration of the semiconduction polymer into the brush will occur to some extend. This will not influence the limitations of the channel dopant layer though, as the concentration of dopant is still highest at the bottom of the channel and the concentration of hole-conductor still highest at the top of the channel.

Another effect of increasing dopant layer thickness is, that hysteresis occurs between switching the device on and off. This hysteresis could be the result of the dopant effect in combination with recombination in the on-state: when switching the device on, the doping effect causes that many charges can be mobilized already at high gate biases. When going from the on- (V_g<0) to the off-state (V_g >0) however, a major part of the positive charges have been able to recombine with or have become immobilized at the negative charged dopant interface, so the current can drop at a relatively low gate voltage. The effect of higher turn-on voltages as described by Rawcliffe[22] therefore is also notable for the turn-on voltages in the devices with higher dopant levels described here, although the effect is less prominent in the turn-off voltages as a result of the positioning of the dopant in the channel.

Rawcliffe also reports an increase in stability of FETs upon intentional doping.[22] This effect was not apparent in the devices studied here. Possibly the total amount of dopant plays a role here. In this study dopant was only present at the dielectric interface, hence the total amount of dopant was much lower than in the study by Rawcliffe.

It is clear that the effects of doping in the channel is totally different from the effects of bulk dopant. Due to the positioning of the monolayers and brushes the advantageous effects of creating more charges are cancelled by more recombination driven by the field. Very thin dopant (mono-)layers however can be used to lower the off current.

To take advantage of extra charges created by a dopant aided by charge separation by the electric field, the dopant ideally has to be situated in a thin layer just above, instead of at the bottom of the channel. In the off-state this dopant layer could help trapping charges and thus lowering the off-current as

well. This layer could be accessible by polymer brush technology (with the dopant situated in the second block of a diblock co-polymer), but was beyond the scope of this research.

3.4.1 Comparison with devices with an OTS monolayer

For comparison also devices were fabricated using a substrate with an OTS SAM. OTS and other silylating agents are an often used surface treatment for FETs as they react with the hydroxyls at the surface, enhancing the alignment of the conjugated polymers. Figure 3.9 compares the device with a TCNQ SAM with the device with an OTS SAM. It is clear that the turn-on voltage of the device with the TCNQ SAM is lower (at 10 V vs. 35 V), which is advantageous. It has to be noted though, that the huge shift in turn-on voltage for the OTS device is not confirmed by literature.[42] The on/off ratio is about an order of magnitude larger for the OTS device, though the off-current is significantly lower for the TCNQ device.

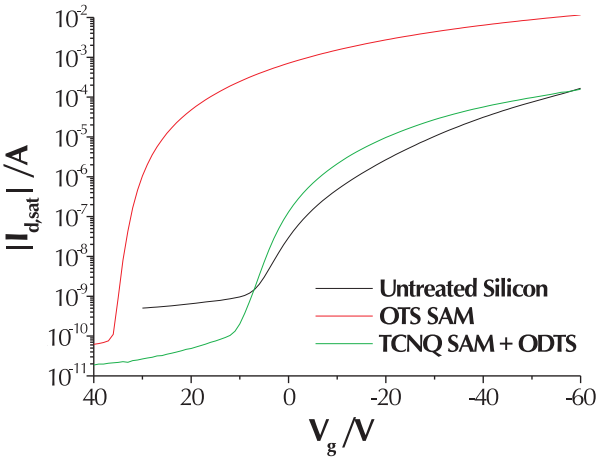

Figure 3.9: Transfer plot for devices with PBTTT using no surface treatment, an OTS monolayer and a TCNQ monolayer (with ODTS post treatment).

3.5 Conclusions and outlook

In this chapter the synthesis of dopant monolayers and polymer brushes with TCNQ units for application in FETs is shown. The dopant concentration can be tuned by varying the concentration of alcohol functionalized TCNQ compared to a dummy in the case of the monolayer and by varying the brush thickness, though the reactivity between the TCNQ moiety and the monolayer is limited by steric effects.

In contrast to bulk dopants, dopants situated at the interface of dielectric and semiconductive polymer layer hardly have any effect on on-currents as the additional charges created by charge transfer can not be separated by the electric field in the device. On the other hand the off-currents are lowered for thin layers of dopant due to trapping of the holes by negative charges on the TCNQ units. With increasing dopant layer thickness however the off-current increases due to the formation of extra charges by charge transfer.

Due to the lower off-currents devices with TCNQ monolayers have a better on/off ratio than devices on untreated silicon and compare well with devices with an OTS monolayer. It is speculated that positioning a dopant layer right above the semiconductive channel in a FET, instead of at the bottom of the channel as in this study, might result in an optimized dopant effect that results in higher on-currents and lower off-currents.

3.6 Materials and methods

General procedures

Oven dried glassware was used for all reactions in non-aqueous solvents.
Ellipsometric measurements on monolayers and polymer brushes were carried out using either an EL X-02C ellipsometer from Dr Riss Ellipsometerbau GmbH with a 632.8 nm laser at 70 ° angle of incidence or using a JA Woollam Alpha-SE spectroscopic ellipsometer. In case of the monochromatic ellipsometer refractive indices of 1.50 and 1.45 were used for polymer and initiator layers respectively, in case of the spectroscopic ellipsometer a model with spline and/or cauchy layer on top of a silicon oxide layer was used.
FT-IR spectroscopy on surface-initiated polymers and surface monolayers was carried out using a Bio-Rad FTS 6000 spectrometer. Spectra of surface-initiated polymers were taken in transmission mode using a background of the same bare Si wafer that was used for polymer growth.
Plasma oxidation of substrates was performed in air in an Emitech K1050X plasma oxidizer for 10 minutes at 100 W.
UV/Vis spectra were recorded on a Varian Cary 4000 UV/Vis Spectrometer.
Atomic Force Microscopy was performed on a Digital Instruments Nanoscope® Dimension™3100 Atomic Force Microscope. Topographical and phase images were recorded.
Contact Angle Goniometry was performed using a home-built combination of a kdScientific syringe controller and pump, a micro-syringe, a paper background screen illuminated by a KL1500LCD lamp and a Cohu CCD camera connected to a computer. Infusion and withdrawal rates of 4 μL minute^{-1} were used.
Electrical characterization of field effect transistors was carried out in a dry nitrogen atmosphere using a computer controlled Agilent 4155C Semiconductor Parameter Analyser. For stability tests the characterization was carried out in air and a semiconductor parameter analyser connected to an automated stage was used to take measurements at regular time intervals. Measurements were taken on four devices with channel length 10 μm for each

sample preparation.

X-ray Photoelectron Spectroscopy (XPS) and Ultraviolet Photoelectron Spectroscopy (UPS)[¶] analyses were performed using a Scienta ESCA 200 under monochromatic Al Kα radiation (1486.6 eV) and a nonmonochromatized HeI and HeII source (21.2, 40.8 eV). A step size of 1 eV was used for survey spectra. Step sizes of 0.1 eV were used to obtain high energy resolution spectra of selected regions.. Charge-neutralising equipment was used to compensate for sample charging and the binding scale was referenced to the CH component of C 1s spectra at 285.0 eV.

Materials

Dioxydiethanol TCNQ, poly(2,5-bis(3-alkylthiophen-2-yl) thieno[3,2-b]thiophene) (PBTTT, M_n = 24800, M_w = 42600) and poly-(3-hexylthiophene) (P3HT, M_n = 14600, M_w = 21900) were donated by Merck Chemicals Ltd. All other chemicals were purchased from Aldrich, Lancaster or Fisher and used as received unless stated otherwise. Triethylamine was distilled from and stored over potassium hydroxide. Toluene was distilled from sodium and stored over molecular sieves. Copper(I) chloride was 99+ % purity and was stored *in vacuo*. Dichloromethane and toluene were distilled prior to use. Methanol and ethanol were Analytical Reagent grade and used as received. The trichlorosilane initiator (2-bromo-2-methylpropionic acid 3-trichlorosilanylpropyl ester) was synthesized in the lab[‖] following a reported procedure,[45] however using allyl alcohol instead of 5-hexene-1-ol. Silicon wafers were obtained from Compart Technology Ltd. (100 mm diameter, phosphorous-doped, <1 0 0> orientation, polished one side). FET substrates were provided by Merck Chemicals Ltd. These substrates were highly doped silicon substrates with a thermally grown silicon oxide (SiO_2) insulating layer of 230 nm, where the substrate served as a common gate electrode. Transistor source-drain gold electrodes had been photolithographically defined on the SiO_2 layer.

[¶] See the footnotes on page 67 and 71

[‖] This synthesis was performed by Andy Brown and Ron Oren, Melville Laboratory for Polymer Synthesis

Immobilization of the initiator monolayer on the substrate Silicon substrates (including FET substrates) were plasma oxidized before functionalization. Glass and quartz samples were sonicated for 2 minutes in a soap solution, subsequently for 2 minutes in demineralized water and finally for 2 minutes in ethanol and dried in a nitrogen stream. After this physical cleaning step they were oxidized in the plasma oxidizer. The silicon and/or glass substrates were placed in a crystallising dish and 30 mL of dry toluene, 50 μL of triethylamine and 10 μL of the trichlorosilane initiator was added. The dish was covered with foil and left overnight at room temperature. The wafer was then washed sequentially with toluene, acetone and absolute ethanol and dried under a nitrogen stream.

Immobilization of a monolayer of 3-glycidoxypropyl trimethoxysilane The procedure for deposition of a monolayer of 3-glycedoxypropyl trimethoxysilane was adapted from literature.[27] Silicon wafers and FET substrates were plasma oxidized before functionalization. Glass samples were sonicated for 2 minutes in a soap solution, subsequently for 2 minutes in demineralized water and finally for 2 minutes in ethanol and dried in a nitrogen stream. After this physical cleaning step they were oxidized in the plasma oxidizer. The silicon, FET and/or glass substrates were placed in a crystallising dish and covered with 30 mL of toluene. 300 μL of glycidoxypropyl trimethoxysilane was added with a syringe and the solution was swirled. The dish was covered with aluminium foil and left overnight. The wafer was cleaned subsequently with toluene, acetone and absolute ethanol and dried under a stream of nitrogen.
IR: $\nu_{max}/\mathrm{cm}^{-1}$: 3000-2600 (epoxy C—H stretch, m), 1500 (alkyl C—C stretch, s) 1300-1000 (O—C—C and C—O—C (asymmetric) stretches, s), 873 (epoxy asymetric ring stretch).

Surface-initiated polyglycidyl methacrylate The reaction mixture was prepared following a literature procedure.[28] Glycidyl methacrylate (GMA) (20 mL, 146.8mmol), water (4mL) and methanol (16mL) were purged with nitrogen for 20 minutes. Then copper(I) chloride (0.145 g, 1.468 mmol), copper(II) bromide (0.0164 g, 0.073 mmol) and bipyridine (0.572 g, 3.66 mmol) were added and the mixture was purged with nitrogen for 15 minutes. Two substrates at a time were put back to back in Radley tubes. All the tubes were evacuated and refilled with Nitrogen through four cycles. The reaction mixture was added to all the

tubes. The reaction was run for different time periods between 0.25 hour and 4 hours stopping the reaction in one of the tubes at a time. After the reaction the substrates were rinsed with toluene, acetone and methanol subsequently. The increase in thickness of the polymer layer was linear over time and was 120 nm after 4 hours of reaction.
IR: ν_{max}/cm^{-1}: 3040-2900 (epoxy C—H stretch, s), 1750 (carbonyl C=O stretch, s), 1500-1320 (alkyl C—C stretch, m), 1320-1085 (O—C—C and C—C(=O)—O (asymmetric) stretches, s), 850-750 (epoxy asymetric ring stretch, s).

TCNQ Functionalization of the monolayers and surface grafted polymers A saturated solution of dioxydiethanol TCNQ (0.2 g, 0.62 mmol) in dichloromethane (45 mL) was purged with nitrogen for 15 minutes. For (partial) endcapping with dummy, phenyl ethanol was used at concentration of 15.4 mmol L^{-1} to (partially) substitutute TCNQ. Glass, silicon or FET substrates with either a 3-glycedoxypropyl trimethoxysilane monolayer or a layer of surface grafted PGMA were placed in Radley tubes and the tubes were evacuated and refilled with Nitrogen for three cycles. The solution was added to the Radley tubes. BF_3-diethyl etherate (0.10 mL, 0.79 mmol) was added to each tube and the reaction was left overnight.

The substrates were cleaned by a soxhlet extraction in ethanol overnight.
IR (SAMs): ν_{max}/cm^{-1}: 3050-2850 (aromatic C—H stretch, s), 2120 (nitrile C≡N stretch, w), 1720 (carbonyl C=O stretch, s), 1600 (conjugated C=C stretch, m), 1500-1340 (alkyl C—C stretch, s), 1300-1000 (O—C—C and C—O—C (asymmetric) stretches, s) 1000-870 (aromatic isolated C—H, s).
IR (Brushes): ν_{max}/cm^{-1}: 3070-2830 (aromatic C—H stretch, s, and epoxy C—H stretch, w); 2221 (nitrile C≡N stretch, w), 1750 (carbonyl C=O stretch, s), 1585-1525 (conjugated C=C stretch, m),1525-1350 (alkyl C—C stretch, m), 1300-1100 (O—C—C and C—C(=O)—O (asymmetric) stretches, s), 1100-1000 (primary alcohol C—OH stretch, m).

Treatment of hydroxy groups with isobutyryl chloride or decanoyl chloride A solution of isobutyryl chloride (2.4 mmol, 0.25 mL) or decanoyl chloride (2.4mmol, 0.5mL) in distilled dichloromethane (10mL) was added dropwise to a solution of pyridine (3.6 mmol, 0.3 mL) in distilled dichloromethane (20 mL) containing samples with TCNQ functionalized surface grafted polymers or

monolayers at 0 °C under a nitrogen atmosphere. The mixture was allowed to come to room temperature and left stirring under nitrogen for 16h.
IR (Brushes): ν_{max}/cm^{-1}: 3040-2900 (epoxy C—H stretch, w), 1750 (carbonyl C=O stretch, s), 1525-1350 (alkyl C—C stretch, m), 1300-1100 (O—C—C and C—C(=O)—O (asymmetric) stretches, s); 1100-1000 (primary alcohol C—OH stretch, m).

Treatment of hydroxy groups with silanes The silicon, FET and/or glass substrates with TCNQ functionalized monolayer or brush were placed in a crystallising dish and covered with 30 mL of Toluene. 300 μL of octadecyl trichlorosilane or pentyl dimethoxychlorosilane was added with a syringe and the solution was swirled. The dish was covered with aluminium foil and left overnight.
IR (Brushes): ν_{max}/cm^{-1}: 3070-2830 (aromatic C—H stretch, s, and epoxy C—H stretch, w); 2221 (nitrile C≡N stretch, w), 1750 (carbonyl C=O stretch, s), 1585-1525 (conjugated C=C stretch, m),1525-1350 (alkyl C—C stretch, m), 1300-1100 (O—C—C and C—C(=O)—O (asymmetric) stretches, s).

Fabrication of field effect transistors Thin-film organic field-effect transistors (OFETs) were fabricated in a dry nitrogen glove box environment by spin coating of either P3HT or PBTTT on top of pre-treated FET substrates.

References

[1] J. H. Burroughes, C. A. Jones, and R. H. Friend, *Nature* **335**, 137 (1988).

[2] A. G. MacDiarmid, *Angew. Chem., Int. Ed.* **40**, 2581 (2001).

[3] K. E. Ziemelis, A. T. Hussain, D. D. C. Bradley, R. H. Friend, J. Rühe, and G. Wegner, *Phys. Rev. Lett.* **66**, 2231 (1991).

[4] D. M. deLeeuw, M. M. J. Simenon, A. R. Brown, and R. E. F. Einerhand, *Synth. Met.* **87**, 53 (1997).

[5] R. J. Kline, M. D. McGehee, and M. F. Toney, *Nature Materials* **5**, 222 (2006).

[6] K. Pernstich, S. Haas, D. Overhoff, C. Goldmann, D. Gundlach, B. Batlogg, A. Rashid, and G. Schitter, *J. Appl. Phys.* **96**, 6431 (2004).

[7] H. Sugimura, K. Hayashi, N. Saito, N. Nakagiri, and O. Takai, *Appl. Surf. Sci.* **188**, 403 (2002).

[8] S. Kobayashi, T. Nishikawa, T. Takenobu, S. Mori, T. Shimoda, T. Mitani, H. Shimotani, N. Yoshimoto, S. Ogawa, and Y. Iwasa, *Nat. Mater.* **3**, 317 (2004).

[9] K. P. Pernstich, C. Goldmann, C. Krellner, D. Oberhoff, D. J. Gundlach, and B. Batlogg, *Synth. Met.* **146**, 325 (2004).

[10] L.-L. Chua, J. Zaumseil, J.-F. Chang, E.-W. Ou, P. K.-H. Ho, H. Sirringhaus, and R. H. Friend, *Nature* **434**, 194 (2005).

[11] R. J. Kline and M. D. McGehee, *Polymer Reviews* **46**, 27 (2006).

[12] H. Sirringhaus, R. J. Wilson, R. H. Friend, M. Inbasekaran, W. Wu, E. P. Woo, M. Grell, and D. D. C. Bradley, *Appl. Phys. Lett.* **77**, 406 (2000).

[13] G. M. Wang, J. Swensen, D. Moses, and A. J. Heeger, *J. Appl. Phys.* **93**, 6137 (2003).

[14] X. Zhou, M. Pfeiffer, J. Blochwitz, A. Werner, A. Nollau, T. Fritz, and K. Leo, *Appl. Phys. Lett.* **78**, 410 (2001).

[15] W. Y. Gao and A. Kahn, *Appl. Phys. Lett.* **79**, 4040 (2001).

[16] J. Blochwitz, T. Fritz, M. Pfeiffer, K. Leo, D. Alloway, P. Lee, and N. Armstrong, *Organic Electronics* **2**, 97 (2001).

[17] W. Y. Gao and A. Kahn, *Appl. Phys. Lett.* **82**, 4815 (2003).

[18] W. Y. Gao and A. Kahn, *Organic Electronics* **3**, 53 (2002).

[19] J. Blochwitz, M. Pfeiffer, T. Fritz, and K. Leo, *Appl. Phys. Lett.* **73**, 729 (1998).

[20] M. Pfeiffer, A. Beyer, B. Plönnigs, A. Nollau, T. Fritz, K. Leo, D. Schlettwein, S. Hiller, and D. Wohrle, *Sol. Energy Mater. Sol. Cells* **63**, 83 (2000).

[21] B. Maennig, M. Pfeiffer, A. Nollau, X. Zhou, K. Leo, and P. Simon, *Phys. Rev. B* **64**, 195208 (2001).

[22] R. Rawcliffe, *Chapter 3*, PhD thesis, Imperial College London, UK, 2006.

[23] H. Skulason and C. D. Frisbie, *Langmuir* **14**, 5834 (1998).

[24] H. Skulason and C. D. Frisbie, *J. Am. Chem. Soc.* **124**, 15125 (2002).

[25] M. L. Chabinyc, X. X. Chen, R. E. Holmlin, H. Jacobs, H. Skulason, C. D. Frisbie, V. Mujica, M. A. Ratner, M. A. Rampi, and G. M. Whitesides, *J. Am. Chem. Soc.* **124**, 11730 (2002).

[26] R. W. Day, G. Inzelt, J. F. Kinstle, and J. Q. Chambers, *J. Am. Chem. Soc.* **104**, 6804 (1982).

[27] I. Luzinov, D. Julthongpiput, A. Liebmann-Vinson, T. Cregger, M. D. Foster, and V. V. Tsukruk, *Langmuir* **16**, 504 (2000).

[28] S. Edmondson and W. T. S. Huck, *J. Mater. Chem.* **14**, 730 (2004).

[29] I. Luzinov, D. Julthongpiput, H. Malz, J. Pionteck, and V. V. Tsukruk, *Macromolecules* **33**, 1043 (2000).

[30] A. Olszewski-Ortar, P. Gros, and Y. Fort, *Tetrahedron Lett.* **38**, 8699 (1997).

[31] R. C. Wheland and E. L. Martin, *J. Org. Chem.* **40**, 3101 (1975).

[32] R. Silverstein, G. Bassler, and T. Morrill, *Spectrometric identification of organic compounds, fifth edition*, John Wiley & Sons, inc, 1991.

[33] I. Yagi, K. Tsukagoshi, and Y. Aoyagi, *Appl. Phys. Lett.* **86**, 103502 (2005).

[34] T. Solomons, *Organic Chemistry, sixt edition*, p.826, John Wiley & Sons, inc., 1996.

[35] Y.-J. Lin, Y.-C. Hong, J.-H. andLien, and B.-Y. Liu, *Appl. Phys. Lett.* **89**, 262110 (2006).

[36] G. Inzelt, R. W. Day, J. F. Kinstle, and J. Q. Chambers, *J. Phys. Chem.* **87**, 4592 (1983).

[37] I. McCulloch, M. Heeney, C. Bailey, K. Genevicius, I. Macdonald, M. Shkunov, D. Sparrowe, S. Tierney, R. Wagner, W. Zhang, M. Chabinyc, R. Kline, M. M.D., and M. Toney, *Nat. Mater.* **5**, 328 (2006).

[38] H. Sirringhaus, N. Tessler, and R. H. Friend, *Science* **280**, 1741 (1998).

[39] H. Sirringhaus, P. J. Brown, R. H. Friend, M. M. Nielsen, K. Bechgaard, B. M. W. Langeveld-Voss, A. J. H. Spiering, R. A. J. Janssen, E. W. Meijer, P. Herwig, and D. M. de Leeuw, *Nature* **401**, 685 (1999).

[40] X. Z. Wang, D. J. Zhou, T. Rayment, and C. Abell, *Chem. Commun.* , 474 (2003).

[41] R. J. Kline, M. D. McGehee, E. N. Kadnikova, J. S. Liu, and J. M. J. Fréchet, *Adv. Mater.* **15**, 1519 (2003).

[42] Y. Wu, P. Liu, B. Ong, T. Srikumar, N. Zhao, G. Botton, and S. Zhu, *Appl. Phys. Lett.* **86**, 142102 (2005).

[43] D. Kim, Y. Park, Y. Jang, H. Yang, Y. Kim, J. Han, D. Moon, S. Park, T. Chang, C. Chang, M. Joo, C. Ryu, and K. Cho, *Adv. Funct. Mater.* **15**, 77 (2005).

[44] C. Jarrett, R. H. Friend, A. Brown, and D. De Leeuw, *J. Appl. Phys.* **77**, 6289 (1995).

[45] M. Husemann, E. E. Malmström, M. McNamara, M. Mate, D. Mecerreyes, D. G. Benoit, J. L. Hedrick, P. Mansky, E. Huang, T. P. Russell, and C. J. Hawker, *Macromolecules* **32**, 1424 (1999).

Chapter 4

Surface-Grafted Polythiophenes using Polymer Brushes as a Template

Synopsis: In polymer electronics, performance is strongly correlated with molecular order. Surface-initiated growth of conjugated polymers could potentially improve the performance of devices like LEDs and photovoltaic cells. In this chapter a template assisted growth of surface-grafted polythiophenes is presented, allowing for selective grafting of the conjugated polymer. Thick layers (up to 150 nm) with low roughness were obtained, that show interesting and potentially useful properties as polychromism and fluorescence.

4.1 Introduction

There is a tremendous research effort to use organic and polymeric (semi-) conducting material in solar cells,[1,2] light emitting diodes (LEDs),[3,4] and field effect transistors (FETs).[5–7] Advantages include low costs, solution processing[3,8] and the possibility for patterning by soft lithographic techniques.[9–11] Polythiophene (PT) and its derivatives are of particular interest due their high mobilities of up to 0.1 cm^2/Vs, although this is critically affected by regioregularity[12] and molecular weight[13] resulting in variations of the mobility by several orders of magnitude.

4.1.1 Influences of molecular weight and morphology on charge transport

In photovoltaic cells and FETs, the performance is highly dependent on charge transport within the device. Generally regioregular polymers with (for conjugated polymers) relatively high molecular weights are chosen, that align to form well ordered structures.[14]

Without side chains, polymers are insoluble and have high melting points, so side chains of conjugated polymers are essential for processibility. However, the presence of these side chains reduces the intermolecular overlap and thus intermolecular charge transfer.[15]

Regioregular conjugated polymers are more planar, which results in a better packing and better intermolecular overlap. The influence of molecular weight on the mobility of P3HT has been investigated perpendicular to the substrate[16] and in the plane of the substrate.[13] In both cases the mobility increases with molecular weight, even though crystalline order is less for high molecular weight molecules. The increase in mobility with molecular weight is four orders of magnitude in the plane of the substrate and 'only' a factor 15 perpendicular to the substrate.

The mobilities measured for FETs along the channel are often a few orders of magnitude higher than for PV cells (measured perpendicular to the substrate), even when the same materials are used.[15] This is partially explained by the fact that the charge carrier density is much higher in FETs than in PV cells. Additionally it has been suggested that this is due to the orientation of the polymers. The polymer backbone preferentially aligns along the substrate. In regioregular, semicrystalline polymers the insulating side chains then orient perpendicular to the substrate, reducing the efficiency of charge transport in that direction.[12] To enhance the charge transport perpendicular to the substrate. Coakley *et al.* used this knowledge by infiltrating P3HT into pores of alumina.[17] The resulting hole mobility was improved by more than an order of magnitude.

McCullough route

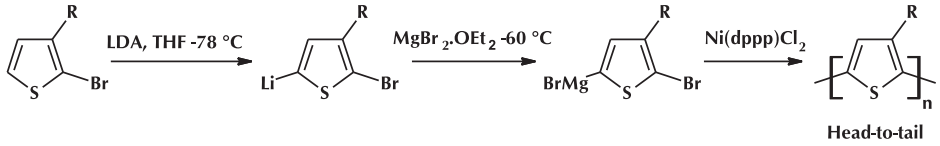

Rieke route

Scheme 4.1

4.1.2 Synthesis of polythiophenes

Three main routes exist for the synthesis of polythiophenes, namely electrochemical coupling of thiophenes, oxidative coupling of thiophenes and organometallic coupling of 2-halo-5-metallo di-substituted monomers. Two approaches in the last class have been developed by Rieke[18] and McCullough (scheme 4.1).[19] Whereas McCullough *et al.* polymerized 2-bromomagnisio-5-bromothiophene using a nickel catalyst, Rieke and co-workers used zinc instead of magnesium in the organometallic group. Both methods yield very regioregular head-to-tail polymers.

Electrochemical polymerization is assumed to proceed via the coupling of two radical cations, as shown in the top half of scheme 4.2.[20] The dimer has a lower oxidation potential and is hence more easily oxidized. The polymer deposits in its oxidized, conducting form on the electrode and allows the polymerization to proceed. This has the advantage that electrochemical polymerization will mainly be limited to the surface of the electrode. Regioregularity is not controlled with electrochemical polymerization and some 2,4-coupling does occur.[21]

Oxidative polymerization initiates with the oxidation of the thiophene by ferric chloride and is assumed to then proceed via proton elimination to the coupling of the neutral radical to a thiophene (see bottom half of scheme 4.2).[21,22] Again the dimer is more easily oxidized. The reaction only takes

place in solvents that do not dissolve ferric chloride completely and it is suggested that the polymerization requires solid ferric chloride. A ratio of 4:1 ferric chloride to thiophene is normally used, as part of the ferric chloride is consumed by complexation with HCl formed in the reaction. This method is partially selective toward head-to-tail coupling and the regioregularity can be increased by performing the reaction at low temperatures with low monomer concentration[23] or by slow addition of $FeCl_3$.[24]

Cross-linking can occur in 3-alkylthiophenes via the side chain α-alkyl position.[25] Also some coupling at the 4-position of the thiophene has been reported and results in non-linear PT and thus limitation of the conjugation length.

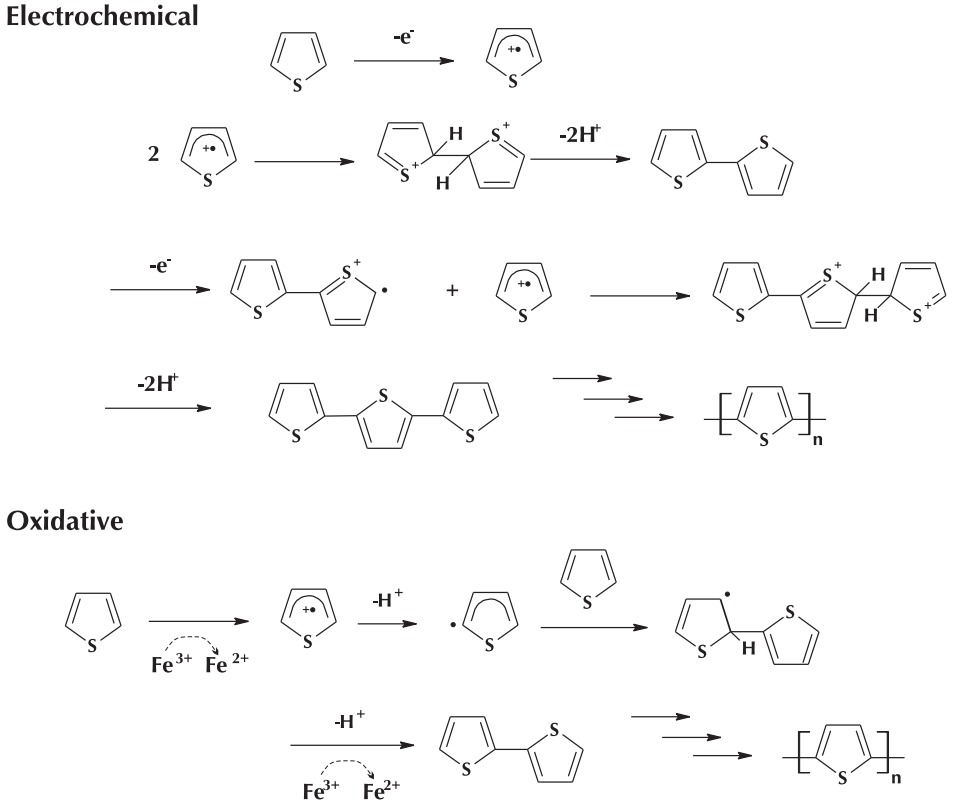

Scheme 4.2

4.1.3 Thiophene polymerization from inorganic substrates

The deposition of conjugated polymers is usually done by solution processing, i.e. inkjet printing[26], screen printing,[27] doctor blading,[28] layer by layer self-assembly[29] or spin coating.[1] However: this is only possible for soluble polymers. Polymers without side chains like unsubstituted PT can not be processes in this way. The way to obtain an insoluble polymer on the surface is to either precipitate it onto the substrate during synthesis or to grow it directly from the surface. As we have seen, when solution processed, the orientation of the thiophenes with reference to the substrate is usually in the plane of the substrate. Growing the polymer from the surface would result in an orientation perpendicular to the substrate, which would be advantageous for applications in solar cells or LEDs.

Surface-confined polymerization of PT is often started with the deposition of a thiophene functionalized monolayer. The deposition of thiophene functionalized monolayers has been described in detail by Appelhans *et al.*[30] and Berlin and Zotti.[29]. In their approach the deposition of the monolayer was followed by either electropolymerization[31,32] or oxidative polymerization of thiophene.[21,33]. Fikus *et al.* started with depositing a undecyl trichlorosilane with a thiophene end group,[33] followed by oxidative polymerization of thiophene. The concentration of the thiophene monomer and of $FeCl_3$ was varied, resulting in a variation of the thickness of the PT layer. However: only the thin films (3.7 nm) were relatively smooth, the thicker films (up to 34 nm) showed a porous network of polymer chains. Zotti reported patterned polymers from thiophene derivatives of up to 15 nm grown by electropolymerization from terthiophene SAMs on gold and ITO.[31] Kang reported PT grown by electropolymerization from a monothiophene functionalized silane monolayer on indium tin oxide (ITO), but unfortunately did not report film thicknesses.[32]

Other approaches for the deposition of a monolayer have been reported as well. Kumru synthesized PT, polypyrrole and polycarbazoles grown from carbon fibers.[34] The first step in that case was "electro-deposition". The resulting polymer coating on the fibers is 1.7 μm thick, a thickness not reported so far (to the authors knowledge) for flat substrates of silicon, gold or ITO. Labaye *et*

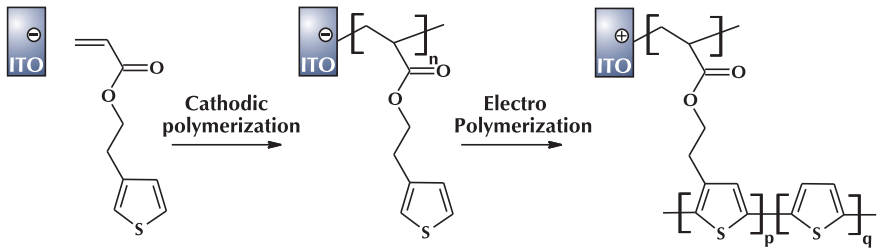

Scheme 4.3: Surface grafted polythiophenes as obtained by the approach of Labaye. First an acrylate functionalized thiophene was electrografted followed by cathodic polymerization of this thiophene derivative. Then PT was grown by electro-polymerization.

al. used cathodic electro-grafting of the first acrylate functionalized thiophene to ITO followed by cathodic polymerization of the acrylate functionality and finally growth of PT from this template by electropolymerization (scheme 4.3).[35] This resulted in inhomogeneous deposition of PT humps of about 1 μm wide and 1 μm high.

4.1.4 Co-polymers with polythiophene functionality

Polythiophenes on polymeric substrates and co-polymers with a polythiophene block have also been reported. Xia *et al.* coupled alkene functionalized thiophenes to a polysiloxane backbone followed by electrochemical polymerization to form cross-links.[36]

Guner *et al.* synthesized a random co-polymer from a thiophene functionalized methacrylate (methylthienyl methacrylate, MTM) and a methyl methacrylate by free radical polymerization and use this as a template for PT growth by electropolymerization.[37] The resulting graft co-polymers PMMA-*co*-MTM-*graft*-PT showed a conductivity of $4\ 10^{-1}$ S cm^{-1}, an increase by more than two orders of magnitude compared to the template polymer PMMA-*co*-PTM which had been electrochemically treated under the same conditions.

Çirpan *et al.* used a methacrylate functionalized thiophene homopolymer to synthesize a polymer by free radical polymerization and then grew grafts of PT and polypyrrole from this polymer by oxidative and electrochemical polymerization.[38]

Bergbreiter *et al.* obtained oligothiophenes in hyperbranched grafts on polyethylene by first grafting poly-*tert*-butacrylate onto polyethylene followed by

conversion of the butacrylates into acrylic acids, then post-functionalizing by a condensation reaction with amine functionalized thiophenes.[39] Finally the side-chain thiophenes were oligomerized with ferric chloride.

Patterned surface-grafted PT has been reported by Fabre and Wayner[9], who used a technique based on photo-etching before deposition of a thiophene functionalized monolayer, Hagberg and Carter[40], who used nanocontact molding of a supporting thiophene functionalized acrylate matrix, and Zotti *et al.*,[31] who used micro-contact printing (μCP).

To summarize, many approaches to grow polythiophenes from inorganic substrates or polymers have already been suggested in literature. It seems to be essential that the thiophene monolayer at the graft substrate is dense or that the concentration of these units at the surface of a polymer is high to yield homogeneous films of polythiophene. Even then, thick layers seldom show low surface roughness at the same time. Promising techniques of using thiophene functionalized poly(meth)acrylates have been applied to bulk polymers but have not yet been successfully translated in surface-grafted polymers.

As we have seen in the introductory chapter, polymer brushes have been suggested to form dense layers and can easily be combined with facile patterning techniques like photo-deposition and μCP. In this chapter the surface-initiated polymer growth of thiophene functionalized polymethacrylates will be discussed, followed by the synthesis of PT and polythiophene derivatives using the thiophene units on the substrate as starting units or "template". Template assisted deposition would allow selective deposition of a semiconducting polymer, which could find many applications in polymer electronics. The aim is to form thick (in the order of 100 nm) and smooth layers of the conjugated polymer in combination with patterning by μCP.

4.2 Surface-initiated polymers of thiophene functionalized methacrylate.

A grafting template based on surface-initiated polymers was chosen as these polymers are shown to form dense layers.[41] In the case of thiophene functionalized polymers this would mean that there is a high concentration of thiophene units at the surface available for template assisted polymerization of thiophene in a next step.

The monomer 3-ethylthienyl methacrylate (EThMA) was synthesized by a condensation reaction of 3-thiophene ethanol with methacryloyl chloride in the presence of triethylamine and was obtained in a 73% yield (see the top reaction in scheme 4.4). The methacrylate functionalized monomer was chosen preferentially over an acrylate as in radical polymerization the radical is more stabilized in methacrylates.

Glass, quartz, silicon, ITO and titanium dioxide were used as substrates for surface-initiated polymerization. First a monolayer of initiator molecules was deposited by immersing the substrates in a dilute solution of the initiator silane. As the covering with silanes is relatively low on ITO and titanium dioxide due to the intrinsic roughness of the substrates and especially low on

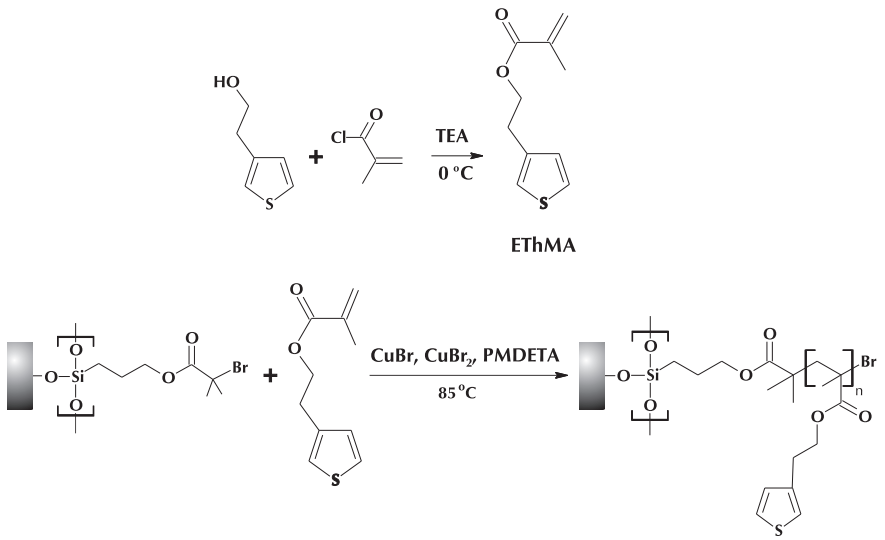

Scheme 4.4

ITO due to the low concentration of hydroxyls at the surface,[42] these substrates were left to react for three days, whereas the other substrates were removed from solution after reaction overnight.

Surface-initiated polymerization of EThMA was performed on silicon to optimize the reaction conditions (bottom reaction in scheme 4.4). Different reaction conditions were investigated by varying the copper(I) bromide and copper(II) bromide concentrations and the reaction temperature. The reaction conditions used eventually were copper(I) bromide and copper(II) bromide as catalytic activator/deactivator system with N,N,N',N",N"-pentamethyl diethylenetriamine (PMDETA) as ligand with a CuBr:$CuBr_2$:PMDETA:EThMA molar ratio of 1:0.5:20:400 at a concentration of the monomer of 2.86 mol/L with regard to the volume of DMF (the total volume increases by ±50% upon addition of the monomer). Surface initiatted ATRP generally has faster kinetics in solvents with high dielectric constants.[43] DMF was chosen as a solvent for this polymerization as it combines this property with being a good solvent for the resulting polymer.

The time resolved growth of PEThMA brushes is plotted in figure 4.1 for several conditions. The reaction kinetics are enhanced by increasing the tem-

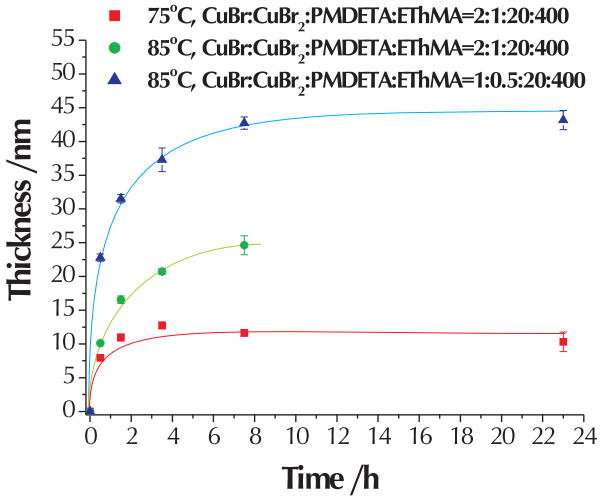

Figure 4.1: Surface-initiated growth of PEThMA.

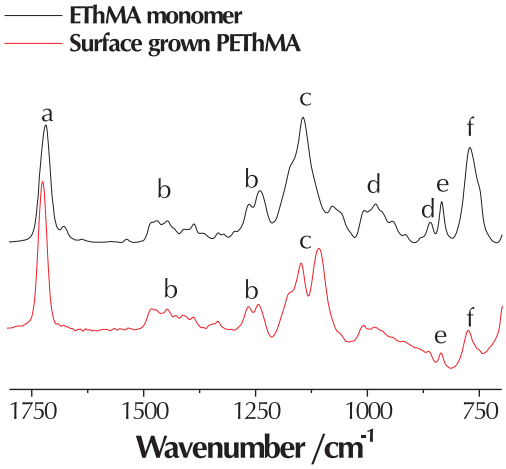

Figure 4.2: FT-IR spectrum of surface-initiated PEThMA, template assisted PT on PEThMA and PT by solution polymerization. The compound specific absorption bands and regions are indicated: a: Carbonyl C=O stretch; b: aromatic C=C stretch, stretching vibrations of thiophene ring; c: C—C(=O)—O (asymmetric) stretches; d: Vinyl out of plane C—H bends; e: C_α—H out of plane bending of 3- substituded thiophene; f: C—H in phase out-of-plane wag of monosubstituted thiophene.

perature up to 85 °C. Above that temperature brush growth becomes slower again. The colour of the solution above this temperature changes to a different shade of blue, which is an indication for dissociation of the catalyst ligand complex. Also thicker polymers can be grown if the concentrations of both of the copper bromides is brought down and the ratio between ligand and catalyst is increased. This enhances the formation of the active complexes. In the IR-spectrum (figure 4.2) of the surface-grown PEThMA the characteristic peaks for the methacrylate backbone (the carbonyl and the ester bands) can be seen as well as the characteristic bands for the thiophene unit (the aromatic ring stretches and the aromatic proton bends), which confirms the synthesis of the thiophene functionalized polymethacrylate brush.

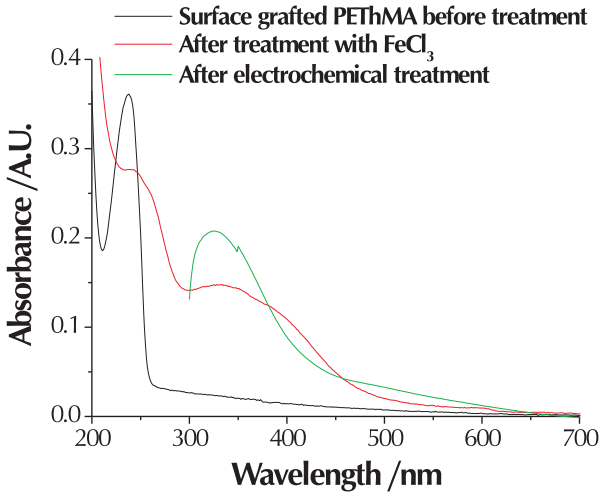

Figure 4.3: UV spectroscopy before and after chemical and electrochemical oxidative oligomerization of the thiophene moieties in a pEThMA polymer brush. Electrochemical polymerization was performed on ITO. The spectrum of this substrate is cut-off at 300 nm, below which the substrate is non-transparent. Polymerization by treatment with ferric chloride was performed on quartz.

4.3 Oligomerization of thiophene units in the brush layer

As has been discussed in the introduction to this chapter, the thiophene side chains of a methacrylate polymer can be coupled to form thiophene oligomers by chemical or electrochemical oxidation and followed by elimination of two protons. Both methods of oxidative coupling were performed on PEThMA polymer brushes.

Figure 4.3 shows the effect of wet chemical oxidation with $FeCl_3$ and electrochemical oxidation using cyclic voltammetry on the UV/Vis absorbance of the surface-grafted polymer. It can be observed visually that the colourless film has turned slightly yellow after either treatment. Before oxidative treatment the surface polymer only shows the typical absorption of thiophene at 230nm.[44] Upon coupling by treatment with $FeCl_3$ or electrochemical treatment using cyclic voltammetry the conjugation length increases and this is vis-

ible in the spectrum as absorbance at higher wavelengths. The increase in the conjugation length is however small, up to ~420 nm (maximum at 340 nm) for electrochemical treatment and ±470 nm for treatment with ferric chloride. These values are significantly below the absorbance for surface grafted polythiophenes reported in the literature, which has an absorption maximum in the range of 370-430nm and an onset around 520-550nm.[29,31] The absorbance for the mono-thiophene stays clearly distinguishable at 230 nm.

Oxidative coupling does not have to be limited to the pendant thiophenes of just one polymer backbone. Oxidative coupling will thus result in cross-links between different polymer strains on the substrate. Besides, because the thiophene units do not have the same dimensions as the corresponding methacrylate unit in the backbone, cross-linking the thiophene units imposes a high strain on the backbone and is therefore unlikely to occur with a high yield. This explains why the increase in conjugation length is limited.

4.4 Surface-grafted polythiophenes using the brush as a template for growth

Several examples of applying thiophene functionalized polymers and monolayers as a starting point or "template" for subsequent polymer growth have been mentioned in the introduction to this chapter. This involves electrochemical or oxidative chemical polymerization under addition of extra thiophene. Oxidative polymerization with ferric chloride has the advantage that polymerization from the surface is limited to the places where the brush layer is deposited, making patterns of PT possible, whereas radicals created near the surface by electropolymerization can also graft to the surface in other areas.[35] However: oxidative polymerization can not be limited to the surface as also the thiophenes in the solution will be oxidized and hence can react with other thiophenes.

By treating the polymer brush with ferric chloride before the addition of the monomer, oligothiophenes can already be created in the brush layer, which will be oxidized easier than the monothiophenes that are added, giving the polymerization at the surface a head-start over polymerization in solution.

Adding the ferric chloride to the substrates before adding the monomer is opposite to the majority of procedures mentioned in literature, but was chosen deliberately because of this advantage and because the disadvantage, forming more regio-irregular PT, does not play a role with unsubstituted thiophenes.

Additionally, the thiophenes in the brush layer are substituted thiophenes. Due to the electron donating character of the alkyl at the 3-position, these thiophenes are more readily oxidized than unsubstituted thiophenes. This adds to the templating effect of the brush layer. This templating effect is schematically shown in scheme 4.5, together with the formation of oligothiophenes within the brush layer.

After reaction an additional polymer layer had polymerized on top of the brush layer. This layer has been characterized by ellipsometry and atomic force microscopy (AFM) and is, depending on the reaction conditions, up to 20 nm thick. The film is stable under ultrasonic washing with a variety of solvents, soxhlet extraction with dichlorobenzene and scotch tape test.

Figure 4.4 shows the topographical images on the surface-grafted

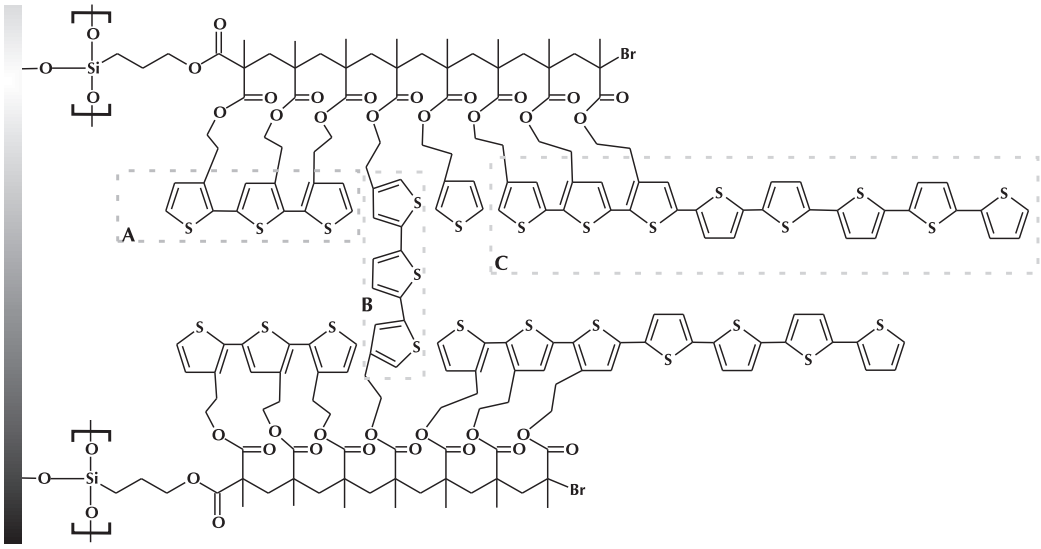

Scheme 4.5: The formation of oligothiophenes by crosslinking of the thiophene side-chains within one single polymer backbone (A) and between two polymer backbones (B) and the templating effect for subsequent polythiophene growth from the oligomerized thiophene side-chains (C).

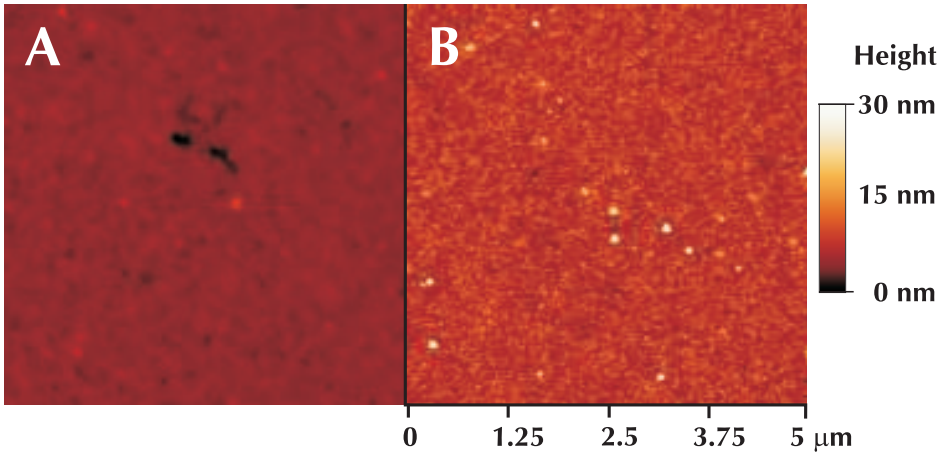

Figure 4.4: Topographic AFM on A) a PEThMA brush and B) PT grown from this template.

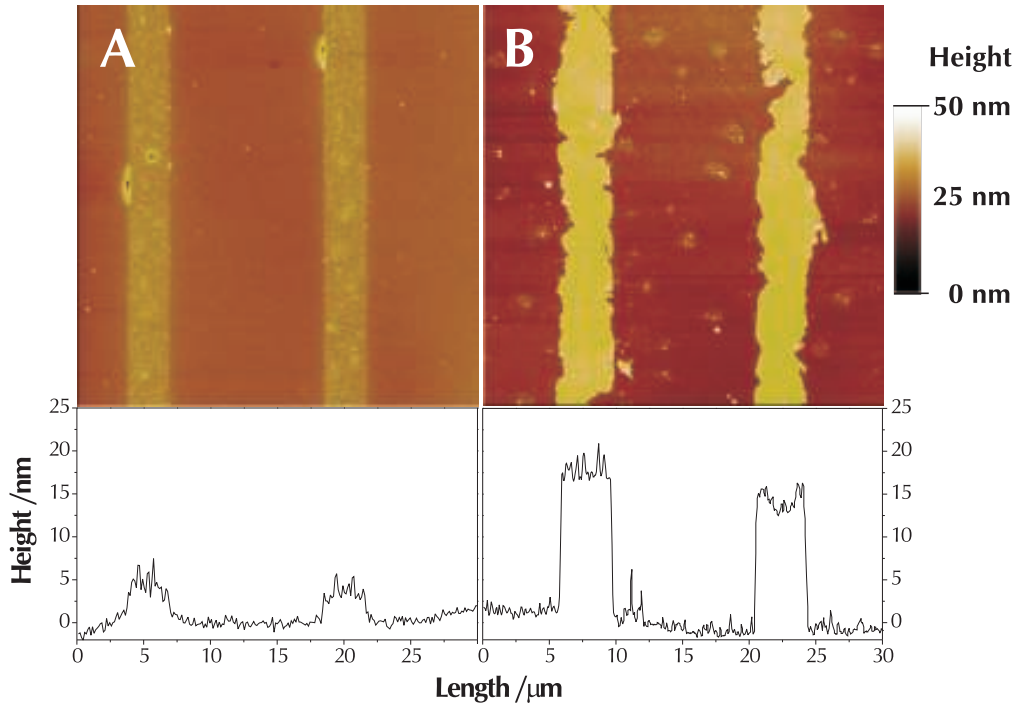

Figure 4.5: A) Topographic AFM on a patterned PEThMA brush B) the patterned brush has served as a template for subsequent PT growth from the surface.

PEThMA polymer and on the PEThMA-PT co-polymer layer. It can be seen that the surface roughness does increase. This is partly caused by small crystallites of bulk polymer that have precipitated from solution. However these layers are still much more homogeneous and thicker than thiophene functionalized monolayers reported in the literature.[33]

To prove the role of the polymer brush template on the deposition of PT, μCP was used to selectively deposit a patterned initiator monolayer for surface-initiated ATRP on silicon substrates. A pattern of 5 μm lines at a 15 μm pitch was used. After the growth of PEThMA brushes these substrates were used for template assisted polymerization of thiophene. This resulted in a pattern of deposited polymer, which was characterized by AFM (see figure 4.5). The topographical image clearly shows that surface-grafted PT only grows from areas where thin films of surface-initiated PEThMA was present and is proof for the template function of the polymer brush.

The IR spectrum of template grown PT on PEThMA is shown together with the PEThMA spectrum in figure 4.6. A strong difference with the spectrum of PEThMA itself is the disappearance of the peak at 775 cm^{-1} which is associated with the C—H in phase out-of-plane wag of monosubstituted thiophenes,[45] and the appearance of a peak at 790 cm^{-1} which is associated with 2,5-coupling of the thiophenes and is also visible in the PT that precipitated out of solution. The solution polymer also shows a small band around 830-850 cm^{-1}, which could be an indication for some non-linear coupling.

In optimising reaction conditions it was found that dichloromethane as a solvent gave the best surface polymerization results. It is suggested in the literature that solid ferric chloride particles should be present for the reaction to proceed.[22] It was found however, that the polymerization also proceeds when only the clear yellow solution above precipitated ferric chloride was used in the reaction, or even filtered with a 1μm filter. The use of these saturated solutions instead of precipitates strongly enhanced the reproducibility. The concentration of the saturated solution was measured by evaporation of the solvent and was approximately 15 mM. It is still possible that $FeCl_3$-microcrystals were still present in this solution and were responsible for the initiation of the reaction.

In a preliminary experiment, template assisted polymerization was also

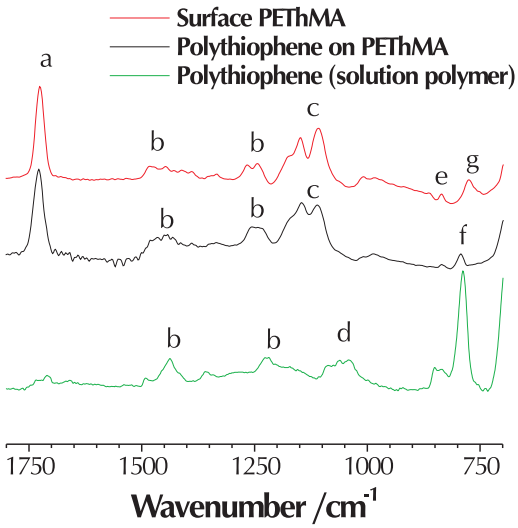

Figure 4.6: FT-IR spectrum of surface-initiated PEThMA, template assisted PT on PEThMA and PT by solution polymerization. The compound specific absorption bands and regions are indicated: a: Carbonyl C=O stretch; b: aromatic C=C stretch, stretching vibrations of thiophene ring; c: C—C(=O)—O (asymmetric) stretches; d: Thiophene C—H in plane bending; e: C_α—H out of plane bending of 3- substituted thiophene; f: C-H_β out of plane bending of 2,5-disubstituted thiophene; g: C—H in phase out-of-plane wag of monosubstituted thiophene.

performed with 3,4-ethylene-dioxy-thiophene (EDOT), of which the polymer is a highly transparent conductive polymer. After polymerization the PEDOT layer was not visible by eye, but the formation of an extra layer of 28±1.8 nm was confirmed by ellipsometry.

4.4.1 Influence of thiophene concentration on film thickness and re-initiation.

The concentration of thiophene for template assisted polymerization was optimized. The concentration of monomer in the solution that resulted in the highest surface-grafted PT thickness was 0.4 M as can be seen in figure 4.7. This means that in this case thiophene is in a huge excess, opposed to the 4:1 excess of $FeCl_3$ suggested in literature. However: it can be seen that further

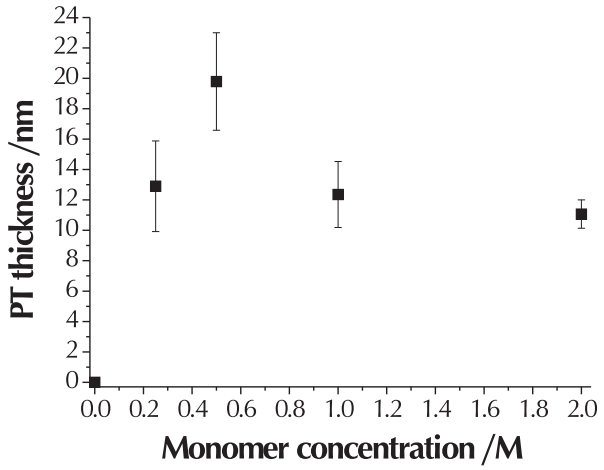

Figure 4.7: Monomer concentration dependency of the thickness of template assisted grown polythiophene.

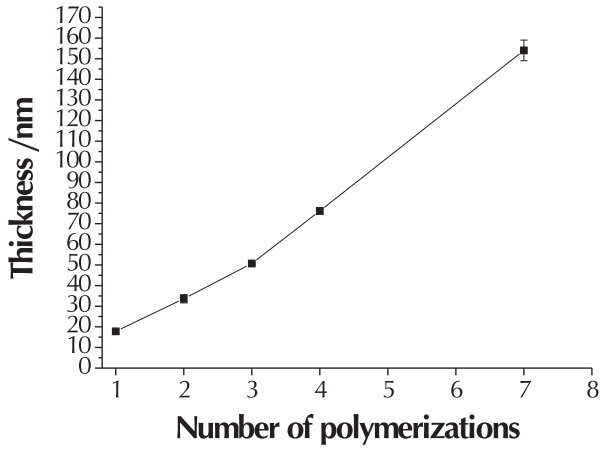

Figure 4.8: Increase in polymer thickness for template grown PT upon re-initiated polymerization. The thickness is ellipsometric thickness of the total layer without the original PEThMA brush layer.

reduction of the thiophene concentration results in less thick polymer layers due to depletion of monomer.

The growth of PT layers can be re-initiated, using the PT layer grown in a first step as template in a second oxidative polymerization of thiophene. For PT the average increase of thickness in each step was 22 nm and a total layer thickness of 154 nm was achieved in seven steps (no more steps were attempted, see figure 4.8). By AFM these thick layers seemed to have the same overall roughness as the thin layers, although defects and bulk polymer crystallites were more prominent.

4.5 Optical characterization and polychromic behaviour

Polychromic behaviour, the change of colour upon chemical or electrochemical stimuli, is often observed for polythiophenes and polythiophene derivatives. Upon oxidation of PT the colour changes from the usual red/orange to dark blue/grey. This chemical doping of polythiophenes to obtain colour change has been extensively studied.[45–48] Reversible colour change was also observed for template grafted PT. After the chemical oxidation reaction the films is highly doped and appears blue-grey. Upon reduction, by either wash-

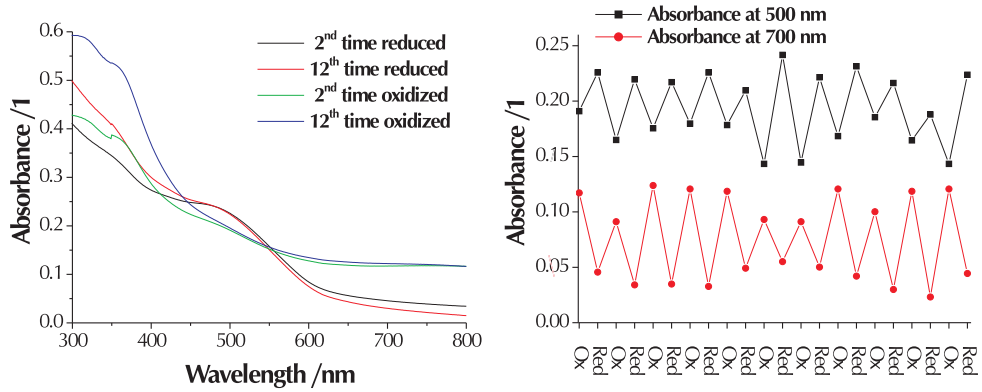

Figure 4.9: UV/Vis spectrum of a grafted PT film. The film is oxidized by $FeCl_3$ and reduced by hydrazine for over 10 cycles.

ing in ammonia or a hydrazine/chloroform emulsion the films turn orange-red. This colour change is reversible as can be observed from the UV/vis absorbance traces in figure 4.9, although the reversibility of the colour change below 400 nm seems to decrease after about 10 oxidations and reductions. To obtain electro-chromic devices with patterned colour changing "pixels" patterned template grafted PT could be combined with an electrolyte and patterned electrodes. This was however beyond the scope of this research.

If the UV/Vis absorption spectrum of PT grafted on top of PEThMA is compared to the spectrum of PEThMA alone (figure 4.3 on page 97), it can be seen that the absorbance has shifted considerably to the red. This is caused by an increase in conjugation length, which lowers the band gap of the polymer. These values are comparable with values reported for bulk (insoluble) polymer, but are significantly higher than values for other surface grafted polythiophenes reported in the literature (absorption maximum 370-430 nm and onset 520-550 nm).[29,31] This suggests that the layers fabricated in this study are of higher conjugation length.

4.6 Fluorescence

Under illumination with UV/blue light, the PT layer shows fluorescence. On patterned substrates this results in patterned fluorescence as is shown in the

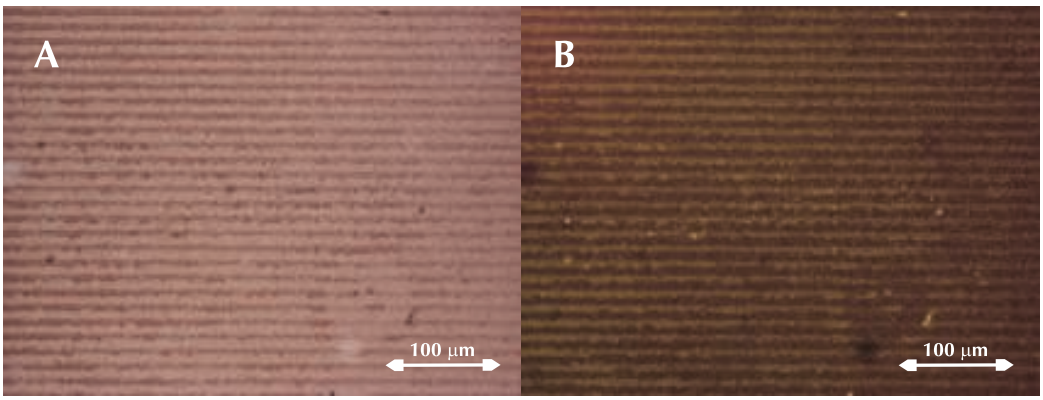

Figure 4.10: Fluorescence microscopy on thiophenes grown from a patterned brush A) normal illumination B) illumination with violet/blue light 450-490 nm filter: DM 505 BA 520 nm.

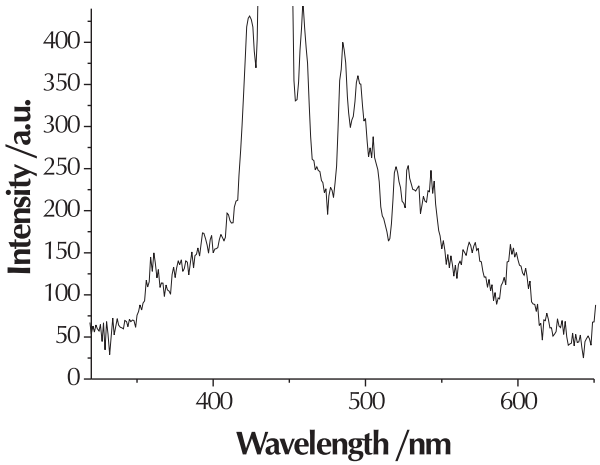

Figure 4.11: Photoluminescence spectrum for thiophenes grown from a thiophene functionalized polymer brush at $\lambda_{ex} = 220$ nm.

microscope image in figure 4.10. This clearly shows that the sample only shows fluorescence in the areas where first the initiator was deposited, then the polymer brush was grown and finally PT was grown by template assisted polymerization from the brush. Fluorescence is normally quenched in highly ordered films, which suggests that the films prepared in this way are amorphous, which is in contrast to what is normally expected in the case of polymers grafted *from* the surface.

The fluorescence was further investigated by photoluminescence spectroscopy (PL).* The photoluminescence spectrum is shown in figure 4.11. The spectrum shows that the sample fluoresces from 350 - 650 nm with a maximum around 425 nm, which means it emits light in almost the entire visible spectrum, with a maximum in the blue. This maximum occurs at a much higher energy than values reported in literature, where 550 nm is reported for a comparable surface grafted polythiophene.[39] The spectrum also shows narrow bands of higher emission. It is well known that luminescence spectra originating from thin films can be distorted due to interference effects, which

*Photoluminescence spectra were recorded by Saghar Khodabakhsh, Melville laboratory of Polymer Chemistry/Cavendish Laboratory, University of Cambridge, Cambridge, United Kingdom.

can explain these spikes.[49] One of these bands, the peak at 440 nm is an artefact of the double excitation wavelength.

Patterned deposition in combination with fluorescence makes this a potentially interesting technique for polymer-LED displays.

4.7 Electrochemical characterization

A surface-grafted PEThMA-PT layer on TiO_2 was analysed with cyclic voltammetry (CV, see figure 4.12). The substrate used had a PT layer of 50 nm on top of a PEThMA brush of 20 nm. The upper limit of 1.75 V for the CV measurement was chosen as there are reports of over-oxidation above 1.8 V.[32] The voltammogram shows that oxidation of the polymer takes place already at approximately 0.0 V with respect to the $Ag/AgNO_3$ electrode. This corresponds to ∼0.29 V *vs.* SCE. Typically, an adjustment value of ∼4.6 eV is used in converting energy values *vs.* SCE into energy values *vs.* vacuum. Therefore, the HOMO level is estimated to be ∼4.9 eV. This corresponds well with values reported in literature (HOMOs of 4.2 to 5 eV).[50,51]

The polymer layer is stable over more than 30 sweeps.

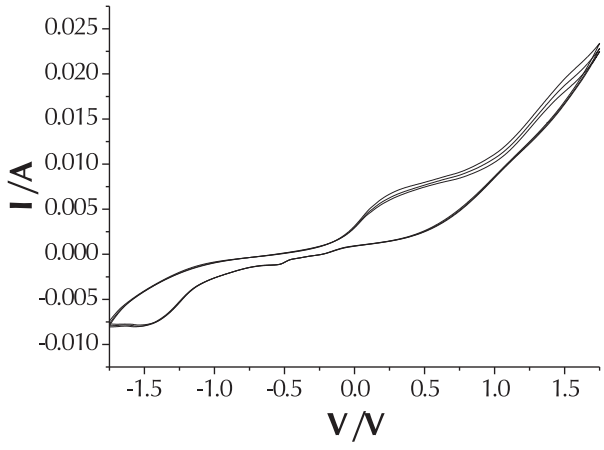

Figure 4.12: Cyclic Voltammetry on surface-grafted polythiophene. Reference electrode $Ag/AgNO_3$.

4.8 Conclusions

Surface-initiated polymers of PEThMA can function as a template to stimulate growth of PT and polythiophene derivatives directly from the surface by a facile wet-chemical oxidative polymerization. This technique can be combined with μCP to obtain patterned surface-grafted PT. Grafted PT layers obtained in this way are typically 20 nm thick. Layers of up to 154 nm thick were obtained by repeating the thiophene growing step. The controllable thickness and low roughness are an improvement over existing procedures.

These PT layers are easily doped and show polychromism upon doping. This colour change, the photoluminescence and the possibility to obtain patterned features using soft lithographic techniques make this method potentially attractive for electronic device fabrication.

4.9 Materials and methods

General procedures

Oven dried glassware was used for all reactions in non-aqueous solvents.
Ellipsometric measurements on monolayers and untreated polymer brushes were carried out using either an EL X-02C ellipsometer from Dr Riss Ellipsometerbau GmbH with a 632.8 nm laser at 70° angle of incidence or a JA Woollam Alpha-SE spectroscopic ellipsometer. In case of the monochromatic ellipsometer refractive indices of 1.50 and 1.45 were used for polymer and initiator layers respectively, in case of the spectroscopic ellipsometer a model with two Spline layers and one Cauchy layer on top of a silicon oxide layer was used.
FT-IR spectra of compounds were recorded on a Perkin Elmer Spectrum One FT-IR Spectrometer equipped with a Universal ATR sampling accessory.
FT-IR spectra of surface-initiated polymers were recorded using a Bio-Rad FTS 6000 spectrometer. Spectra of surface-initiated polymers were taken in transmission mode using a background of the same bare Si wafer that was used for polymer growth.
Plasma oxidation of substrates was performed in air in an Emitech K1050X plasma oxidizer for 10 minutes at 100 W.
^{1}**H-NMR and** ^{13}**C-NMR** spectra were recorded on a 400 MHz Bruker Avance 400 QNP Ultrashield or a 500 MHz Bruker Avance 500 Cryo Ultrashield in $CDCl_3$ using tetramethylsilane as an internal reference.
Mass spectrometry was performed on a Bruker Daltonics FTICR Bioapex II by electron spray ionization with detection of the positive ions (ESI+).
UV/Vis spectra were recorded on a Varian Cary 4000 UV/Vis Spectrometer. Spectra were recorded on quartz, unless stated otherwise and were recorded using a bare substrate as a reference.
Photoluminescence emission spectra[†] were recorded at room temperature using a spectrograph with an optical fiber input coupled to a cooled charge

[†]Photoluminescence spectra were recorded by Saghar Khodabakhsh, Melville laboratory of Polymer Chemistry/Cavendish Laboratory, University of Cambridge, Cambridge, United Kingdom.

coupled device array (Oriel Instaspec IV). The system response was calibrated using a tungsten lamp. Excitation for the photoluminescence was from the multiline UV mode of an argon ion laser.

Atomic Force Microscopy was performed on a Digital Instruments Nanoscope® Dimension™3100 Atomic Force Microscope. Both topographical and phase images were recorded.

Cyclic voltammetry experiments were conducted at room temperature on a Autolab PGStat30 Potentiostat/Galvanostat on coated ITO or TiO_2 samples. The electrochemical cell was purged with nitrogen before the scan was started and scans were taken under and atmosphere of nitrogen. The electrolyte was 0.1 M tetrabutylammonium hexafluorophosphate (TBAHP) solution in acetonitrile. The reference electrode was an $Ag/AgNO_3$ non-aqueous wire electrode. Scans were taken with -2.0 V as minimum potential and 1.8 V as maximum potential. Scan speed was 100 mV/s. The Fc/Fc^+ signal was observed at 0.093V which means that the $Ag/AgNO_3$ electrode has a redox potential of 0.29 V vs. SCE.

Light microscopy was performed at room temperature on a Nikon Eclipse ME600 microscope with a Nikon DN100 digital net camera connected to a computer.

Materials

Dow Corning Sylgard 184 Base silicon elastomer and Sylgard 184 Silicon curing agent were purchased from VWR. All other chemicals were purchased from Aldrich, Lancaster or Fisher and used as received unless stated otherwise. Copper (I) bromide was of 99.999 % purity and was stored *in vacuo*. Triethylamine, Dichloromethane and toluene were distilled prior to use. Methanol and ethanol were Analytical Reagent grade and used as received. The trichlorosilane initiator (2-bromo-2-methylpropionic acid 3-trichlorosilanylpropyl ester) was synthesized in the lab[‡] following a reported procedure,[52] however using allyl alcohol instead of 5-hexene-1-ol. PDMS Stamps were fabricated following reported procedures.[11] Silicon wafers were

[‡]This synthesis was performed by Andy Brown and Ron Oren, Melville Laboratory for Polymer synthesis

obtained from Compart Technology Ltd. (100 mm diameter, phosphorous-doped, <1 0 0> orientation, polished on one side).

Immobilization of the initiator monolayer on the substrate Silicon and TiO_2 wafers were plasma oxidized before functionalization. Glass and ITO samples were sonicated for 2 minutes in a soap solution, subsequently for 2 minutes in demineralized water and finally for 2 minutes in ethanol and dried in a nitrogen stream. After this physical cleaning step they were oxidized in the plasma oxidizer. For initiation of the entire surface, the silicon and/or glass substrates were placed in a crystallising dish and 30 mL of dry toluene, 50 μL of triethylamine and 10 μL of the trichlorosilane initiator was added. The dish was covered with foil and left overnight at room temperature. The wafer was then washed sequentially with toluene, distilled acetone and absolute ethanol and dried under a nitrogen stream. For a patterned immobilization of the initiator monolayer on glass substrates by micro-contact printing, a flat piece of PDMS was used as an "ink pad". This piece was soaked in a solution of 5 μL of the trichlorosilane initator in 20 mL of hexane and blown dry in a nitrogen stream for 60 s. A patterned PDMS stamp was inked by putting it on the flat piece of PDMS and leaving it for 30 s without applying additional pressure. The stamp was than transferred to a silicon or glass substrate and left there for 30 s without applying additional pressure. The substrate with the pattern of trichlorisilane initiator was then rinsed with subsequently hexane, dichloromethane and ethanol and dried in a stream of nitrogen.

Synthesis of 3-Ethylthienyl Methacrylate (EThMA) A solution of methacryloyl chloride (84.2 mmol, 8.80 g) in distilled dichloromethane (50 mL) was added drop-wise to a mixture of 2-(3-thienyl)ethanol (70.2 mmol, 9 g) and distilled triethyl amine (140 mmol, 19.6 mL) in distilled dichloromethane (100 mL) at 0 °C, under a nitrogen atmosphere. The mixture was allowed to come to room temperature and left stirring under nitrogen for 18 h. The reaction was quenched with 100 mL 0.01 M aqueous hydrochloric acid. The organic layer was collected and the aqueous layer was extracted with DCM. The combined organic layers were washed with subsequently an aqueous saturated sodium bicarbonate solution and brine. The organic layer was dried over anhydrous magnesium sulfate, filtered and the solvents were evaporated. The compound was purified by column chromatography over silica using ethyl ethyl acetate

(3-10%) in PET-ether (40:60) as an eluent and obtained as a colourless oil. Yield: 9.85g (73%)
^{1}H-NMR ($CDCl_3$) : 7.25 (dd, 1H, Th–*H*), 7.02 (m, 1H, Th–*H*), 6.97 (dd, 1H, Th–*H*), 6.08 (m, 1H, vinyl–*H*), 5.54 (m, 1H, vinyl–*H*), 4.34 (t, 2H, Th–CH_2–CH_2), 3.00 (t, 2H, Th–CH_2), 2.03 (s, 3H, CH_3)
^{13}C-NMR ($CDCl_3$) : 167.58 (*C*=O), 138.40 (C–CH_3), 136.58 (Th-*C*–CH_2–), 128.57 (Th-*C*), 125.85 (Th-*C*), 125.79 (–CH_2), 121.84 (Th-*C*), 64.83 (CH_2–O–), 29.86 (Th–CH_2–CH_2), 18.58 (CH_3)
MS (MW=196.0558): m/z=196.0557
Analytically calculated for $C_{10}H_{12}O_2S$: C: 61.20%, H: 8.92%; Found: C: 61.42%, H: 6.20%

Surface-initiated poly-(3-ethylthienyl methacrylate) by ATRP A solution of 3-ethylthienyl methacrylate (3.9 g, 20 mmol) in N,N'-dimethyl formide (7 mL) was purged with nitrogen for 20 minutes. Copper(I) bromide (7.2 mg, 0.05 mmol), copper(II):bromide (5.6 mg, 0.025 mmol) and N,N,N',N",N"-pentamethyl diethylenetriamine (209 μl, 1 mmol) were added and the mixture was purged with nitrogen for another 20 minutes. Initiator coated substrates were put in Radley tubes. The tubes are evacuated and refilled with Nitrogen through three cycles. The reaction mixture is added using a syringe and heated to 80 °C. Substrates were removed at different time intervals to record a time resolved growth of the polymers and subsequently rinsed with dichloromethane, acetone and 2-propanol.
IR: ν_{max}/cm^{-1}: 1735 (C=O stretch, s), 1600-1200 (aromatic C=C stretch, ring stretch, w), 1250-1050 (O—CH_3 and C—C(=O)—O (asymmetric) stretches, w), 830 (3-subst.Th-C_α—H out of plane bend, s), 775 (monosubst.Th-C—H, in phase out-of-plane)

Template grown polythiophenes Substrates coated with a surface-initiated poly-(3-ethylthienyl methacrylate) layer were put upside down in Schlenk tubes and evacuated and refilled with Nitrogen trough three cycles. A suspension of 320 mg of iron(III) chloride ($FeCl_3$) in 20 mL of dichloromethane was stirred and purged with nitrogen for 20min to obtain a saturated solution. The mixture was left to rest for five minutes and 2.5 mL of the clear solution (approx. 2.5 mg/mL $FeCl_3$) was added using a syringe to each tube containing a substrate. 100 μL of thiophene was added and the reaction was left for

30 minutes. After reaction the substrates appeared green/blue. The bulk polymer formed in this reaction was collected by suction filtration and washed with dichloromethane, acetone and 2-propanol. The substrates were cleaned by sonication in subsequently chloroform, acetone and 2-propanol and the coating turned red in the acetone wash step.
Surface polymers: IR: ν_{max}/cm^{-1}: 1735 (C=O stretch, s), 1600-1200 (aromatic C=C stretch, ring stretch, w), 1250-1050 (O—CH_3 and C—C(=O)—O (asymmetric) stretches, w), 830 (3-subst.Th-C_α—H out of plane bend, s), 790 (2,5-disubst.Th-C—H_β out of plane bend, s) Solution polymer: IR: ν_{max}/cm^{-1}: 1600-1200 (aromatic C=C stretch, ring stretch, w), 1100-1000 (Th-C—H in plane bend, w), 830 (3-subst. Th-C_α—H out of plane bend, s), 790 (2,5-disubst.Th-C—H_β out of plane bend, s)

References

[1] S. E. Shaheen, C. J. Brabec, N. S. Sariciftci, F. Padinger, T. Fromherz, and J. C. Hummelen, *Appl. Phys. Lett.* **78**, 841 (2001).

[2] K. M. Coakley and M. D. McGehee, *Chem. Mater.* **16**, 4533 (2004).

[3] S. R. Forrest, *Nature* **428**, 911 (2004).

[4] M. Granström, *Polym. Adv. Technol.* **8**, 424 (1997).

[5] H. Sirringhaus, N. Tessler, and R. H. Friend, *Science* **280**, 1741 (1998).

[6] F. Garnier, R. Hajlaoui, and M. El Kassmi, *Appl. Phys. Lett.* **73**, 1721 (1998).

[7] F. Würthner, *Angew. Chem., Int. Ed.* **40**, 1037 (2001).

[8] M. D. McGehee and M. A. Topinka, *Nat. Mater.* **5**, 675 (2006).

[9] B. Fabre and D. D. M. Wayner, *Langmuir* **19**, 7145 (2003).

[10] Z. Q. Liang, M. Rackaitis, K. Li, E. Manias, and Q. Wang, *Chem. Mater.* **15**, 2699 (2003).

[11] Y. N. Xia and G. M. Whitesides, *Angew. Chem., Int. Ed.* **37**, 551 (1998).

[12] H. Sirringhaus, P. J. Brown, R. H. Friend, M. M. Nielsen, K. Bechgaard, B. M. W. Langeveld-Voss, A. J. H. Spiering, R. A. J. Janssen, E. W. Meijer, P. Herwig, and D. M. de Leeuw, *Nature* **401**, 685 (1999).

[13] R. J. Kline, M. D. McGehee, E. N. Kadnikova, J. S. Liu, and J. M. J. Fréchet, *Adv. Mater.* **15**, 1519 (2003).

[14] Y. Kim, S. Cook, S. M. Tuladhar, S. A. Choulis, J. Nelson, J. R. Durrant, D. D. C. Bradley, M. Giles, I. Mcculloch, C. S. Ha, and M. Ree, *Nat. Mater.* **5**, 197 (2006).

[15] R. J. Kline and M. D. McGehee, *Polymer Reviews* **46**, 27 (2006).

[16] C. Goh, R. J. Kline, M. D. McGehee, E. N. Kadnikova, and J. M. J. Fréchet, *Appl. Phys. Lett.* **86**, 122110 (2005).

[17] K. M. Coakley, B. S. Srinivasan, J. M. Ziebarth, C. Goh, Y. X. Liu, and M. D. McGehee, *Adv. Funct. Mater.* **15**, 1927 (2005).

[18] T. A. Chen and R. D. Rieke, *J. Am. Chem. Soc.* **114**, 10087 (1992).

[19] R. D. McCullough, R. D. Lowe, M. Jayaraman, P. C. Ewbank, D. L. Anderson, and S. Tristram-Nagle, *Synth. Met.* **55**, 1198 (1993).

[20] W. J. Feast, J. Tsibouklis, K. L. Pouwer, L. Groenendaal, and E. W. Meijer, *Polymer* **37**, 5017 (1996).

[21] N. Chanunpanich, A. Ulman, Y. M. Strzhemechny, S. A. Schwarz, J. Dormicik, A. Janke, H. G. Braun, and T. Kratzmüller, *Polym. Int.* **52**, 172 (2003).

[22] V. M. Niemi, P. Knuuttila, J. E. Österholm, and J. Korvola, *Polymer* **33**, 1559 (1992).

[23] S. Amou, O. Haba, K. Shirato, T. Hayakawa, M. Ueda, K. Takeuchi, and M. Asai, *J. Polym. Sci., Part A: Polym. Chem.* **37**, 1943 (1999).

[24] J. Laakso, H. Järvinen, and B. Skagerberg, *Synth. Met.* **55**, 1204 (1993).

[25] O. R. Gautun, H. J. Carlsen, E. J. Samuelsen, and J. Mårdalen, *Synth. Met.* **58**, 115 (1993).

[26] H. Sirringhaus, T. Kawase, R. H. Friend, T. Shimoda, M. Inbasekaran, W. Wu, and E. P. Woo, *Science* **290**, 2123 (2000).

[27] S. E. Shaheen, R. Radspinner, N. Peyghambarian, and G. E. Jabbour, *Appl. Phys. Lett.* **79**, 2996 (2001).

[28] F. Padinger, C. J. Brabec, T. Fromherz, J. C. Hummelen, and N. S. Sariciftci, *Opto-Electr. Rev* **8**, 280 (2000).

[29] A. Berlin and G. Zotti, *Macromol. Rapid Commun.* **21**, 301 (2000).

[30] D. Appelhans, D. Ferse, H. J. P. Adler, W. Plieth, A. Fikus, K. Grundke, F. J. Schmitt, T. Bayer, and B. Adolphi, *Colloids Surf., A* **161**, 203 (2000).

[31] G. Zotti, S. Zecchin, G. Schiavon, B. Vercelli, and A. Berlin, *J. Electroanal. Chem.* **575**, 169 (2005).

[32] J. F. Kang, J. D. Perry, P. Tian, and S. M. Kilbey, *Langmuir* **18**, 10196 (2002).

[33] A. Fikus, W. Plieth, D. Appelhans, D. Ferse, H. J. Adler, B. Adolphi, and F. J. Schmitt, *J. Electrochem. Soc.* **146**, 4522 (1999).

[34] M. E. Kumru, J. Springer, A. S. Saraç, and A. Bismarck, *Synth. Met.* **123**, 391 (2001).

[35] D. E. Labaye, C. Jérôme, V. M. Geskin, P. Louette, R. Lazzaroni, L. Martinot, and R. Jérôme, *Langmuir* **18**, 5222 (2002).

[36] C. Xia, X. W. Fan, M. K. Park, and R. C. Advincula, *Langmuir* **17**, 7893 (2001).

[37] Y. Guner, L. Toppare, Y. Hepuzer, and Y. Yagci, *Eur. Polym. J.* **40**, 1799 (2004).

[38] A. Çirpan, S. Alkan, L. Toppare, Y. Hepuzer, and Y. Yagci, *J. Polym. Sci., Part A: Polym. Chem.* **40**, 4131 (2002).

[39] D. E. Bergbreiter and M. L. Liu, *J. Polym. Sci., Part A: Polym. Chem.* **39**, 4119 (2001).

[40] E. C. Hagberg, *Polymer Preprints* **46**, 356 (2005).

[41] S. Edmondson and W. T. S. Huck, *Adv. Mater.* **16**, 1327 (2004).

[42] I. Markovich and D. Mandler, *J. Electroanal. Chem.* **500**, 453 (2001).

[43] D. M. Jones and W. T. S. Huck, *Adv. Mater.* **13**, 1256 (2001).

[44] R. Silverstein, G. Bassler, and T. Morrill, *Spectrometric identification of organic compounds, fifth edition*, John Wiley & Sons, inc, 1991.

[45] M. E. Nicho, H. L. Hu, C. López-Mata, and J. Escalante, *Sol. Energy Mater. Sol. Cells* **82**, 105 (2004).

[46] H. C. Ko, S. A. Park, and H. S. Lee, *Synth. Met.* **143**, 31 (2004).

[47] E. Said, N. D. Robinson, D. Nilsson, P. O. Svensson, and M. Berggren, *Electrochem. Solid-State Lett.* **8**, H12 (2005).

[48] C. R. Granqvist, *Nat. Mater.* **5**, 89 (2006).

[49] R. Furstenberg and J. O. White, *J. Opt. A: Pure Appl. Opt.* **9**, 741 (2007).

[50] S. Tepavcevic, A. T. Wroble, M. Bissen, D. J. Wallace, Y. Choi, and L. Hanley, *J. Phys. Chem. B* **109**, 7134 (2005).

[51] Q. Q. Qiao and J. T. McLeskey, *Appl. Phys. Lett.* **86**, 153501 (2005).

[52] M. Husemann, E. E. Malmström, M. McNamara, M. Mate, D. Mecerreyes, D. G. Benoit, J. L. Hedrick, P. Mansky, E. Huang, T. P. Russell, and C. J. Hawker, *Macromolecules* **32**, 1424 (1999).

Part II

New Techniques for Surface-initiated Polymers

Chapter 5

Effects of Micro-confinement on Surface-initiated Polymerization by ATRP

Synopsis: Using micro-reactors for surface-initiated atom transfer radical polymerization has recently drawn attention as a useful technique for surface modification in micro-fluidic devices. Additionally, a reduction in reactor volume could result in a reduction in waste of monomer. However, the effects of changed diffusion kinetics are barely understood. This chapter investigates the effect of reduction of reactor volume with glass beads. The reaction kinetics change dramatically, depending on reactor dimensions and reagent concentrations. The effects of bead size, bead surface treatment and reaction conditions are described empirically and advantages of this technique are discussed.

5.1 Introduction

Due to the development of cheap micro-fabrication techniques and following the need for reliable chemical detectors and biosensors, the use of micro-fluidic devices has become increasingly widespread.[1–6] Lab-on-a-chip technology combines sample preparation and analysis in one small device and finds applications in drug discovery,[7,8] and DNA microarrays.[9,10] Other applications of micro-fluidics can be found in optics[11] and information technology.[12]

Surface modification plays a crucial role because of its ability to direct the fluids within such devices.[13] Stimuli responsive polymer surface coatings that switch between hydrophilic and hydrophobic have been developed using surface-initiated polymers by atom transfer radical polymerization (ATRP).[14] These coatings have also been synthesized *in situ*,[15–17] *i.e.* in the micro-fluidic device, but the number of examples is limited.

Research into reducing the volume of ATRP reactors is not only interesting from a micro-fluidic point of view. Theoretically only nanograms of monomer would be needed for a polymer layer of several square centimeters and around 100 nm thick. However to obtain sufficient coverage of the substrate with the reaction mixture, grams of monomer are typically employed. For many of the device applications, highly functionalized monomers are used. The synthesis of these monomers often is laborious and expensive. Therefore reduction of the reactor volume should result in a more efficient use of monomer.

5.1.1 Mass and heat transfer

Mass and heat transfer in reactors are studied in the field of fluid dynamics. In fluid dynamics a great number of dimensionless numbers is used to describe the nature of the flow of heat and mass.

Most of these numbers describe mass and heat transfer in moving fluids. Perhaps the most frequently applied of all these dimensionless numbers is the Reynolds number, which describes the ratio of inertial forces to viscous forces:

$$Re = \frac{\rho v^2/L}{\mu v/L^2} = \frac{\rho v L}{\mu} = \frac{vL}{\nu} = \frac{\text{Inertial forces}}{\text{Viscous forces}} \tag{5.1}$$

With v is the mean fluid velocity, L is the characteristic length, μ is the absolute dynamic fluid viscosity, ν is the kinematic fluid viscosity and ρ is the fluid density. The Reynolds number quantifies the relative importance of the inertial forces and the viscous forces and can thus be used to identify different flow regimes, such as laminar and turbulant flow. For flow in a pipe, for instance, the characteristic length is the pipe diameter. At low pipe diameter, the viscous forces gain importance over the inertial forces: the Reynolds number becomes low. At low Reynolds numbers, the flows become laminar and

is described by smooth constant fluid motion, while turbulent flow occurs at high Reynolds numbers and has many flow fluctuations.

Mass transfer can take place by diffusion, the random Brownian motion of individual particles in the fluid, and by advection, in which matter or heat is transported by the larger-scale motion of currents in the fluid. The sum of these two is called convection. The Péclet number relates the rate of advection of a fluid to its rate of diffusion and is defined as:

$$Pe = \frac{Lv}{\mathcal{D}} \tag{5.2}$$

with $\mathcal{D}$ is the diffusion coefficient or diffusivity. For heat transfer the Péclet number takes the form:

$$Pe = \frac{Lv}{\alpha} \tag{5.3}$$

with α is the thermal diffusivity:

$$\alpha = \frac{k}{\rho c_p} \tag{5.4}$$

With k is the thermal conductivity and c_p is the heat capacity. The Péclet number shows, that at small length scales the advection is only small compared to the diffusion, or in the case of heat transfer: the conductive component of the heat transfer.

Currents in the fluid are not only caused by external forces, but can also be caused by diffusion as a result of high concentration differences in the fluid (due to, for instance, a reaction at an interface). The Sherwood number describes the total convective mass transfer with respect to the mass transfer by diffusion only:

$$Sh = \frac{K_c L}{\mathcal{D}} = \frac{\text{Convective mass transfer}}{\text{Diffusive mass transfer}} \tag{5.5}$$

With K_c is the overal mass transfer coefficient. Again it is shown, that at small length scales the diffusion contribution to convection becomes more prominent till in the limit case $K_c = \mathcal{D}$, the advection part to convection is zero and convection is equal to diffusion.

The heat transfer equivalent to the Sherwood number is the Nusselt number:

$$Nu = \frac{hL}{k} = \frac{\text{Convective heat transfer}}{\text{Conductive heat transfer}} \tag{5.6}$$

With h is the convective heat transfer coefficient.

Diffusion is described by Fick's first and second law. The first law is used, when the concentration ithin the diffusion volume does not change over time. In one dimension the law has the following form:

$$J = -\mathcal{D}\frac{\partial \phi}{\partial x} \tag{5.7}$$

Or in the case of more dimensions:

$$J = -\mathcal{D}\nabla\phi \tag{5.8}$$

With J is the diffusion flux, ϕ is the concentration and x is the position.

Fick's second law is used in non-steady state situations, *e.g.* when the concentration within the diffusion volume changes with time:

$$\frac{\partial \phi}{\partial t} = \mathcal{D}\nabla^2\phi \tag{5.9}$$

To summarize, heat and mass transfer are influenced by the dimensions of the reactor. At low characteristic lengths, flow becomes more laminar, viscosity becomes more important for the flow characteristics and diffusion and conduction become the major contribution to mass and heat transfer respectively.

5.1.2 Micro-confined ATRP

Xu *et al.* used ATRP in micro-channels of 0.3 mm high by 8 mm wide by 4.5 cm long (total volume = 0.11 μL) to investigate the influence of solution composition on the formation of polymer brushes by use of a stable concentration gradient in the channel.[15] In this study, the volume of the reaction mixture is effectively reduced. The paper provides a calculation and computer model based on Fick's second law to support their claim, that the diffusion effects on

the gradient in the channel are negligible. However, the kinetic consequences of reducing the reaction volume were not investigated.

ATRP in capillaries has been performed by Feldmann *et al.*[18] and by Bruening *et al.*[19] for applications in capillary electrophoresis and capillary eletrochromatography respectively. Neither of these two reports investigates the influence of the confinement on the polymerization, although in another report Bruening comments that the thickness of a film grown in the capillary is up to 1.5 times higher than grown under similar conditions on a flat surface.[20]

Petrie investigated the confinement effect on surface-initiated MMA in nanometer-sized pores.[21] In this study he found that in pores <50 nm the polymers grown are restricted in size to a maximum of 20 monomer units. He attributes this to the small pores severely restricting the space for polymerization and diffusion of monomer.

5.1.3 Diffusion effects and micro-confinement

In micro-reactors, heat transport, mass transport and mixing are much faster than conventional reactors due to the shorter diffusion lengths.[22,23] This is because the surface to volume ratios for the reactor wall and for the contact areas of different phases present in the reactor are much higher for smaller volumes. Mass transfer coefficients can be up to two orders of magnitude larger than for standard laboratory-scale reactors.[24] A reduction of reactor volume can thus strongly affect the reaction kinetics, especially in diffusion limited reactions.[25]

The influence of diffusion is highest for fast reactions and reactions involving large molecules or complexes.[26] For solution ATRP this means that the activation and deactivation are influenced, as these reactions involve a polymer chain and a copper complex, and termination by recombination is influenced, as this reaction involves two polymer chains. Propagation, which involves a polymer chain and a (smaller) monomer is also influenced by diffusion effects, although to a lesser extend.

The influence of diffusion limitations on termination occurs mainly at higher conversions due to a gelation effect, which has been confirmed by statistical modelling by the method of moments.[27–29] For surface-initiated

polymerizations, these effects are expected to be of less importance as polymerization preferentially occurs at the surface only and surface-initiated polymerizations result in low conversions of monomer, reducing the effect of viscosity or gelation on termination. However, the influence of enhanced mass transfer on activation, deactivation and propagation will play a role.

Genzer modeled surface-initiated polymerization by ATRP with Monte-Carlo simulations.[30] He concluded that termination in an early stage of the polymerization plays a more important role in surface confined polymerizations, as the radicals created at the surface are in close proximity to each other. The availability of monomer is not limiting in this simulation. Wang on the other hand concluded from an experimental study using Electron spin resonance, that termination in an early stage takes place till a critical concentration of the deactivating copper(II) complex is formed.[26]

To summarize, there have been some studies modeling diffusion effects in ATRP, both in solution and on surfaces. Most of these studies focus on reduced diffusion at high conversions. The knowledge about the effects of micro-confinement on surface-initiated polymerization however is very limited. In this chapter a method to reduce the reactor volume will be discussed and the effects of reducing reaction dimensions to the micrometer regime on the reaction kinetics and the influence of the reactor wall surface treatment will be investigated in an empirical study.

5.2 Micro-confined polymerization: kinetic effects

The kinetic effects of reducing the reaction dimensions were studied using a model system of surface-initiated brush growth of polymethyl methacrylate (PMMA) following a recipe by Jones *et al.*[31] A copper(I) bromide / bipyridine (BPY) catalyst complex was used with a relative [CuBr]:[BPY]:[MMA] mole ratio of 1:3:100 with a mixture of methanol and water as solvent. Although in this method no copper(II) is used, the polymerization by this procedure is usually reasonably controlled. This is due to the rapid creation of copper(II) in the initiation step.

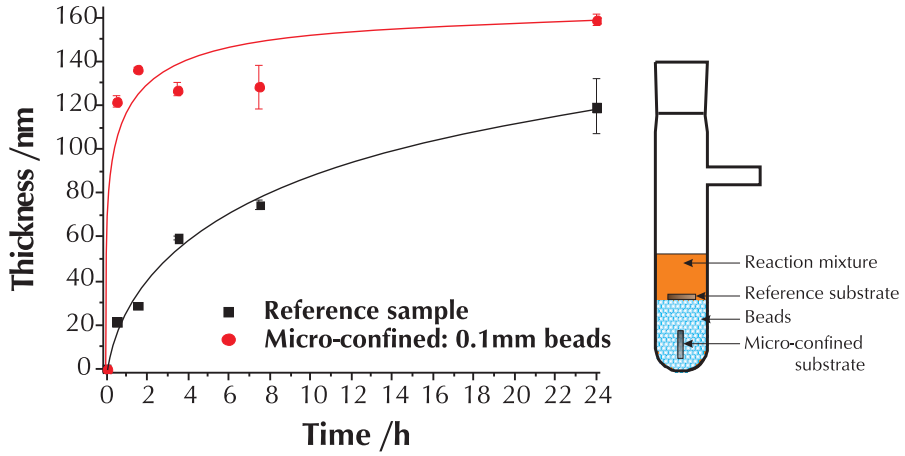

Figure 5.1: Left: time resolved PMMA brush growth in micro-confinement with 0.1 mm beads and for the reference without beads. Right: schematic for the reaction set-up: the reference and micro-confined sample were exposed to the same reaction conditions in the same tube.

Beads were used to fill the background volume surrounding the substrates. The interstitial volume was filled with reaction mixture so substrates were in contact with both the closely packed beads and the reaction mixture.

When beads with a diameter below 0.5 mm are used the reaction kinetics are influenced. Figure 5.1 shows the time resolved brush growth on substrates immersed in polymerization solution in presence of beads of 0.1 mm in diameter in comparison to brush growth in absence of beads. The initial rate of polymerization in this micro-confinement is very high: in just thirty minutes a polymer layer of 120 nm thickness has formed, much faster than on the reference sample. The reaction then slows down and stops.

The thicknesses reported here are average ellipsometric thicknesses of four points at the surface. The surface of the samples showed microscopic imprints of where the beads had been in contact with the surface. These imprints will be discussed later. The thickness measured by ellipsometry was confirmed by inspection of the thin film interference colour and in many cases also by atomic force microscopy (AFM).

In the micro-confined situation, the reaction mixture has become viscous toward the end of the polymerization, indicating that solution polymer has formed. This solution polymer is formed by auto-initiation and by radical transfer from the surface radicals. Although solution polymer is also formed

in reference reactions without beads, the viscosity was much higher in the micro-confined situation, indicating that not only the surface-initiated polymerization, but also the solution polymerization had been enhanced.

The reference reaction without beads initially has more living character and only slows down after four hours of reaction. Even though it has far more living character, the eventual brush thickness is still less than that obtained in the micro-confined reaction. The formation of thicker brushes in micro-confinement is in agreement with reports in literature.[20]

As has been discussed in the introduction to this chapter, mass and heat transport can be greatly influenced by micro-confinement and diffusion can have a major impact on reaction kinetics. In chapter 1, section 1.3, the reaction kinetics for ATRP were discussed and the following equation was derived:

$$R_p = k_{app}[\mathrm{M}] = k_p K_{eq}[\mathrm{I}_0]\frac{[\mathrm{Cu(I)}]}{[\mathrm{Cu(II)X}]}[\mathrm{M}] \tag{5.10}$$

With:

$$K_{eq} = \frac{k_a}{k_{da}} \tag{5.11}$$

Effects of mass and heat transfer can affect the propagation constant k_p and the equilibrium constant K_{eq} of the equilibrium between activation (k_a)and deactivation (k_{da}). Heat transfer from the reactor wall is not expected to play an important role here, because although the surface area of the reactor walls has increased, the heat capacity of the reactor wall is only limited, as the beads share only minimal contact area with each other and are not connected to a heat source or heat sink.

In terms of mass transfer, the reactions that can be affected are the reactions that involve molecules in the solution: activation, deactivation and propagation. If at least activation or propagation are enhanced, faster polymer growth will be the result. The experimental observations are in agreement with this explanation: the micro-confined brush growth takes place at shorter time scales. Note that in surface-confined polymerizations termination by recombination does not involve molecules in the solution and is therefore not expected to be influenced by a change in mass transport. Faster deactivation, *i.e.* end-capping by the copper(II)-bromide complex, would result in less

termination events, but would lower the reaction rate. Therefore enhanced termination and deactivation are not expected to be responsible for the quicker brush growth. Reduced deactivation, however, would have similar effects to enhanced activation.

It should also be noted that the increased surface to volume ratio could distort the equilibrium between molecules adsorbed on the bead walls and molecules in solution. Another explanation could be that the diffusion near the surface has been affected and that, *e.g.* copper complexes stay closer to the surface, hence influencing the equilibrium constant.

If local differences in concentrations would occur, this would also influence the reaction kinetics. However, the concentrations right at the start of the reaction are expected to be the same for both the reference reaction and the micro-confined polymerization, so this can not explain the difference in the initial reaction rate.

An explanation for the early termination in brush growth, however, could well be related to local differences in concentration. One explanation could be that as a result of the faster activation and propagation (by faster diffusion within each void) the monomer concentration in each void near the surface decreases fast and that the supply of more monomer from adjacent voids is not sufficient to maintain the rate of polymerization. For the growth of a 120 nm thick PMMA layer on an area of $4.3\ 10^{-9}$ m^2 (the area of a triangle formed by three beads of 0.1 mm touching) approximately 0.5 ng of monomer would be needed. As this is only about 5% of the monomer present in each tetrahedral void at the start of the polymerization, this would not be sufficient to explain quick drop in rate of polymerization. However, as the formation of polymer in solution is enhanced as well, this could explain the early termination.

5.2.1 Void size and degrees of freedom

If the faster brush growth is caused by the micro-confinement, the volume of the interstitial voids between the beads will be of importance and hence, as these void sizes are cubicly dependent on the bead diameter, the dimensions of the beads will have a strong influence. Table 5.1 gives the approximate value for void sizes in a cubic close (bcc) packing. A bcc packing was assumed to

Table 5.1: Void sizes for each bead diameter asuming a bcc packing, also see the appendix to this chapter on page 141.

Bead diameter (mm)	Void size (m^3) tetrahedral	Void size (m^3) octahedral
2.5	$3.6 \cdot 10^{-10}$	$1.4 \cdot 10^{-9}$
1	$2.3 \cdot 10^{-11}$	$9.2 \cdot 10^{-11}$
0.5	$2.9 \cdot 10^{-12}$	$1.2 \cdot 10^{-11}$
0.1	$2.3 \cdot 10^{-14}$	$9.2 \cdot 10^{-14}$
0.035	$9.8 \cdot 10^{-16}$	$3.8 \cdot 10^{-15}$
0.011	$3.0 \cdot 10^{-17}$	$1.2 \cdot 10^{-16}$

calculate the sizes of the tetrahedral and octahedral voids, but in a hexagonal close packing only tetrahedral voids will exist, see the Appendix on page 141.

The void fraction of closely packed beads was determined experimentally for beads of 0.1 mm by filling the voids of a known volume of beads with water and measuring the increase in mass. The volume fraction of the voids was 35%, so higher than the theoretical value of 26%. This deviation can be caused by a small variation in the bead size and irregular packing in some areas.

The diameter of the beads was varied between 11 μm and 3.5 mm and the thickness of the polymer layer was measured after three hours of reaction. For bead diameters $\geqslant$0.5 mm the polymer brush layer thickness after three hours is not significantly different from the thicknesses achieved by conventional surface grown polymers in absence of beads as can be seen in figure 5.2. For bead diameters of 0.1 mm and smaller, there is a strong effect: the smaller the bead dimensions, the thicker the resulting polymer brush layers. For beads with a diameter of 11 μm the brush thickness after three hours of reaction is 180 nm, which is three times as thick as for brushes grown in the conventional way. This dependency of bead diameter was very reproducible, although the deviation of the thickness after three hours was significantly higher in case of the smallest beads (11 μm and 35 μm).

For the brushes grown on substrates in presence of the smallest beads (11 μm and 35 μm) the surface after reaction looked matt, as a consequence of the indentations caused by the beads. Due to this, ellipsometry did not always

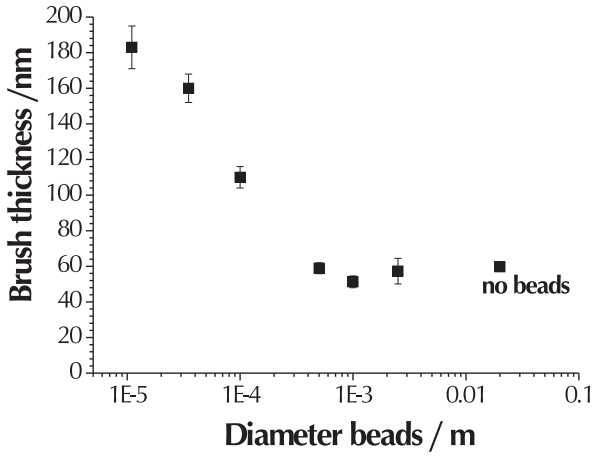

Figure 5.2: The influence of bead size on the polymer thickness. The thickness was measured after three hours of surface-initiated PMMA growth by ATRP, the data point at 2 cm is a reference point for conventional brush growth (in absence of beads).

give a meaningful value. In these cases the thickness was measured by both inspection of the thin film interference colour and by AFM measurements.

Similar experiments were also performed in which two substrates were clipped together face to face separated by bead spacers. As for the smaller spacers (<0.5 mm) it was impossible to deposit just one bead at each corner, two small lines of beads were deposited at opposite sides of the substrate and the samples were carefully clipped together. After reaction there were no significant differences in brush thickness between the different samples, apart from those locations on the sample were the small lines of beads had been positioned. In those locations the brush layers were thicker and the thickness was in the same regime as observed in the case were the tube was filled with beads.

Apparently reducing the dimensions of the reaction volume in just one of the three dimensions does not have a significant influence — at least not in the regime that has been studied here.

Preliminary experiments were performed to investigate whether confinement in two dimensions had any influence on the reaction kinetics. To this end polydimethyl siloxane (PDMS) stamps with channel widths in the mi-

crometer regime were put in contact with initiator coated substrates and the channels were filled with reaction mixture. The results of these experiments suggest that also confinement in two out of three dimensions does not have a significant influence, although it has to be noted that observations by Bruening *et al.* indicated otherwise.[20] Apparently, at the length scales studied here, the reactor volume has to be reduced in all three dimensions to enhance the reaction kinetics.

5.2.2 Influence of the concentration of Cu^{2+}

As the growth of surface-initiated polymers in presence of beads levels off after only thirty minutes, a copper(II) halide was added to increase the living character of the reaction. Copper(II) bromide was added in a 10 % molar concentration with regards to Cu^{1+}. For the conventional reaction this prolongs the linear growth from four hours to eight hours after which the reaction starts to level off as shown in figure 5.3. Also the linear growth in presence of 0.1mm beads is extended to about eight hours, after which the reaction becomes less linear and finally slows down. For the conventional polymerization the

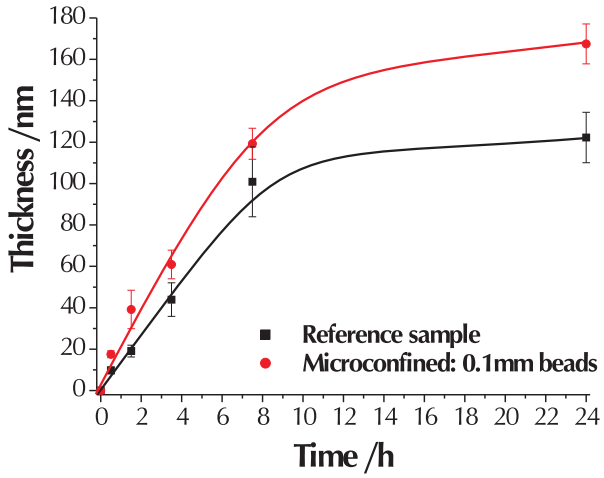

Figure 5.3: Time resolved brush growth of PMMA in presence and in absence of beads using a reaction mixture containing 10 mole-% copper(II) bromide with respect to the concentration of copper(I) bromide.

enhanced living character at the start of the polymerization does not eventually result in a thicker brush, as the reaction is slowed down over the entire time scale.

Although initially the reaction rate is also lower for the micro-confined reaction, the repression of termination in the second half of the reaction results in thicker brushes than in absence of copper(II) bromide and with ~167 nm this polymer layer is about a third thicker than in a non-micro-confined way. So also when the ratio between copper(I) and copper(II) is changed and the equilibrium between active and dormant state is enhanced, micro-confined polymerization outperforms conventional polymerization in reaction speed and eventual thickness.

An early stop in polymerization as was observed in the reaction without copper(II) is not observed here. With the slower initial brush growth the supply of monomer is expected to be less of a problem. Also the formation of solution polymer is reduced considerably. Termination seems to be slightly more prominent in the polymerization without beads under these conditions, which could be explained by less efficient propagation (with regards to termination).

5.2.3 Lowering the concentration of monomer

It was discussed in the introductory chapter (page 15) that the rate of polymerization is linearly dependent on the concentration of monomer, but that in practice when the concentration of monomer is lowered, termination takes over and the growth of polymer is stopped in an early stage. In the case of polymer growth in presence of beads, the increase of thickness *vs.* time is much higher. This is either due to either a higher propagation constant or a different equilibrium between active and dormant state, as the concentrations of all reactants were kept the same.

To get an insight into the reaction kinetics, the monomer concentration was lowered from 4.3 M to 1.7 M and finally to 0.4 M, while keeping the molar ratio between monomer, catalyst and ligand the same. The time resolved brush growth is shown in figure 5.4. Lowering the concentration from 4.3 M to 1.7 M yields a similar time resolved polymer growth, although the equilibrium

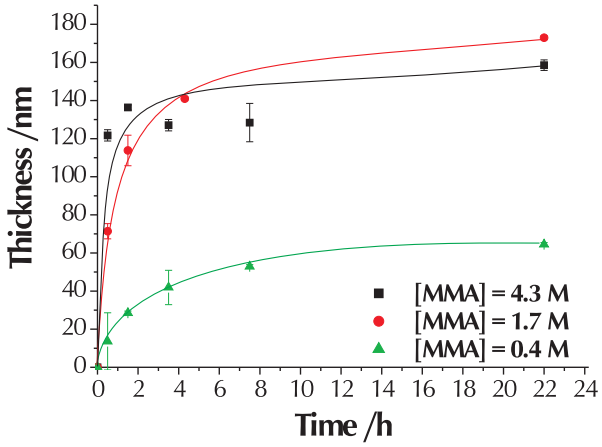

Figure 5.4: Time resolved micro-confined brush growth at various concentrations of the monomer in presence of 0.1 mm beads. The concentrations of Cu(I) and ligand are lowered accordingly keeping [M]:[Cu^{1+}]:[BiPy] constant at 100:1:3.

between living and dormant state is affected: the reaction is more controlled at the start. This can be explained by the lower copper(I) concentration: the ratio between copper(I) and copper(II), which is created by the initiation reaction, is affected.[32]

When the concentration of monomer is lowered from 1.7 M to 0.4 M the change in reaction rate is more pronounced: the initial reaction rate decreases by a factor 5 and the polymer thickness after 22 hours decreases by a factor 2.7. On the reference sample without micro-confinement, no polymer grows at this concentration as the active radical site goes back into the dormant state or terminates before a monomer molecule has the chance to collide with it (the reaction rate for most side reactions does not depend on monomer concentration). This is a known effect to occur in ATRP.[33]

Apparently in presence of beads the chance for a monomer molecule to collide with an active site is increased relative to side reactions occurring. In section 5.2 the increased reaction rate was attributed to either a change in k_p or in K_{eq} as a consequence of changed mass transfer of either the monomer or the catalyst complex. As a change in K_{eq} would not affect the ratio between propagation and side reactions, it is most probable, that the increased reaction

rates relate to a change in k_p and as such to a changed mass transfer of monomer.

5.2.4 Enhanced polymerization with other monomers

As was suggested in the introduction to this chapter, reduction in amounts of reagents needed could be very interesting for the polymerization of highly functionalized monomers. Therefore micro-confinement was also tested with the polymerization of the liquid crystalline monomer described in chapter 2. This polymerization was chosen as the reaction needs high concentrations of monomer, is difficult to optimize and polymerization at the surface is hindered by formation of solution polymer.

Reactive mesogen RM488 was polymerized following a recipe with a 3.6 times lower concentration of monomer compared to the procedure described in section 2.2 on page 41. For conventional polymerization this resulted in brushes of 2.9 nm after 10 h of reaction. For the reaction performed in micro-confined condition using 0.1 mm beads this resulted in 18.3 nm thick brushes, comparable to the thicknesses achieved for the same reaction time following the recipe with higher concentration of monomer without beads. A 65% reduction in reaction volume of reaction mixture combined with a 72% reduction in monomer concentration results in a total reduction of 90% for the amount of monomer needed, although it has to be noted, that also by this procedure it was impossible to grow brushes thicker than 20 nm.

The considerable reduction in functionalized monomer needed shows that this technique can be very attractive from an economical perspective.

5.3 Influence of bead surface energy

In micro-reactors the nature of the surface plays an important role. In this case the bead surface energy plays a major role as the total surface area per volume increases with decreasing bead diameter. The influence of the nature of the surface of the beads on reaction kinetics was investigated. The surface of 0.1 mm beads was oxidized by plasma treatment to increase hydrophilicity. The beads were stirred between successive treatments, to ensure all the sides

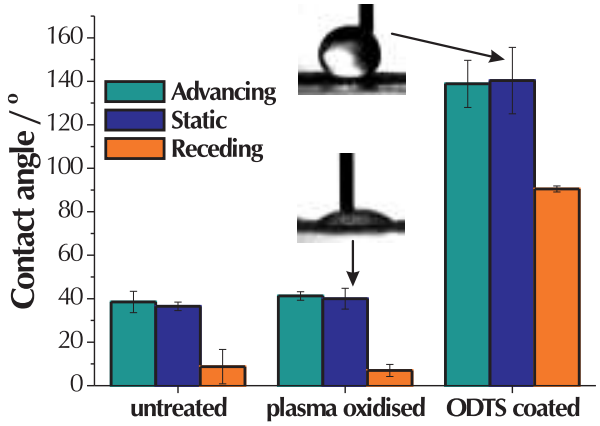

Figure 5.5: Contact angles of water on untreated beads, beads with a plasma oxidized surface and beads that underwent a treatment with ODTS. Insets show photographs of the static contact angle on both of the treated substrates.

of all the beads had been exposed to the plasma. Part of these beads were then treated with octadecyl trichlorosilane (ODTS).

Contact angles were measured on a close packed monolayer of beads stuck to a glass substrate by double sided adhesive tape. As can be seen from figure 5.5 there is no significant difference in contact angle between non-treated beads and plasma treated beads. The influence of the ODTS treatment on the other hand is very significant. The static contact angle increases from 40 ° to 140 °. This contact angle is larger that the value of 105 ° reported in literature and the value of 107 ° reported in chapter 2 for water on an ODTS monolayer.[34] This can be partly explained by the fact that the monolayer of beads on a flat glass substrate forms a micro-structured surface. This micro-structure amplifies the hydrophilic or hydrophobic properties of the surface,[13] by an amount given by the Young-Wenzel equation:[35,36]

$$r(S_S - S_{SL}) = S_L \cos\theta \tag{5.12}$$

With:

$$r = \frac{\text{actual surface}}{\text{geometric surface}} \tag{5.13}$$

and S_S, S_{SL}, S_L the free interface tensions of a solid-air, a solid-liquid and a

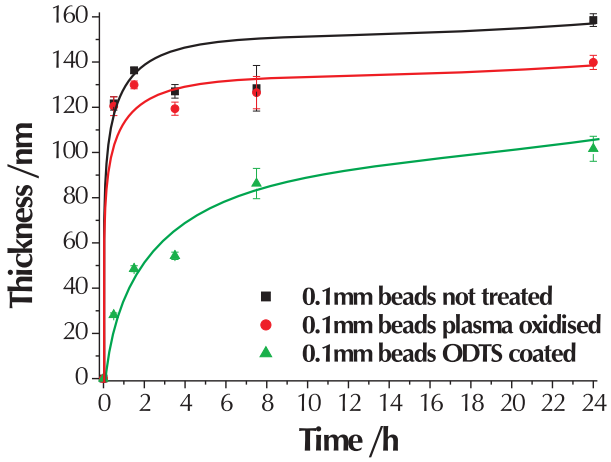

Figure 5.6: Time resolved brush growth of PMMA in presence of bare, plasma treated and ODTS coated beads.

liquid-air interface respectively and θ the contact angle.

When substituting the measured contact angles, a value of r=3 is obtained, which is higher than the value of r=2, which would be obtained by deviding the area of a half sphere by the area of a circle. The difference may be explained by irregularities on the bead surface and air trapped between the beads.

The time resolved polymer growth in presence of these treated beads is displayed in figure 5.6. The kinetics in presence of the plasma treated beads are similar to the situation with non-treated beads, which is in agreement with their similarity in hydrophilicity. For the ODTS coated beads however, the development of reaction rate follows a pattern that lies between growth in presence of untreated beads and conventional growth without beads: the brushes grow faster at the start than in conventional polymer brush growth but slower than in the case of untreated or plasma treated beads. After four hours the growth slows down considerably, but the reaction rate is still higher than for the reaction with untreated beads. For both treatments the polymerization rates are different from the conventional polymerization, but micro-confined polymerization with plasma oxidized beads and with untreated beads show the biggest discrepancies from polymerization without beads.

Due to the higher surface to volume ratio the nature of the surface plays

a much bigger role than in conventional reactors.[22] The nature of the reactor walls influences the mass transfer near the wall as the surface energy of the wall influences the orientation of water and other molecules near the wall,[37] and hence could influence the mass transfer of monomer and catalyst. This could explain the differences in reaction kinetics when changing the nature of the micro-reactor walls, although the exact mechanism is not fully uncovered yet.

5.4 Micro-patterning

In section 5.2.1 it was suggested that the packing of the beads is either a bcc or a hexagonal close packing. Hexagonal close packing and bcc packing both are built up from single layers of hexagonally packed spheres with the position of each third layer as the only difference. Polymer brush growth in presence of beads gives rise to a pattern of indentations in the polymer layer (figure 5.7) as no polymer can grow in the point where the bead touches the surface. This pattern is indeed hexagonal, although not very regular. The irregularities may be caused by small deviations in bead size and local irregularities in the lattice.

In an attempt to utilize these indentations to create micro-patterns a monolayer of polystyrene colloid beads of 1 μm was spin coated on top of an initiator coated substrate and 20 nm thich polymer brushes were grown from the sub-

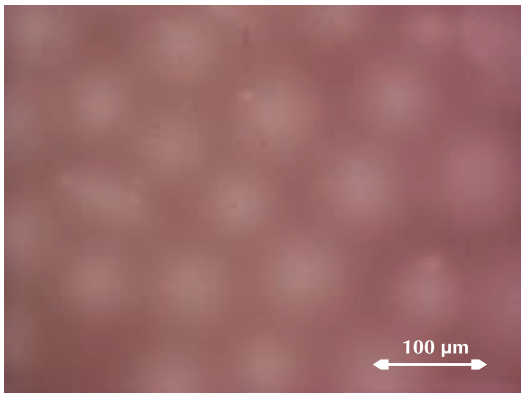

Figure 5.7: Optical microscopy on a substrate after micro-confined surface-initiated polymerization with 0.1 mm beads. The dark regions are of larger brush thickness.

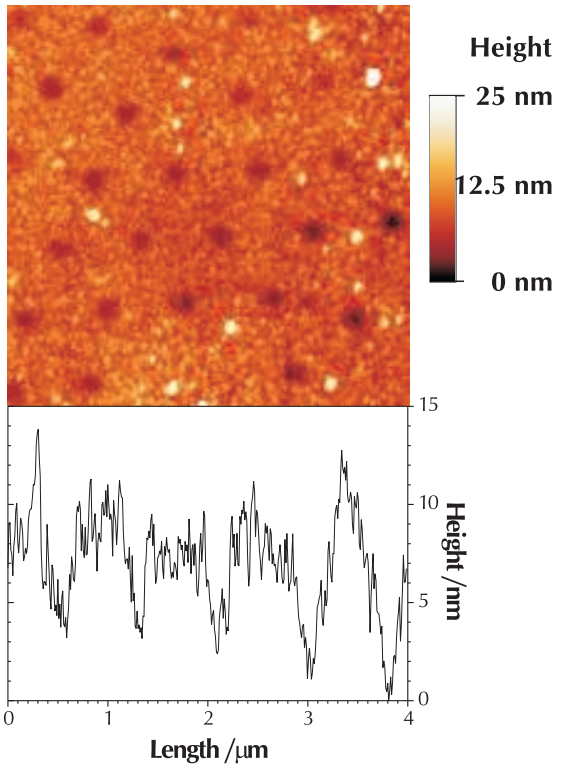

Figure 5.8: Topographical AFM on a substrate with surface-initiated PMMA grown in presence of 1 μm colloid beads.

strate.* The substrate was then characterized by AFM. The polymerization between the colloid beads results in a regular pattern in some of the regions on the substrate as is shown in figure 5.8.

*This experiment was performed by Sarah Kim, Melville laboratory for polymer chemistry, University of Cambridge, Cambridge, United Kingdom / Superlattice nanomaterials lab, Korea advanced institute of science and technology, Daejeon, Republic of Korea

5.5 Conclusions and outlook

Using beads to reduce reactor volume can be an effective way to reduce the amount of monomer needed for the reaction. When beads with diameter <0.5 mm are used, the reaction kinetics are influenced: thicker brushes are formed and shorter reaction times are needed. This is attributed to an enhanced rate of propagation, due to a changed mass transfer of the monomer. The size of the beads and the nature of their surface has a significant effect on reaction kinetics, being most beneficial with the smallest beads and with hydrophilic surfaces. Due to the enhanced propagation step in micro-confined polymerization, monomer concentrations could be reduced by a factor 2.5 without effect on the eventual brush thickness and with a factor 10, without causing early termination of the reaction. At this concentration surface-initiated polymerizations performed following conventional procedures without beads terminate because of monomer deficiency.

Enhanced reaction kinetics by micro-confinement are shown for a model monomer MMA, but also for a more functionalized monomer, the liquid crytalline RM488. In the latter case the amount of monomer needed could be reduced with 90% while obtaining brush layers with the same thickness as following procedures without beads.

Performing polymerization in presence of beads results in patterns of indentations in the formed polymer layer. A regular 1 μm hexagonal pattern was obtained after polymerization in the voids of a colloid monolayer, making micro-patterning a potentially interesting additional application of this technique.

The studies described in this chapter are limited and still leave many questions open: the exact mechanism of the enhanced mass transfer in the presence of beads, the optimal bead size for enhanced polymerization *etc.* Nevertheless the results presented in this chapter clearly show a distinct influence of the reactor volume on the surface-initiated polymerization kinetics, which potentially has many applications and which makes this a promising line for future research.

5.6 Materials and methods

General procedures

Ellipsometric measurements on monolayers and untreated polymer brushes were carried out using either an EL X-02C ellipsometer from Dr Riss Ellipsometerbau GmbH with a 632.8 nm laser at 70° angle of incidence or a JA Woollam Alpha-SE spectroscopic ellipsometer. Refractive indices of 1.50 and 1.45 were used for polymer and initiator layers respectively with the monochromatic ellipsometer. In the case of the spectroscopic ellipsometer a model with two Spline layers and one Cauchy layer on top of a silicon oxide layer was used.
Plasma oxidation of substrates was performed in air in an Emitech K1050X plasma oxidizer for 10 minutes at 100 W.
Spin Coating of colloids was carried out on a Süss Microtec lithography GmbH Delta 10TT. Colloids were spin coated from the original solution at various speeds.[†]
Atomic Force Microscopy was performed on a Digital Instruments Nanoscope® Dimension™3100 Atomic Force Microscope. Both topographical and phase images were recorded.
Optical Microscopy was performed on a Nikon Eclipse ME600 microscope equiped with a Nikon DN100 digital net camera.
Contact Angle Goniometry was performed using a home-built combination of a kdScientific syringe controller and pump, a micro-syringe, a paper background screen illuminated by a KL1500LCD lamp and a Cohu CCD camera connected to a computer. Infusion and withdrawal rates of 4 μL min^{-1} were used.

Materials

Spheriglass® glass beads with diameter of approximately 11 μm and 35 μm (5000CPOO and 3000CPOO respectively) were donated to the laboratory by Unipath. Biospec glass beads with diameters of 0.1 mm, 0.5 mm, 1 mm

[†]Please see footnote on page 136

and 2.5 mm were purchased from Thistle Scientific. Aqueous colloidal polystyrene (PS) spheres with a diameter of 1.01 μm were purchased from Magsphere. Dow Corning Sylgard 184 Base silicon elastomer and Sylgard 184 Silicon curing agent were purchased from VWR. All other chemicals were purchased from Aldrich, Lancaster or Fisher and used as received unless stated otherwise. Triethylamine was distilled from and stored over potassium hydroxide. Toluene was distilled from sodium and stored over molecular sieves. copper(I) bromide was of 99.999 % purity and was stored *in vacuo*. Dichloromethane and toluene were distilled prior to use. Methanol and ethanol were Analytical Reagent grade and used as received. MMA was purified over a short plug of alumina before use. The trichlorosilane initiator (2-bromo-2-methylpropionic acid 3-trichlorosilanylpropyl ester) was synthesized by members of the lab following a reported procedure,[38] using allyl alcohol instead of 5-hexene-1-ol. Silicon wafers were obtained from Compart Technology Ltd. (100 mm diameter, phosphorous-doped, <1 0 0> orientation, polished on one side).

Immobilization of the initiator monolayer on the substrate Silicon wafers were plasma oxidized before functionalization. The silicon substrates were placed in a crystallising dish and 30 mL of dry toluene, 50 μL of triethylamine and 10 μL of the trichlorosilane initiator was added. The dish was covered with foil and left overnight at room temperature. The wafer was then washed sequentially with toluene, distilled acetone and absolute ethanol and dried under a nitrogen stream.

Performing micro-confined polymerizations by volume-reduction with beads (typical procedure) The reaction mixture was prepared following a literature procedure by Jones *et al.*:[31] Methyl methacrylate (MMA) (20 mL, 169.9 mmol), water (4 mL) and methanol (16 mL) were purged with nitrogen for 20 minutes. Then copper(I) bromide (0.24 g, 1.699 mmol) and bypiridine (0.8 g, 5.1 mmol) were added and the mixture was purged with nitrogen for 15minutes. Two substrates at a time were put back to back in Radley tubes. Glass beads were then added to the tubes until the substrates were fully covered with beads. A third substrate was carefully put on top of the beads in each tube, facing up. In the case of sandwiched substrates with spacers, a small amount of beads was carefully distributed over the top side substrate, a second substrate was put on top

of first substrate, facing down. Both substrates were gently pressed together between thumb and index finger, the top substrate was displaced with small circular movements to obtain monolayers of beads between the substrates. Both substrates were then clipped together using Rapesco® Supaclip 40 paper clips and put in separate Radley tubes. All the tubes were evacuated and refilled with Nitrogen through four cycles. The reaction mixture was added to all the tubes. The reaction was run for different time periods between 0.5 h and 24 h stopping the reaction in one of the tubes at a time. After reaction the substrates were rinsed with toluene, acetone and methanol subsequently. In case substrates with polystyrene colloid monolayers were used, the substrates were put *back-to-back* in the reaction tubes. The monolayer was stable during polymerization and was removed in the rinsing steps after reaction.

Synthesis of polymer brushes of RM 488 on silicon (micro-confined procedure, compare page 51) A solution of RM488 (1.5 g, 2.93 mmol) in DMF (7mL) was purged with nitrogen for 20 minutes and Copper(I) bromide (0.6 mg, 4.2 μmol), copper(II) bromide (0.1g, 0.44 μmol) and PMDETA (10μL, 0.5 μmol were added. The reaction mixture was then heated to 50 °C and purged for another 15 minutes Two substrates at a time were put back to back in Radley tubes. Glass beads were then added to the tubes until the substrates were fully covered with beads. A third substrate was carefully put on top of the beads in each tube, facing up. All the tubes were evacuated and refilled with Nitrogen through four cycles. The reaction mixture was added to all the tubes. Surface-initiated polymerization was performed at 50 °C for 16 h After the reaction the substrates were rinsed with dichloromethane (under sonication), toluene, acetone and methanol subsequently. Ellipsometric thickness: 18.3 nm.

Treatment of beads Beads with diameter 0.1 mm were plasma oxidized before functionalization. The beads were placed in a crystallising dish and 30 mL of dry toluene, 50 μL of triethylamine and 10 μL of octadecyltrichlorosilane was added. The dish was covered and left overnight at room temperature. The beads were then washed sequentially with toluene, distilled acetone and absolute ethanol and dried under vacuum overnight.

Appendix

Assuming a face-centred cubic packing of spheres (Keppler conjecture):

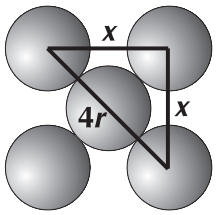

For spheres of radius r, touching along the face diagonal, the cubic unit cell parameter x is calculated as:

$$x = 2\sqrt{2}r$$

The total unit cell volume is:

$$V_{cell} = x^3$$

$$V_{cell} = 16\sqrt{2}r^3$$

The occupied volume by spheres is:

$$V_{occ} = 8 \cdot \frac{1}{8}V_{sphere} + 6 \cdot \frac{1}{2}V_{sphere}$$

$$V_{occ} = 4V_{sphere}$$

$$V_{occ} = \frac{16\pi r^3}{3}$$

Space filling factor is:

$$FF_{vol} = \frac{V_{occ}}{V_{cell}} = \frac{\pi}{3\sqrt{2}} = 74\%$$

The total amount of interstitial volume per unit cell is:

$$V_{interst} = V_{cell} - V_{occ} = 16\sqrt{2}r^3 - 16\frac{\pi}{3}r^3$$

The interstitial volume consists of 8 tetrahedral voids and 4 octahedral voids per unit cell. The tetrahedrons enclosing the tetrahedral voids each have height, base area and volume:

$$h_{tetr} = \frac{2\sqrt{6}}{3}$$

$$A_{base,tetr} = \sqrt{3}r^3$$

$$V_{tetr} = \frac{1}{3}\sqrt{3}r^2\frac{2\sqrt{6}}{3} = \frac{2\sqrt{2}}{3}r^3$$

The octahedrons enclosing the octahedral voids consist of two identical pyramids with height, base area and volume:

$$h_{pyr} = 2r\sqrt{2}$$

$$A_{base,pyr} = 4r^2$$

$$V_{pyr} = \frac{1}{3}4r^2r\sqrt{2} = \frac{4\sqrt{2}}{3}r^3$$

So the volume each octahedrons is:

$$V_{oct} = 2V_{pyr} = \frac{8\sqrt{2}}{3}r^3 = 4V_{tetr}$$

Assuming that in both the octahedron and the tetrahedron the spheres take up a more or less equal part of space with regards to the total volume of the body, it can be stated by approximation that the volume of the voids compare likewise. And that:

$$V_{tetrvoid} \approx \frac{1}{32}V_{interst} = \frac{1}{2}\left(\sqrt{2} - \frac{\pi}{3}\right)r^3 \approx 0.183r^3$$

$$V_{octvoid} \approx \frac{4}{32}V_{interst} = 2\left(\sqrt{2} - \frac{\pi}{3}\right)r^3 \approx 0.734r^3$$

It should be noted however, that all the voids are connected. If the beads form a hexagonal pattern at the surface, both the tetrahedral and the octahedral voids are adjacent to the surface and the volume of the voids at the surface is slightly larger due to the absence of the sphere at one corner of the tetrahedron.

References

[1] H. Löwe and W. Ehrfeld, *Electrochim. Acta* **44**, 3679 (1999).

[2] J. C. McDonald and G. M. Whitesides, *Acc. Chem. Res.* **35**, 491 (2002).

[3] E. Verpoorte and N. F. de Rooij, *Proc. IEEE* **91**, 930 (2003).

[4] S. K. Sia and G. M. Whitesides, *Electrophoresis* **24**, 3563 (2003).

[5] A. J. deMello, *Nature* **442**, 394 (2006).

[6] G. M. Whitesides, *Nature* **442**, 386 (2006).

[7] P. S. Dittrich and A. Manz, *Nature* **5**, 210 (2006).

[8] B. H. Weigl, R. L. Bardell, and C. R. Cabrera, *Adv. Drug Delivery Rev.* **55**, 349 (2003).

[9] E. Lagally, P. Simpson, and R. Mathies, *Sens. Actuators, B* **63**, 138 (2000).

[10] A. T. Wooley and R. A. Mathies, *Proc. Natl. Acad. Sci. USA* **91**, 11348 (1994).

[11] P. Mach, M. Dolinski, K. Baldwin, J. Rogers, C. Kerbage, R. Windeler, and B. Eggleton, *Appl. Phys. Lett.* **80**, 4294 (2002).

[12] T. Thorsen, S. Maerkl, and S. Quake, *Science* **298**, 580 (2002).

[13] A. Shastry, M. J. Case, and K. F. Böhringer, *Langmuir* **22**, 6161 (2006).

[14] O. Azzaroni, A. A. Brown, and W. T. S. Huck, *Angew. Chem., Int. Ed.* **45**, 1770 (2006).

[15] C. Xu, W. Tao, C. M. Drain, J. D. Batteas, and K. L. Beers, *Macromolecules* **38**, 6 (2005).

[16] T. Wu, Y. Mei, J. T. Cabral, C. Xu, and K. L. Beers, *J. Am. Chem. Soc.* **126**, 9880 (2004).

[17] D. L. Huber, R. P. Manginell, M. A. Samara, B.-I. Kim, and B. C. Bunker, *Science* **18**, 352 (2003).

[18] A. Feldmann, U. Claussnitzer, and M. Otto, *J. Chromatogr., B: Anal. Technol. Biomed. Life Sci.* **803**, 149 (2004).

[19] M. L. Bruening, M. D. Miller, A. M. Balachandra, W. X. Huang, and G. L. Baker, *Polymer Preprints* **44**, 467 (2003).

[20] M. D. Miller, G. L. Baker, and M. L. Bruening, *J. Chromatogr. A* **1044**, 323 (2004).

[21] R. J. Petrie, *Polymerization in Confined Geometries*, PhD thesis, North Carolina State University, Raleigh, USA, 2005.

[22] J. Atencia and D. J. Beebe, *Nature* **437**, 648 (2005).

[23] J. B. Knight, A. Vishwanath, J. P. Brody, and R. H. Austin, *Phys. Rev. Lett.* **80**, 3863 (1998).

[24] M. W. Losey, M. A. Schmidt, and K. F. Jensen, *Ind. Eng. Chem. Res.* **40**, 2555 (2001).

[25] M. Brivio, W. Verboom, and D. N. Reinhoudt, *Lab Chip* **6**, 329 (2006).

[26] A. R. Wang and S. P. Zhu, *Macromolecules* **35**, 9926 (2002).

[27] O. Delgadillo-Velazquez, E. Vivaldo-Lima, I. A. Quintero-Ortega, and S. P. Zhu, *AIChE J.* **48**, 2597 (2002).

[28] M. Zhang and W. H. Ray, *J. Appl. Polym. Sci.* **86**, 1630 (2002).

[29] M. Al-Harthi, J. B. R. Soares, and L. C. Simon, *Macromol. Mater. Eng.* **291**, 993 (2006).

[30] J. Genzer, *Macromolecules* **39**, 7157 (2006).

[31] D. M. Jones, A. A. Brown, and W. T. S. Huck, *Langmuir* **18**, 1265 (2002).

[32] J. Pyun, T. Kowalewski, and K. Matyjaszewski, *Macromol. Rapid Commun.* **24**, 1043 (2003).

[33] K. Matyjaszewski, *Curr. Org. Chem.* **6**, 67 (2002).

[34] T. Huang, T. Geng, J. Sturgis, H. B. Li, R. Gomez, R. Bashir, A. K. Bhunia, J. P. Robinson, and M. R. Ladisch, *Enzyme Microb. Technol.* **33**, 958 (2003).

[35] R. N. Wenzel, *Ind. Eng. Chem.* **28**, 988 (1936).

[36] R. N. Wenzel, *J. Phys. Chem.* **53**, 1466 (1949).

[37] J. Allen, S. Kuyucak, and S.-H. Chung, *J. Chem. Phys.* **111**, 7985 (1999).

[38] M. Husemann, E. E. Malmström, M. McNamara, M. Mate, D. Mecerreyes, D. G. Benoit, J. L. Hedrick, P. Mansky, E. Huang, T. P. Russell, and C. J. Hawker, *Macromolecules* **32**, 1424 (1999).

Chapter 6

Mixed ATRP/NMP initiator monolayers by controlled surface modification

Synopsis: Atom transfer radical polymerization and nitroxide mediated polymerization both are living radical polymerizations that allow for control of thickness when used to grow surface-initiated polymers. Mixed polymer brushes and block co-polymers potentially have interesting applications in biosensors and microchip fabrication. Current techniques to obtain mixed polymer brushes by these two polymerizations require the separate synthesis of an NMP and an ATRP silane initiator. Surface grafted block co-polymers grown by a combination of two different polymerization techniques are not known to date. In this chapter the synthesis of mixed polymer brushes and block co-polymers based on the conversion of an ATRP-active bromo end-group into an NMP-active nitroxide is shown. The grafting density dependent surface morphology and the switching of this morphology upon exposure to different solvents is studied.

6.1 Introduction

Nitroxide mediated polymerization (NMP) has been introduced in the introductory chapter (section 1.2.2 on page 8) as one of the controlled radical polymerizations that are used to obtain surface-initiated polymers. NMP has been

proposed to be an attractive alternative to atom transfer radical polymerization (ATRP) as no catalyst is needed. This leads to a tolerance for complex forming monomers and easier purification.[1] However, ATRP is still a preferred method for the polymerization of many non-complex forming acrylates and methacrylates, as polymerization by ATRP is often possible at room temperature.[2]

6.1.1 Block co-polymers and mixed brushes

Most polymers are immiscible and most blends of polymers tend to phase separate. Di-block co-polymers are two different types of polymer connected with a covalent bond and therefore can not phase separate at macroscopic length scales. Instead they form ordered structures, like lamellar layers and perpendicular cylinders with domain dimensions in the order of 20-40 nm.[3,4] The domain size and shape depend on the relative volume fraction of the two blocks.

The micro-phase separation of block co-polymers is of interest to tune wettabilities, to increase cell adhesion and to increase surface to volume ratios for biosensors. An area of particular interest is to assist lithographic techniques to obtain smaller patterns,[5,6] a field that finds commercial applications in microchip fabrication.[7]

The formation of block co-polymers in surface-initiated polymer brushes by living radical polymerizations is accessible as the brush in the dormant form can be transferred from one reaction mixture to the other and be re-initiated.[8,9] This approach has been used succesfully for polymer brushes formed using NMP and ATRP.[10–14]

In the case of surface grafted polymers, forcing two different polymers together is not only possible by a covalent bond between them, but two polymers are also confined to the same region if their anchoring points to the substrate are homogeneously distributed. As with all polymer brushes, these can be formed either by grafting *from* and grafting *to* the substrate (see section 1.2).

Ionov *et al.* obtained a mixed brush by grafting acid functionalized poly-2-vinylpyridine and polyisoprene to an epoxy functionalized monolayer on silicon.[15] They then cross-linked the polyisoprene polymers by exposure to UV-light in patterned areas. When exposed to a selective solvent, the soluble

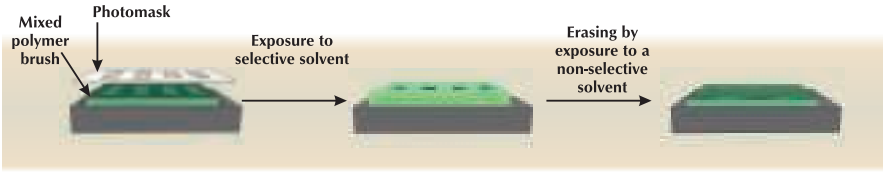

Scheme 6.1: Schematic of photolithography on mixed polymer brushes of polyvinylpyridine and polyisoprene as followed by Ionov *et al.*[15] Upon illumination through a photomask the brushes cross-link. The pattern can be developed by exposing it to a selective solvent, either acidic water or toluene. Exposure to ethanol (a non-selective solvent for both polymers) the image is erased.

polymer swells, but not in the areas where cross-linked polymer is present (see scheme 6.1). In this way patterns can be obtained that are visible only when exposed to certain solvents.

LeMieux *et al.* grafted polystyrene (PS) and poly-*tert*-butyl acrylate (P*t*BA) to an epoxy functionalized surface.[16] They noticed that if both polymers are grafted at the same time, domain sizes are in the order of several hundred nanometers. This is attributed to aggregation in solution before grafting and preferential adsorption of one of the polymers onto the silicon, while the other dewets the surface. This problem is solved by a two-step approach in which P*t*BA is adsorbed first, taking care that it does not consume all the available sites, followed by adsorption of PS. Hydrolysis of P*t*BA results in its conversion into polyacrylic acid. These brush surface layers can then be switched between hydrophilic and hydrophobic by exposure to different solvents.

Klep *et al.* obtained mixed brushes by a combination of grafting *to* and grafting *from*.[17] Polyglycidyl methacrylate (PGMA) was grafted to the silicon

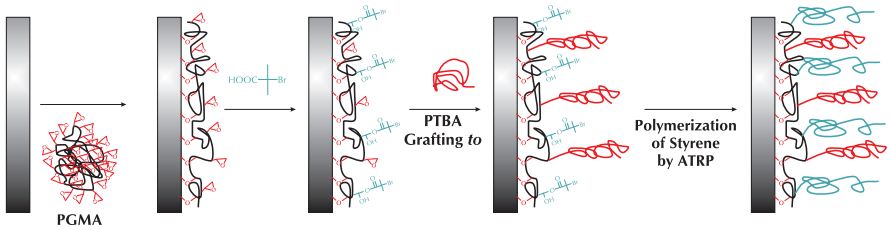

Scheme 6.2: Preparation of mixed polymer brushes in the procedure followed by Klep *et al.* Redrawn from the original publication.[17]

surface, forming a pancake structure, and was treated with bromo-isobutyric acid to obtain a macro-initiator for ATRP. P*t*BA was grafted to the PGMA layer by reaction of the carboxy group with the epoxy to form the first brush-like layer. Finally PS was grown by ATRP from the surface, thus yielding mixed brushes (see scheme 6.2).

Mixed brushes by a grafting *from* approach using free radical polymerization have been synthesized by the groups of Tsukruk and Rühe. Tsukruk and co-workers made use of the fact that not all of the azo-initiators are used in the first free radical polymerization, so they can be used in a second step to form the second polymer and obtain a mixed brush of the glassy co-polymer polystyrene-*co*-2,3,4,5,6-pentafluorostyrene (PSF) and the rubbery polymethyl acrylate (PMA).[18]

Rühe's group on the other hand used the property of an azo-monolayer that it can act as free radical initiator both upon illumination and upon heating.[19] In the first step they illuminate this layer through a mask to obtain patterned brushes, then they use thermal initiation in the second polymerization to obtain mixed brushes in the illuminated areas and pure polymer in the shadowed areas.

Mixed polymer brushes can show micro-phase separation in a similar way to block co-polymers. The phase separation of mixed PSF/PMMA brushes formed by a two step free radical approach upon exposure to selective and non-selective solvents was studied by Minko *et al.*[20] Their self-consistent field calculations suggest that selective solvents enhance perpendicular segregation, in which the unfavoured polymer forms clusters below a layer of the favoured component, resulting in a dimple structured phase separation. In a non-selective solvent a ripple-like phase separation is expected as both polymers will be at the surface and will phase separate laterally. This theory is in agreement with the experiments they report.

Prokhorova *et al.* also synthesized PMMA/PGMA mixed brushes in the two-step free radical grafting *from* approach, and suggest that the conformational changes upon switching these structures by exposure to different solvents could deliver mechanical work.[21] They support this by homogeneously distributing nanoparticles on top of mixed brushes followed by switching the brush layer for a number of times. Depending on the nature of the underlying

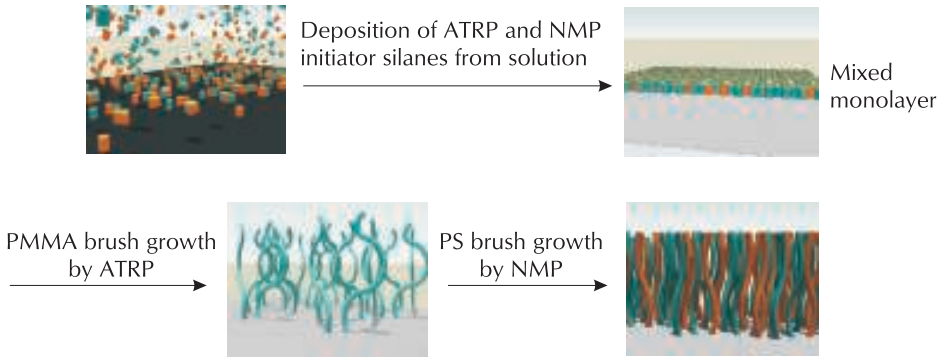

Scheme 6.3: Schematic of the method followed by Ejaz *et al.* to obtain mixed brushes. A mixed monolayer of ATRP and NMP initiator silanes is deposited from solution. PMMA brushes are grown by ATRP followed by PS brushes by NMP.

mixed brush, the nanoparticles then form aggregates, indicating that they have been moved from one region to the other. Particles on a reference substrate had not aggregate which suggests that the aggregation is the result of the switching and not of *e.g.* Brownian motion.

Ejaz *et al.* report mixed deposition of both an NMP and ATRP initiator by self assembly and synthesized the first mixed brush layers by a living grafting *from* approach from these mixed monolayers. They obtain mixed brushes of PMMA and PS in different grafting density ratios and show control over the thickness of both of the polymer layers (scheme 6.3).[22]

In summary, the formation of mixed brushes is a relatively new field with potentially many applications that can add to the possibilities offered by block co-polymers. Examples of the use of living grafting *from* approaches are very limited which is remarkable as they would offer the benefit of control over thickness of both the polymers formed.

6.1.2 Existing approaches for NMP initiator monolayers

Several approaches to obtain NMP initiator monolayers at the surface of silicon and glass substrates exist. There are no examples of NMP monolayers on other substrates to the author's knowledge, but attempts to use NMP to grow polymers from thiol initiators on gold are futile given the instability of thiol monolayers at elevated reaction temperatures.[23]

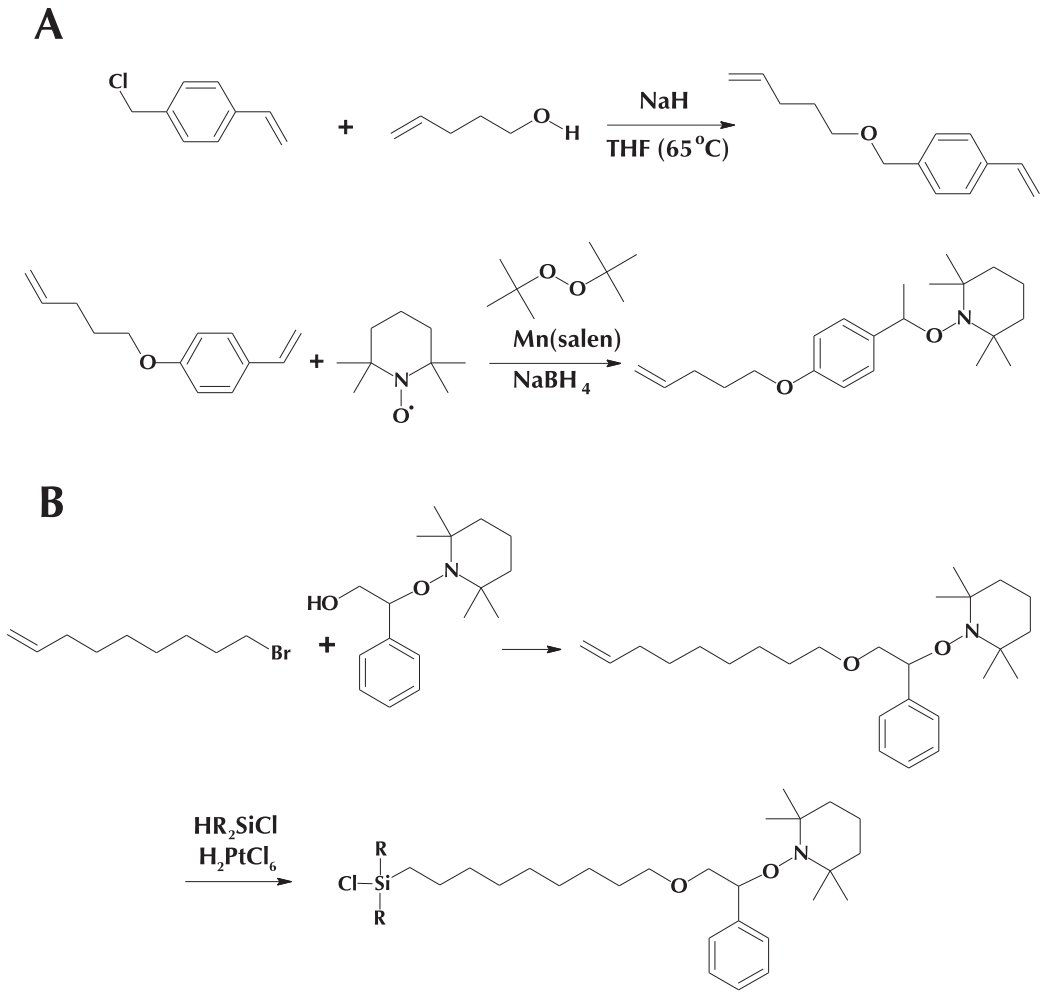

Scheme 6.4: Two routes for the synthesis of an silane initiator for nitroxide mediated polymerizations.

The most widely used approach to obtain a surface grafted initiator for NMP is the three-step synthesis of a trichlorosilane as described by Husseman *et al.*[8] This route starts with the condensation of vinylbenzyl chloride with pent-4-enol followed by the Jacobsen coupling of the product with the nitroxide 2,2,6,6-tetramethyl piperidinoxy (TEMPO, see scheme 6.4 A) and finally a hydrosilation to obtain the initiator silane.

The route for the synthesis of an alternative silane initiator, also suggested by Husseman, can be followed as well.[8,24] In this approach the coupling is

between 8-bromooctene and a hydroxy functionalized unimolecular initiator, followed by a hydrosilation (see scheme 6.4B).

Xu *et al.* synthesized an initiator monolayer by reactions at the surface.[25] They deposit a 3-(trimethoxysilyl)propyl methacrylate on the surface and then convert this monolayer into an NMP monolayer by exposing it to the free radical initiator 2,2'-azobis(isobutyronitrile) (AIBN) in presence of TEMPO at 80 °C. At this temperature radicals are formed in solution by the dissociation of AIBN. This is followed by radical transfer to the surface grafted methacrylate. Finally the surface grafted radicals are then efficiently end-capped by TEMPO to form a bond that is stable at this temperature but responsible for the reversible deprotection during the following polymerization at higher temperatures.

Another approach that uses an initiator in the bulk to create the first radicals at the surface was followed by Mulfort *et al.*[26] They deposited a monolayer of a styrene functionalized silane and then use a bimolecular system of benzoyl peroxide (BPO) and TEMPO to start NMP.

In his review of applications of the persistent radical effect Studer lists seven methods to obtain alkoxyamines.[27] In all of these, the first step is the creation of a radical by oxidation with either a metal complex or a peroxide; this radical is then trapped by TEMPO. The first method discussed is the conversion of halides into alkoxyamines by reaction with Cu(I) in presence of TEMPO. It is this method that was followed by Bon *et al.* to convert the active chain end of a polymer formed by ATRP into an alkoxyamine.[28] However, this procedure has not yet been used to form block-co-polymer brushes with blocks synthesized by ATRP and NMP subsequently or to convert ATRP initiator monolayers into NMP initiator monolayers. This chapter will discuss the controlled conversion of an ATRP initiator monolayer into an NMP initiator monolayer and its use to obtain mixed brushes and ATRP/NMP-based block co-polymers.

6.2 Monolayer conversion

An initiator monolayer for polymerizations by ATRP was deposited on the native silicon oxide layer of silicon substrates by self-assembly. The thickness of this layer was 0.9 nm as measured by ellipsometry. An alkoxyamine functionalized monolayer was obtained by reacting this monolayer with a catalyst complex of copper(I) and *N,N,N',N",N"*-pentamethyl diethylenetriamine in the presence of the alkoxyamine TEMPO, following a similar procedure to Bon *et al.*, who used it for solution polymerization (see scheme 6.5).[28] A ratio of [TEMPO]:[CuBr] = 70:1 in toluene was used. The copper complex removes the bromine endgroup of the monolayer to create a radical which is immediately capped by TEMPO. This reaction was performed at 0 °C, at which temperature the creation of the radical is slow. The objective of this approach was to allow for partial conversion of the bromide end groups when the reaction is carried out at different time scales, so mixed monolayers of silanes with an ATRP initiator functionality and silanes with NMP initiator functionality can be obtained.

For a more complete conversion the reaction is run at elevated temperatures of 90 °C for 16 hours. At this temperature the creation of the radical by removal of the bromine is faster, but the equilibrium of the TEMPO capping reaction is still totally to the capped state.[29] During this reaction the ellipsometric thickness increased from 0.9 nm to 1.4 nm.

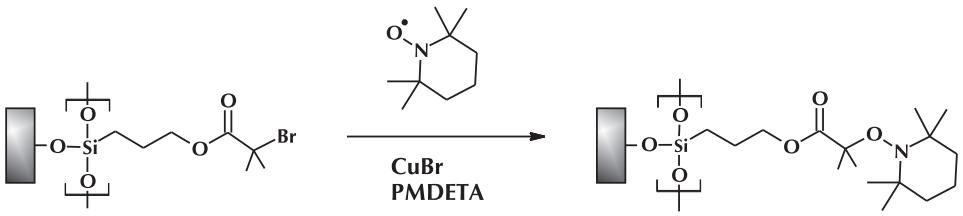

Scheme 6.5

6.2.1 XPS on monolayers*

The reacted monolayers were analysed by X-ray photoelectron spectroscopy (XPS). The nitrogen spectrum and bromide spectrum are shown in figure 6.1 and 6.2 respectively. When the spectra after reaction for 10 minutes and after reaction overnight are compared it can be seen that the concentration of nitrogen increases significantly during the reaction and that the bromide peak completely disappears. It has to be noted that the bromide detection is unreliable as only traces of the bromide can be measured, which results in a much lower value than the actual concentration. The elemental analysis also shows that the atom ratio of carbon increases going from short to long conversion time (see table 6.1), as was expected (the calculated atom ratio of carbon over 'other' atoms increases from 7:7 for an ATRP initiator monolayer to 16:8 for an NMP initiator monolayer, but this excludes the signal of silicon and the native silicon oxide layer).

As can be seen from the values of silicon and oxygen, the analysis goes deep into the substrate. The values are ~5–7% lower for the sample converted for 16 h, which suggests, that the monolayer thickness increased and the measurement goes less deep into the silicon wafer.

XPS measurements were taken from two points at each sample. Generally the concentration of nitrogen and carbon in the second point is much lower than in the first point. This can be explained by dissociation of the alkoxyamine as the sample heats up. This suggests that the NMP initiator is indeed present at the surface. Also the concentration of silicon is higher in the second measurement, which is in agreement with a expected decrease in thickness of the monolayer upon heating.

For a fully converted monolayer an atom ratio of C:N = 16:1 would be expected. The measured atom ratio is 10.4, which means that the concentration of nitrogen measured is much higher (or the carbon signal lower) than can be expected on basis of full conversion. A quantitative analysis of the XPS data is however meaningless as the monolayer is not stable and the signal attributed

*XPS analysis was performed by Dr Madeleine Ramstedt, Melville Laboratory for polymer chemistry, Cambridge, United Kingdom / STI-IMX-LMCH, Ecole Polytechnique Fédérale de Lausanne, Lausanne, Switzerland

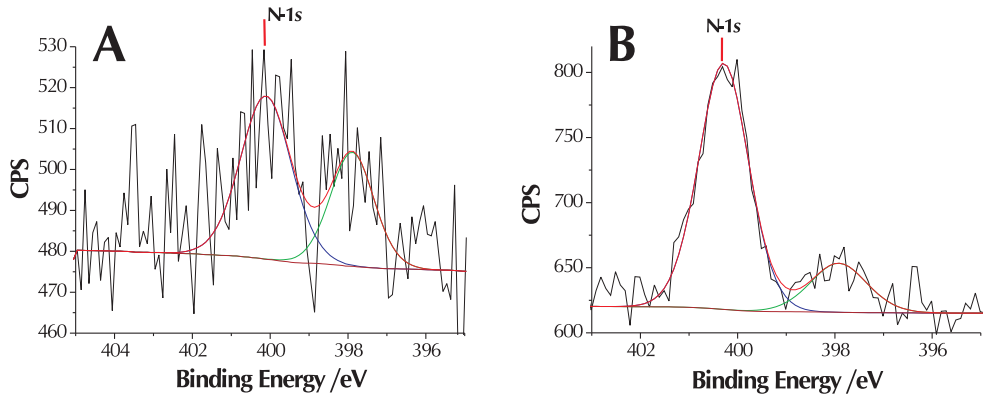

Figure 6.1: XPS analyses of the N-1*s* region for substrates with (partially) converted monolayers. A) Converted at 0 °C for 10 minutes, B) converted at 90 °C for 16 hours.

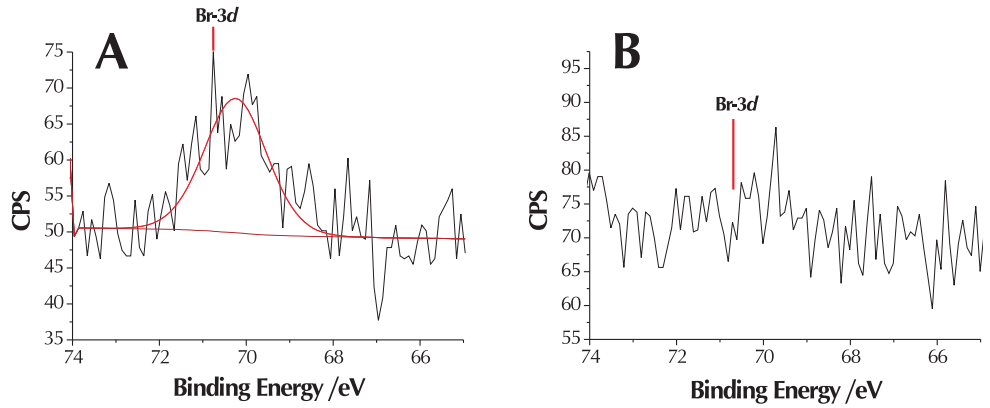

Figure 6.2: XPS analyses of the Br-3*d* region for substrates with (partially) converted monolayers. A) Converted at 0 °C for 10 minutes, B) converted at 90 °C for 16 hours.

Table 6.1: Elemental analysis (in mole-%) by XPS of initiator monolayers converted under various conditions.

	C	N	Br	O	Si
10 min (0 °C)	14.9	0.8	0.1	41.3	42.9
40 min (0 °C)	15.4	0.7	0.2	42.4	41.4
16 h (90 °C)	18.5	1.8	0.0	39.2	39.8

to the monolayer is very small compared to the signal of the substrate resulting in a large error in the measurement. These XPS results should therefore only be interpreted qualitatively.

6.3 Surface-initiated PMMA by ATRP and PS by NMP

The substrates with (partially) converted monolayers were used for the surface initiated polymerization of MMA by ATRP and the polymerization of styrene by NMP.

For the surface initiated polymerization of methyl methacrylate (MMA) by ATRP a standard recipe suggested by Jones *et al.* was followed:[30] A copper(I) / bipyridine(BPY) catalyst complex was used with a relative [CuBr]:[BPY]:[MMA] mole ratio of 1:3:100 with a mixture of methanol and water as solvent.

The PMMA growth is shown in figure 6.3. For the polymerization from all three of the substrates the growth of the polymer is linear with time, which is indicative of living character of the polymerization.[31] It is clear that with increasing monolayer conversion time the thickness increase with time is less. For the monolayer that underwent conversion for only 10 minutes, the thickness after three hours is ~40% of that of PMMA grown from the original

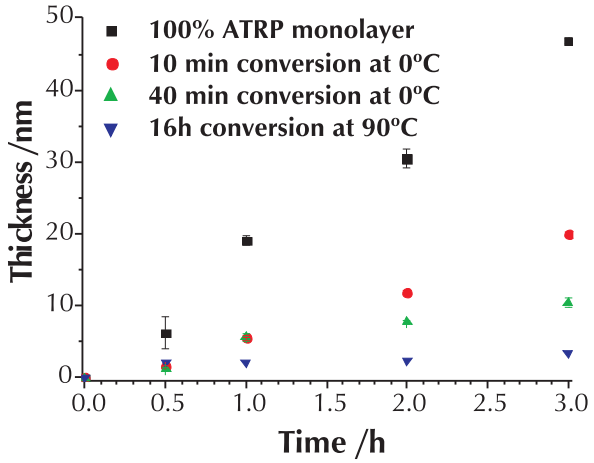

Figure 6.3: Surface-initiated PMMA growth by ATRP on substrates with a 100% ATRP initiator monolayer and on substrates with monolayers that are (partially) converted into NMP initiator monolayers.

ATRP monolayer. For the layer converted for 40 minutes, this thickness is only ~20% and for the one reacted for 16 hours less than ~5%. Since the polymers are expected to have equal chain lengths for equal reaction times this indicates that the grafting density is lower and the brushes have a more coiled and less extended chain conformation (see also section 1.2).

For the polymerization of styrene by NMP a solution of styrene in toluene was used to avoid solidification of the bulk and damage to the sample. The reaction was run in presence of TEMPO or in presence of the unimolecular initiator 2,2,6,6-tetramethyl-1-(phenylethoxy)piperidine, to increase the availability of the endcapping agent and increase the living character of the polymerization. It was found that in absence of a bulk initiator but in presence of TEMPO the brush growth did not start until after approximately 16 h of reaction, after which the thickness increased with time. Addition of a bulk initiator solved this problem and the growth of polymers from the surface started right upon reaching the reaction temperature. The need to add bulk initiator to improve the linearity of the polymerization has been discussed in the introductory chapter on page 14 and can be attributed to the delicate equilibrium between initiators and endcapping agents. Other explanations include

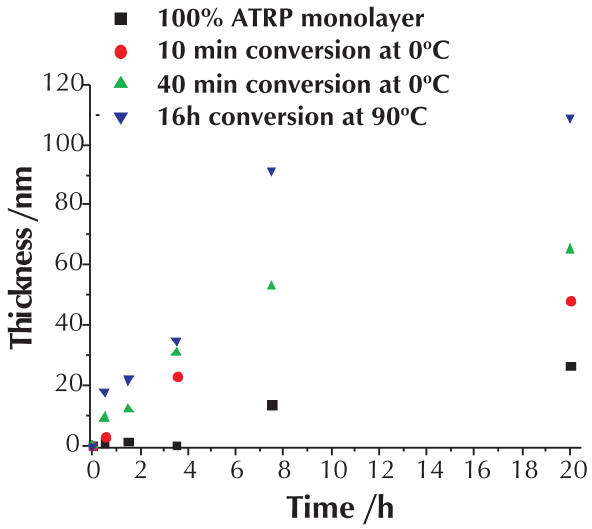

Figure 6.4: Surface-initiated PS growth by NMP on substrates with a 100% ATRP initiator monolayer and on substrates with monolayers that are (partially) converted into NMP initiator monolayers.

the presence of small concentrations of impurities that can be scavenged by the additional radicals in the solution.[8]

The brush growth under these conditions is shown in figure 6.4. Again there is a clear relation between conversion time and eventual brush thickness. The brush thickness increases with monolayer conversion time, which is expected as more NMP polymers are grafted from the surface. However, polymers also grow from an unconverted ATRP monolayer up to 26 nm after 20 h of reaction. This is unexpected, but can be explained by some thermal initiation of the ATRP monolayer.

6.3.1 Grafting density

Several relations between brush height h and grafting density σ have been suggested. They all have the format:[32–36]

$$h = C(\sigma)^y$$

With y equal to 1 (for a dry brush), 1/3 (for a brush in a good solvent), 1/2 (for a brush in a theta solvent). C in this formula is the layer thickness for brushes grown from a complete initiator SAM.

Going from mushroom to brush regime, however, y is not always constant;[37] for the mushroom regime in a good solvent $y = 0$,[38] while this becomes 1/3 for the brush regime. This effect is less for the dry thickness.

In the case described in this study, the thicknesses are dry thicknesses and it is worth to use the above model as it gives the opportunity to calculate approximate values for the grafting density, when this model is applied to the different (unknown) grafting densities of the brushes grown from the partly converted monolayers in this study.

For polymer brushes grown by ATRP from mixed ATRP/NMP initiator monolayers, the relative grafting density can directly be calculated from the dry polymer brush thickness if the model above is applied with $y = 1$. The relative ATRP monolayer grafting density σ_{rel} is then equal to the ratio of the brush thickness for a certain monolayer conversion time and the brush thickness for the ATRP initiator SAM. This is done in table 6.2 for the PMMA polymers obtained by ATRP for 1, 2 and 3 hours. The average ratio is taken as ATRP initiator grafting density for the partially converted monolayers.

Table 6.2: Calculation of the relative ATRP initiator grafting density (σ_{rel}) for the different monolayers. For each reaction time the brush heigth is divided by the brush height obtained on a full ATRP initiator monolayer. The average ratio of $\frac{h}{h_{\sigma=0}}$ is taken as σ for that converted monolayer.

Monolayer conversion time	ATRP 1 h		ATRP 2 h		ATRP 3 h		σ_{rel} = average $\frac{h}{h_{\sigma=1}}$
	Brush thickness (nm)	$\frac{h}{h_{\sigma=1}}$	Brush thickness (nm)	$\frac{h}{h_{\sigma=1}}$	Brush thickness (nm)	$\frac{h}{h_{\sigma=1}}$	
0 minutes ($\sigma = 1$)	19.1	1	30.5	1	46.9	1	1
10 minutes	5.7	0.3	12	0.39	20.1	0.43	0.37
40 minutes	5.6	0.29	7.7	0.25	10.5	0.22	0.26
16 hours	2.25	0.12	2.29	0.08	0.07	0.07	0.09

It is clear that already after 10 minutes of reaction, the ATRP initiator grafting density has dropped significantly to $37\pm7\%$ of the complete monolayer. For future experiments it could be interesting to slow down this reaction to yield intermediate grafting densities with more control. This could be done by lowering the reaction temperature to slow down the creation of radicals by the copper(I) catalyst complex or by using copper(II) bromide in the reaction mixture. In the latter case TEMPO would be in competition with the halide for end-capping the radical.

In figure 6.5 A the PMMA brush thickness is plotted against the calculated grafting density of the ATRP initiator monolayer to visualize the applied model.

If during the conversion of the ATRP initiator into the NMP initiator at the surface side reactions are excluded, *i.e.* the endcapping of radicals by TEMPO would be complete, the NMP initiator grafting density would be: $\sigma_{NMP} = 1 - \sigma_{rel}$. In that case, the brush thickness of PS by NMP as a function of σ_{rel} would also be linear, with zero brush thickness for $\sigma_{rel} = 1$. It can be seen from 6.5 B that this is not valid. It has already been discussed above that thermal initiation of the ATRP initiator could account for the positive deviation at $\sigma_{rel} = 1$.

The PS brush thickness at $\sigma_{rel} = 0.26$ and 0.37 is lower than would be expected for a linear relationship. Incomplete conversion could account for

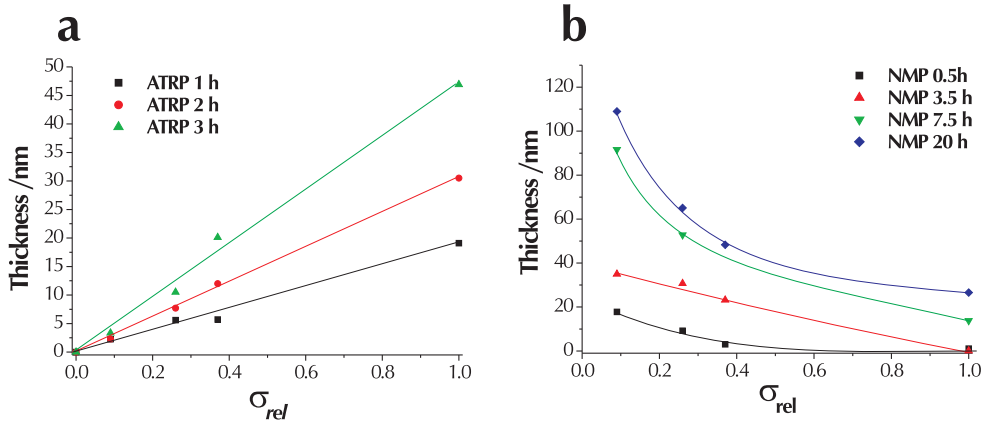

Figure 6.5: Dry thickness for different polymerization times as a function of the relative grafting density of the ATRP initiator monolayer (σ_{rel}) after polymerization by a) ATRP and b) NMP. Brush thicknesses are the same data as in figures 6.3 and 6.4 respectively, but plotted as function of σ_{rel} (as calculated according to table 6.2).

this deviation. The procedure used to stop the conversion of the monolayer was by exposing the reaction mixture to air. This could result in part of the radicals being neither end-capped by a bromide nor by a nitroxide but reacting with oxygen from the air, resulting in the loss of an initiator site. Alternative methods of stopping the reaction while preserving initiator sites could include quenching the reaction by lowering the temperature or by injecting a concentrated solution of a copper(II) complex or by using a low concentration of copper(II) in the reaction mixture during conversion of the monolayer.

At higher conversions there will be less radicals in the uncapped state when the reaction is stopped (as there are less ATRP initiator sites left), so the sum of the relative grafting density of ATRP initiators and NMP initiators will be closer to 1, as can be observed.

6.3.2 Mixed polymer brushes

As mixed monolayers of ATRP and NMP initiators have been obtained it is also possible to grow mixed brushes. To this end, surface initiated polymerization of MMA by ATRP was performed first, followed by surface initiated polymerization of styrene by NMP. This order was chosen as the ATRP

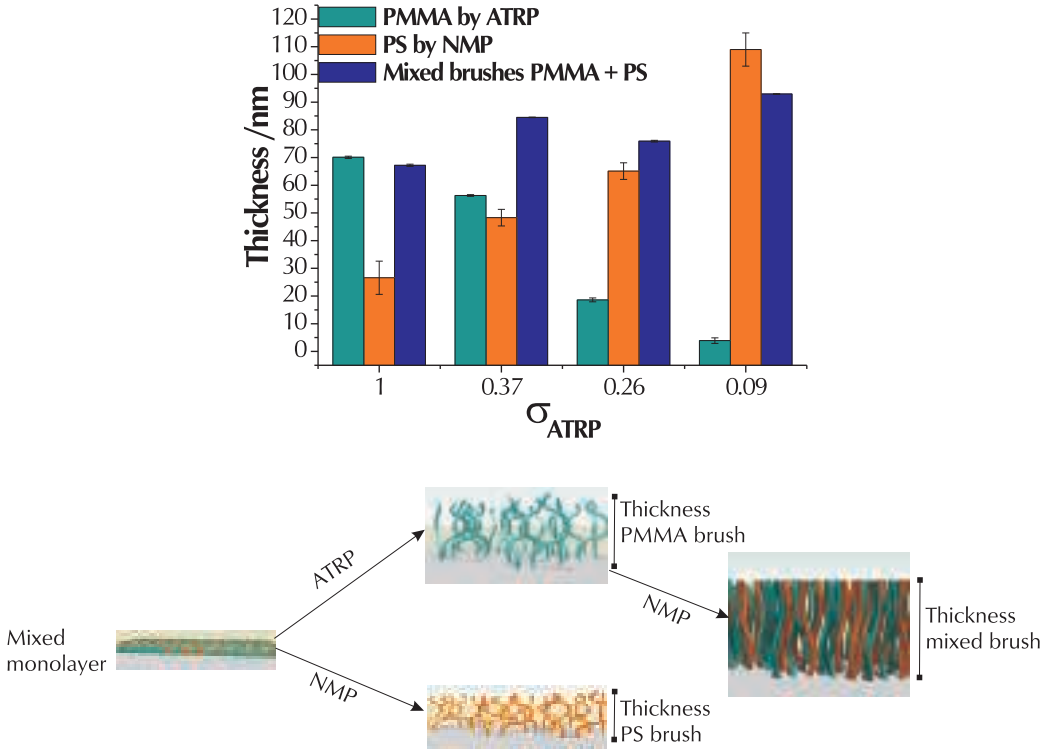

Figure 6.6: Schematic for the formation of homopolymer and mixed brushes on substrates with a mixed monolayer of both NMP and ATRP initiators (bottom). Ellipsometric thickness of polymers grown from 100% ATRP monolayers and (partially) converted monolayers (top). σ_{rel} (calculated as described in section 6.2) on the x-axis is given as indication for the composition of the mixed initiator monolayer. PMMA was grown by ATRP (16 h), Polystyrene was grown by NMP (20 h). Mixed brushes were formed by growing PMMA by ATRP (16h) followed by growing PS by NMP (20h).

initiators are damaged at the elevated temperature required for NMP. As a reference, also homopolymers of PS were grown from these mixed initiator coated substrates. In these polymerizations ATRP of MMA was run for 16 hours and NMP of styrene was run for 20 hours.

Figure 6.6 shows that for the substrates with grafting densities 0.37 and 0.26, performing both polymerizations subsequently results in thicker brush layers than growing either of the corresponding homopolymers from these substrates. Thicker mixed brushes than homopolymers are not observed for the substrate with the full ATRP initiator monolayer ($\sigma_{rel} = 1$) or on the

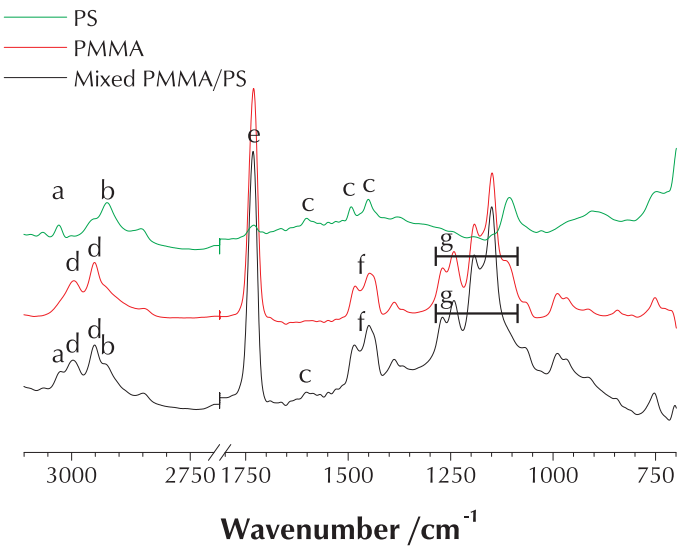

Figure 6.7: FT-IR spectrum of surface-initiated PS, PMMA and mixed polymers (brushes were grown from monolayers that were converted for 0 minutes, 16 hours and 40 minutes respectively). The compound specific absorption bands and regions are indicated: a: aromatic C—H stretch; b: tertiary C—H stretch; c: aromatic ring stretch; d: primary and secondary C—H stretches; e: Carbonyl C=O stretch; f: alkane C—C stretches; g: O—CH_3 and C—C(=O)—O (asymmetric) stretches.

substrate with predominantly NMP initiator ($\sigma_{rel} = 0.09$). In these cases the contribution of PS and PMMA respectively to the total mixed brush thickness is minimal.

Figure 6.7 shows the IR spectrum of a PMMA homopolymer brush of 70.1 nm, a PS homopolymer brush of 109 nm and a PMMA/PS mixed brush (σ_{rel} =0.37, thickness: 84.5 nm) grown from a mixed monolayer following the procedure above. It can be seen that the mixed brush layer shows characteristic absorptions of both the PMMA and the PS polymers, *e.g.* the aromatic C—H (3030 cm^{-1}) and ring stretches (1600 cm^{-1}) on one hand and the ester (1750, 1250-1100 cm^{-1}) and alkyl stretches (1480, 1440 cm^{-1}) on the other. This is evidence that the desired polymers have indeed been obtained.

6.3.3 Block co-polymers

As a preliminary experiment the conversion of an ATRP reactive end group into an NMP reactive end group was also applied to obtain the surface-initiated block co-polymer PMMA-*b*-PS. To this end, brush growth of PMMA from a 100% ATRP initiator monolayer was quenched after 1 hour of reaction at a thickness of 21 nm with a solution of 1 g TEMPO in 10 mL of methanol. Subsequently, this substrate was used for the polymerization of styrene by NMP for 6 h. In the second step the thickness of the polymer layer increased by 21 nm to 39 nm, in the same range as comparable brush growth from converted monolayers (compare figure 6.4). The brush thickness on a reference sample with a PMMA brush grown by ATRP without intermediate quenching by TEMPO did not increase in this step. This indicates that this approach is promising to obtain block co-polymers.

6.4 Surface morphology and solvent treatments

As discussed in the introduction to this chapter, binary brushes (block co-polymer brushes and mixed brushes) show phase separation at the nanometer length scale into different patterns. This phase separation depends on molecular parameters, *i.e.* chain-length and nature of the polymer, and on external parameters, like solvent treatment.

The surface morphology of mixed PMMA/PS brush layers was studied at different grafting density and phase effects upon rinsing with different solvents were investigated. To this end PMMA and PS were grown from mixed monolayer substrates with reaction conditions tuned to obtain a similar brush thickness of approximately 80 nm on all of the substrates.

Figure 6.8 shows topographic AFM images on surfaces with different grafting densities after drying in a nitrogen atmosphere overnight. The last solvent treatment prior to this drying step had been DCM. As can be seen, both the polymer layers grown from an untreated ATRP initiator monolayer (A) and a monolayer with high NMP initiator grafting density (D) are smooth compared to the other substrates without distinct features. On substrates with low (B) and intermediate (C) PS grafting small grain-like features appear. It is likely

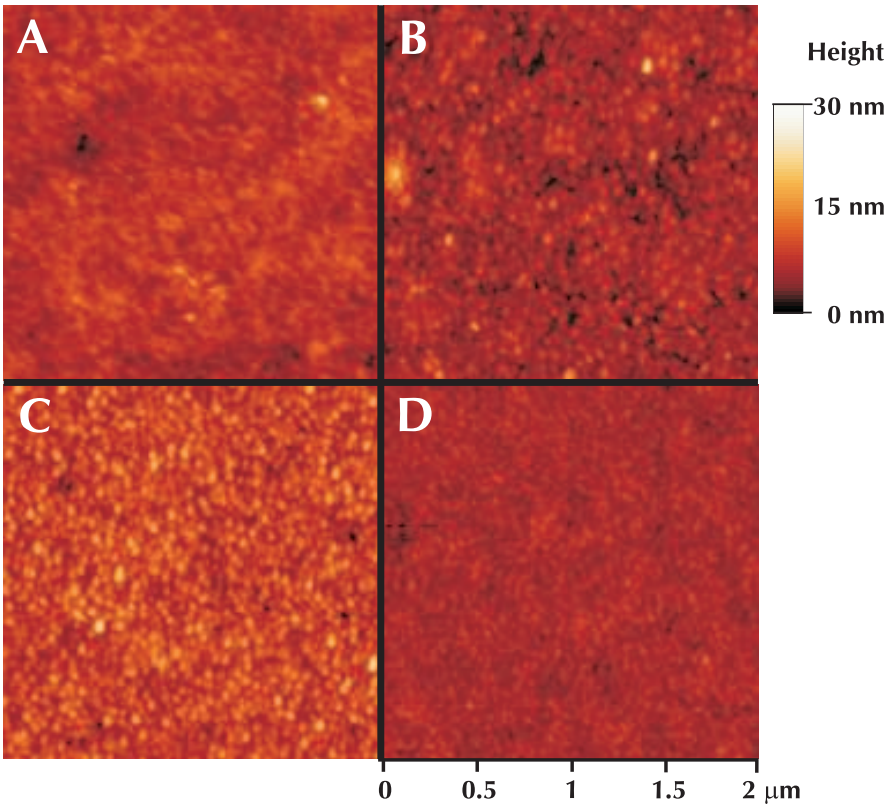

Figure 6.8: Topographic AFM on dry mixed brushes of PMMA and PS grown from different monolayers. Polymers were grown from the same substrates as used in the experiments above: A) σ_{rel} =1; B) σ_{rel} =0.37; C) σ_{rel} =0.26; D) σ_{rel} =0.09.

that the grainy structure is a result of the PS chains phase separating from the PMMA chains.

When a mixed brush is treated with different solvents, different surface morphologies can be distinguished. The samples with mixed brushes were washed with selective good solvents for just one of the polymers and with a good solvent for both of the polymers. Acetone was chosen as a selective solvent for PMMA, cyclohexane as a selective solvent for PS and dichloromethane as a good solvent for both polymers. As can be seen in figure 6.9, washing of the substrate with the highest PS:PMMA ratio (σ_{rel} =0.09) with acetone results in formation of grain-like features, similar to the ones seen in figure 6.8. However as acetone is selective for PMMA these grains are now expected to result from the PMMA brushes that have aggregated between collapsed PS

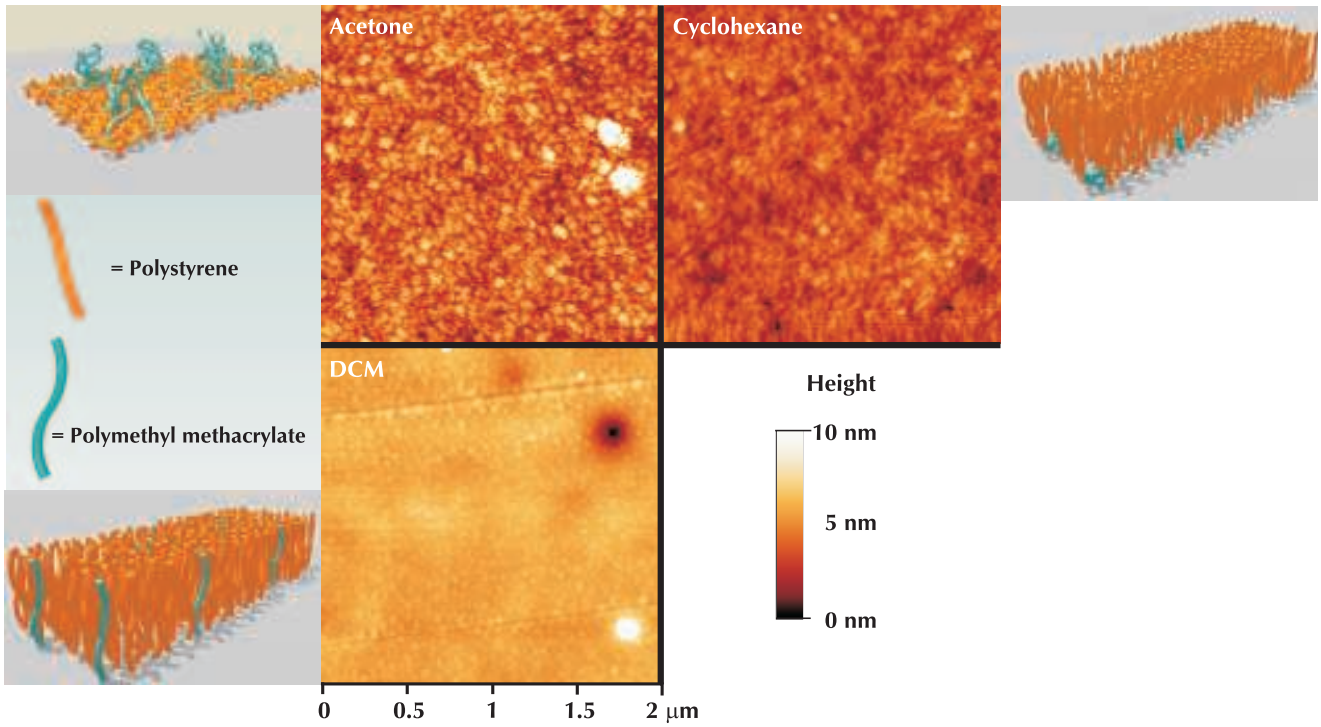

Figure 6.9: Topographical AFM on mixed PMMA/PS surface-initiated polymers (σ_{rel} =0.09, compare substrate D in figure 6.8) after washing with different solvents and schematic representation of the brush layers upon treatment. Upon washing with the selective solvents acetone or cyclohexane, respectively the PS and PMMA chains are expected to collapse giving rise to either a grainy or web-like structure. Upon washing with the non-selective solvent DCM, both polymers regain the brush conformation and the features dissappear.

brushes. Upon drying in air also the PMMA chains collapse on top of the PS layer giving rise to the grainy structure.

After washing with cyclohexane the morphology has changed to a smoother web-like surface with holes, which could be the result of selective swelling of the PS polymers with the collapsed PMMA brushes forming aggregated domains with lower brush thickness. Upon washing with the non-selective solvent dichloromethane, the features dissappear as both polymers are now in the soluted form. The observed switching in surface morphology can be repeated by re-exposure to the various solvents and the results are in agreement with observed morphologies of mixed brushes obtained by other methods.[17,22,39]

6.5 Conclusions

In this chapter mixed ATRP/NMP initiator monolayers are synthesized from ATRP monolayers by a radical conversion reaction at the surface with copper(I) in presence of TEMPO. This conversion has been confirmed by XPS as an increase in nitrogen content. Moreover, the activity of the respective initiators has been proven by growing polymers by ATRP and NMP to yield mixed PMMA/PS brushes with different polymer grafting ratios depending on the conversion of the monolayer. A similar approach has been followed in a preliminary experiment to obtain the surface-initiated block co-polymer PMMA-*b*-PS.

The phase morphology was studied by AFM and showed increasing PS grain-like domains with increasing NMP initiator density on dry substrates. Exposure to selective solvents induces the formation of either grain-like features or holes at the surface. These features are erased upon rinsing with the non-selective solvent dichloromethane.

The combination of mixed polymer brushes and block co-polymers that can be synthesized by this method, makes this approach an accessible and attractive tool to fabricate complex polymer architectures.

6.6 Materials and methods

General procedures

Oven dried glassware was used for all reactions in non-aqueous solvents.
Ellipsometric measurements on monolayers and untreated polymer brushes were carried out using either an EL X-02C ellipsometer from Dr Riss Ellipsometerbau GmbH with a 632.8 nm laser at 70° angle of incidence or a JA Woollam Alpha-SE spectroscopic ellipsometer. In case of the monochromatic ellipsometer refractive indices of 1.50 and 1.45 were used for polymer and initiator layers respectively, in case of the spectroscopic ellipsometer a Spline layer was used as a model for the PS brushes and a Cauchy layer was used to model PMMA brushes.
FT-IR spectra of surface-initiated polymers were recorded using a Bio-Rad FTS 6000 spectrometer. Spectra of surface-initiated polymers were taken in transmission mode using a background of the same bare Si wafer that was used for polymer growth.
Plasma oxidation of substrates was performed in air in an Emitech K1050X plasma oxidizer for 10 minutes at 100 W.
AFM was performed on a Digital Instruments Nanoscope® Dimension™3100 Atomic Force Microscope. Both topographical and phase images were recorded. Substrates were stored under dry nitrogen overnight before analysis. In the case of solvent treatments the substrates were immersed in the solvent for 30 s, dried to air and immediately analysed.
XPS analyses were performed using a Kratos Axis Ultra under monochromatic Al Kα radiation (1486.6 eV). A pass energy of 80 eV and a step size of 1 eV were used for survey spectra. A pass energy of 20 eV and a step size of 0.1 eV were used to obtain high energy resolution spectra of selected regions. Charge neutralising equipment was used to compensate for sample charging and the binding scale was referenced to the CH component of C 1s spectra at 285.0 eV. The concentrations obtained are reported as the percentage of that particular atom species (at %) at the surface of the sample (<10 nm analysis depth).[40]

Materials

All chemicals were purchased from Aldrich, Lancaster or Fisher and used as received unless stated otherwise. Copper(I) bromide was of 99.999 % purity and was stored *in vacuo*. Triethylamine, dichloromethane and toluene were distilled prior to use. Methanol and ethanol were Analytical Reagent grade and used as received. Methyl methacrylate was purified over a short plug of alumina before use. Styrene was purified by passing it over an alumina column followed by vacuum distillation and stored in the freezer before use. The trichlorosilane ATRP initiator (2-bromo-2-methylpropionic acid 3-trichlorosilanylpropyl ester) was synthesized in the lab[†] following a reported procedure,[8] however using allyl alcohol instead of 5-hexene-1-ol. Silicon wafers were obtained from Compart Technology Ltd. (100 mm diameter, phosphorous-doped, <1 0 0> orientation, polished on one side).

Immobilization of the ATRP initiator monolayer on the substrate Silicon wafers were plasma oxidized before functionalization. The substrates were placed in a crystallising dish and 30 mL of dry toluene, 50 μL of triethylamine and 10 μL of the trichlorosilane initiator was added. The dish was covered with foil and left for 16 hours at room temperature. The wafer was then washed sequentially with toluene, distilled acetone and absolute ethanol and dried under a nitrogen stream.

Conversion of an ATRP monolayer into an NMP monolayer A solution of TEMPO (1 g, 24 mmol) in toluene (100 mL) was stirred and purged with nitrogen for 20 minutes. Copper(I) bromide (0.05 g, 0.35 mmol) and *N,N,N',N",N"*-pentamethyl diethylenetriamine (0.21 mL, 1 mmol) were then added and the mixture was cooled down to 0 °C. Radley tubes containing substrates coated with an ATRP initiator monolayer were evacuated and refilled with nitrogen through four cycles. The reaction mixture was then added to the Radley tubes and reaction took place under nitrogen for 40 minutes at 0 °C after which the temperature was raised to 90 °C. Samples were removed from their tubes after reaction for 10 minutes, 40 minutes and 16 hours.

[†]This synthesis was performed by Andy Brown and Ron Oren, Melville Laboratory for Polymer Synthesis

Surface-initiated polymerization of MMA by ATRP The reaction mixture was prepared following a literature procedure by Jones *et al.*:[30] methyl methacrylate (20 mL, 170 mmol), water (4 mL) and methanol (16 mL) were purged with nitrogen for 20 minutes. Then copper(I) bromide (0.24 g, 1.7 mmol) and bypiridine (0.8 g, 5.1 mmol) were added and the mixture was purged with nitrogen for 15 minutes. Substrates were placed in separate Radley tubes and the tubes were evacuated and refilled with nitrogen through four cycles. The reaction mixture was added to all the tubes and left to react under nitrogen for 16 hours, removing the substrates from the tubes at set time intervals and rinsed subsequently with toluene, acetone and ethanol. To obtain a polymer layer that could be used to form block co-polymers, the reaction mixture was quenched after 1h of reaction by injecting a solution of TEMPO (1g, 6.4mmol) in methanol (10 mL) and left for 15 minutes. The substrate was then removed from the reaction mixture and cleaned by rinsing subsequently with toluene, acetone and ethanol.
IR: ν_{max}/cm^{-1}: 2995 (primary C—H strech, m), 2955 (secondary C—H stretch, s), 1730 (Carbonyl C=O stretch, s), 1500-1410 (alkyl C—H bend, m), 1300-1075 (O—CH_3 and C—C(=O)—O (asymmetric) stretches, s)
Surface-initiated polymerization of styrene by NMP 2,2,6,6-tetramethyl-1-(phenylethoxy)piperidine (0.15 g, 0.59 mmol) or TEMPO (0.08 g, 0.51 mmol) was added to a solution of styrene (45 mL, 393 mmol) in toluene (15 mL). The mixture was purged with nitrogen for 20 minutes. Substrates coated with a pure or partly converted monolayer of initiator were placed in Radley tubes. For block co-polymers a sample was used that had undergone polymerization of MMA by ATRP (see the procedure above). The tubes were evacuated and refilled with nitrogen through four cycles. The reaction mixture was added to the Radley tubes and the mixture was heated to 125 °C and left to react under nitrogen for 20 hours, removing the substrates from the tubes at set time intervals and cleaned under sonication with toluene, acetone and ethanol subsequently.
IR: ν_{max}/cm^{-1}: 3027 (aromatic C—H stretch, m), 2955 (secondary C—H stretch, w), 2925 (tertiary C—H stretch, s), 1620-1420 (aromatic ring stretch, m), 1500-1410 (alkyl C—H bend, m)

References

[1] D. G. Benoit, V. Chaplinski, R. Braslau, and C. J. Hawker, *J. Am. Chem. Soc.* **121**, 3904 (1999).

[2] J. Xia, S. G. Gaynor, and K. Matyjaszewski, *Macromolecules* **31**, 5958 (1998).

[3] F. S. Bates, *Science* **22**, 898 (1991).

[4] H.-A. Klok and S. Lecommandoux, *Adv. Mater.* **13**, 1217 (2001).

[5] M. Park, C. Harrison, P. M. Chaiking, R. A. Register, and D. H. Adamson, *Science* **276**, 1401 (1997).

[6] T. Thurn-Albrecht, J. Schotter, G. Kästle, N. Emley, T. Shibauchi, L. Krusin-Elbaum, K. Guarini, C. Black, M. Tuaminen, and T. Russel, *Science* **290**, 2126 (2000).

[7] N. P. Balsara and M. J. Park, *J. Polym. Sci., Part B: Polym. Phys.* **44**, 3429 (2006).

[8] M. Husemann, E. E. Malmström, M. McNamara, M. Mate, D. Mecerreyes, D. G. Benoit, J. L. Hedrick, P. Mansky, E. Huang, T. P. Russell, and C. J. Hawker, *Macromolecules* **32**, 1424 (1999).

[9] S. Edmondson and W. T. S. Huck, *J. Mater. Chem.* **14**, 730 (2004).

[10] K. Matyjaszewski, S. M. Jo, H. J. Paik, and D. A. Shipp, *Macromolecules* **32**, 6431 (1999).

[11] B. Zhao and W. J. Brittain, *Macromolecules* **33**, 8813 (2000).

[12] C. B. Tang, T. Kowalewski, and K. Matyjaszewski, *Macromolecules* **36**, 1465 (2003).

[13] J. N. Kizhakkedathu, K. R. Kumar, D. Goodman, and D. E. Brooks, *Polymer* **45**, 7471 (2004).

[14] H. Y. Zhao, B. P. Farrell, and D. A. Shipp, *Polymer* **45**, 4473 (2004).

[15] L. Ionov, S. Minko, M. Stamm, J. F. Gohy, R. Jérôme, and A. Scholl, *J. Am. Chem. Soc.* **125**, 8302 (2003).

[16] M. C. LeMieux, D. Julthongpiput, K. N. Bergman, P. D. Cuong, H. S. Ahn, Y. H. Lin, and V. V. Tsukruk, *Langmuir* **20**, 10046 (2004).

[17] V. Klep, S. Minko, and I. Luzinov, *Polymeric Materials: Science & Engineering* **226**, U483 (2003).

[18] M. LeMieux, D. Usov, S. Minko, M. Stamm, H. Shulha, and V. V. Tsukruk, *Macromolecules* **36**, 7244 (2003).

[19] R. Konradi and J. Rühe, *Langmuir* **22**, 8571 (2006).

[20] S. Minko, M. Muller, D. Usov, A. Scholl, C. Froeck, and M. Stamm, *Phys. Rev. Lett.* **88**, 035502 (2002).

[21] S. A. Prokhorova, A. Kopyshev, A. Ramakrishnan, H. Zhang, and J. Rühe, *Nanotechnology* **14**, 1098 (2003).

[22] M. Ejaz, K. Ohno, Y. Tsujii, and T. Fukuda, *Polymer Preprints* **44**, 532 (2003).

[23] A. Ulman, *Chem. Rev.* **96**, 1533 (1996).

[24] C. Devaux, J. P. Chapel, E. Beyou, and P. Chaumont, *Eur. Phys. J. E* **7**, 345 (2002).

[25] F. J. Xu, Y. Song, Z. P. Cheng, X. L. Zhu, C. X. Zhu, E. T. Kang, and K. G. Neoh, *Macromolecules* **38**, 6254 (2005).

[26] K. L. Mulfort, J. Ryu, and Q. Y. Zhou, *Polymer* **44**, 3185 (2003).

[27] A. Studer, *Chem. Soc. Rev.* **33**, 267 (2004).

[28] S. A. F. Bon, A. G. Steward, and D. M. Haddleton, *J. Polym. Sci., Part A: Polym. Chem.* **38**, 2678 (2000).

[29] C. J. Hawker, A. W. Bosman, and E. Harth, *Chem. Rev.* **101**, 3661 (2001).

[30] D. M. Jones, A. A. Brown, and W. T. S. Huck, *Langmuir* **18**, 1265 (2002).

[31] K. Matyjaszewski, P. J. Miller, N. Shukla, B. Immaraporn, A. Gelman, B. B. Luokala, T. M. Siclovan, G. Kickelbick, T. Vallant, H. Hoffmann, and T. Pakula, *Macromolecules* **32**, 8716 (1999).

[32] P. Y. Lai and K. Binder, *J. Chem. Phys.* **97**, 586 (1992).

[33] A. Karim, V. V. Tsukruk, J. F. Douglas, S. K. Satija, L. J. Fetters, D. H. Reneker, and M. D. Foster, *Journal de Physique II* **5**, 1441 (1995).

[34] J. I. Martin and Z. G. Wang, *J. Phys. Chem.* **99**, 2833 (1995).

[35] B. Zhao and W. J. Brittain, *Prog. Polym. Sci.* **25**, 677 (2000).

[36] M. Biesalski and J. Rühe, *Macromolecules* **37**, 1166 (2004).

[37] T. L. Li and K. N. Park, *Comp. Theor. Polymer Sci.* **11**, 133 (2001).

[38] T. Wu, K. Efimenko, and J. Genzer, *J. Am. Chem. Soc.* **124**, 9394 (2002).

[39] S. Santer, A. Kopyshev, H. K. Yang, and J. Rühe, *Macromolecules* **39**, 3056 (2006).

[40] B. D. Ratner, D. G. Castner, and J. Vickerman (ed.), *Surface Analyses - The Principal Techniques,* **Chapter 3**, Wiley & Sons: Chichester, UK, 1997.

Outlook

In this thesis surface modification by surface initiated polymers with potential applications in display and polymer electronic devices has been shown. Actual applications in working devices is not shown in this thesis and further research building from these results will be needed. Additionally two techniques were discussed seperately in chapter 5 and 6 of this thesis, enhancing the versatility and attractiveness of polymer brushes. Some of the phenomena observed are not fully understood to date. Better understanding of these could lead to better tuning of the physical and chemical properties of the surface modification layers, the ability to build complex architectures by polymer brushes and higher yields of reactions, due to better insight in polymerization kinetics.

In chapter 2 LC polymer brushes were used to induce homeotropic alignment over large areas and patterned alignment. It was suggested that this could be used in polymer electronic devices (page 36), as alignment of the active layers plays an important role in these devices and LC materials are widely used. Enhanced mobility resulting from enhanced order in the brush layer can best be measured with FETs. The fabrication of FETs utilizing a LC brush alignment layer and comparison of its performance with devices based on other alignment layers (without LC interaction with the active layer) would thus be a logical next step.

In section 2.2.2 a considerable difference in clearing point between surface grafted polymers and solution polymers was observed and explained as a combination of a different entropy contribution for the fact that they are confined to a mere 2D space and for the fact that the surface grafted polymers are forced together and have less motional freedom. One approach for further research could be to investigate the influence of grafting density of the initiator

monolayers and hence the density of polymer brushes. Research into the exact contributions of these factors would open up the ability to tune phase transitions of surface grafted polymers.

In chapter 3 post-functionalizing a glycidyl methacrylate brush by reaction with an alcohol is used as an alternative to synthesizing a functionalized monomer followed by polymerization. This alternative approach could be very useful for introducing functionalities that are incompatible with polymerization by ATRP, like moieties that form complexes with the copper ions or that undergo redox reactions with Cu(I), like the electron acceptor TCNQ in this case. However the yield of the post-functionalization observed with the alcohol functionalized TCNQ is very low. This is attributed to the bulkyness of the reagent. Brush growth with the bulky LC monomer used in chapter 2 was also very low. It can be expected that in confined polymers, like polymer brushes, bulkyness of reagents limits the yield of reactions by a higher degree than in less confined circumstances. It would be very interesting to investigate this phenomenon by growing brushes from monomers of varying bulkyness and by post-functionalizing surface initiated polymers with a variety of alcohols. One tool in this research could be restarting polymerizations with a less bulky monomer polymerization of the first, bulky, monomer has leveled off.

It was suggested in chapter 3 that a dopant situated just above the semi-conducting channel of a FET would have the desired effect of enhancing the mobility in the on-state and reducing the mobility in the off-state of the device. It was also suggested that this could be realized by synthesizing a diblock co-polymer (page 77). This device architecture would be very challenging as the physical properties of both polymer blocks should be tuned to allow penetration of the brush by the semi-conducting polymer while guaranteeing the separation of both blocks into two layers with the dopant block situated above the channel.

Polymers with side chains of electron acceptor have the potential of conducting electrons.[1] It would be interesting to test electron conductance of the TCNQ brushes for potential applications in *e.g.* solar cells.

The FETs tested in chapter 3 showed very much hysteresis. This was explained by the dopant charges that are present when going from the off- to the on-state, but not when going from the on- to the off-state (page 76). In

the off-state this is comparable to a double dielectric layer. Memory devices are devices that utilise the hysteresis that is the effect of a double dielectric.[2] It would therefore be an interesting avenue of research to apply and test the dopant monolayers and brushes presented in this thesis in memory devices.

Chapter 4 showed the growth of polythiophenes from a surface attached template. Polythiophenes find applications in solar cells, LEDs and FETs. Because of the expected geometry of the polymers forming pathways from and to the surface, these polymers may enhance mobility in solar cells. On the other hand, because of their photoluminescence, their application in LEDs may be attractive as well. Applications in FETs however are not a logical next step as these require polymer order parallel to the surface.

The effects of microconfinement on surface initiated growth in chapter 5 are still not fully understood and more research will be needed investigating the key drivers of the changed kinetics. It was shown that both the sizes of the beads and the nature of the walls are of interest. To be able to study the influence of void volume and surface area separately the use of different bead geometries could be a potential approach. Another interesting experiment is further reduction of the bead size. It is expected that when the bead sizes are reduced to the same order of magnitude as the brush thickness the growth of polymers from the surface will be hindered instead of enhanced as the void size decreases towards zero.

The combination of mixed brushes and block co-polymers that can be achieved with the technique presented in chapter 6 can be used to grow complex architectures by a combination of NMP and ATRP. One of the interesting features is that active end-groups can be passified for reaction by ATRP and can be used for NMP later on. To extend the usefulness of this technique it would be interesting to investigate whether this passification can be done by *e.g.* micro-contact printing (out of the polymerization solution but in inert atmosphere) or as a gradient by adding increasing amounts of nitroxide mediator during ATRP. Also it would be useful if the nitroxide mediator could be changed for an ATRP mediator again by adding excess amounts of Cu(II) at elevated temperatures. A factor limiting the success of the technique presented in chapter 6 is the limited conversion, so optimizing reaction conditions to enhance this conversion will be needed.

In conclusion, the techniques, polymers and phenomena described in this thesis offer an interesting mix of starting points for further fundamental research into reaction kinetics, for potential applications in devices and finally of extendable toolkits that could enhance the versatility of surface initiated polymerizations.

References

[1] R. Gómez, D. Veldman, R. Blanco, C. Seoane, J. L. Segura, and R. A. J. Janssen, *Macromolecules* **40**, 2760 (2007).

[2] V. Ioannou-Sougleridis, P. Dimitrakis, V. Em Vamvakas, P. Normand, C. Bonafos, S. Schamm, A. Mouti, G. B. Assayag, and V. Paillard, *Nanotechnology* **18**, 215204 (2007).

Acknowledgements

As with every big project, the research in this thesis would not have been possible without the help and support of many.

First of all, I want to thank my supervisor Wilhelm Huck, who facilitated the place in the lab, arranged the funding and whose almost unlimited stream of ideas was a great source of inspiration.

Alan, Catharine and Celia are thanked for their technical and administrative support.

The research in this thesis would not have been possible either without the funding of Merck Chemicals Ltd, Southampton and a combined studentship of the Cambridge European trust and the Isaac Newton Trust. Also the interdisciplinary research collaboration in Nanotechnology contributed both financially and with facilities, for which I am very grateful.

Merck Chemicals contributed more than only money. For the project of alignment on liquid crystalline polymer brushes and the project of TCNQ brushes as a dopant layer they contributed essential materials. The TCNQ project wouldn't have been possible without the opportunity to use their facilities in Southampton. I really appreciated the patience with which Maxim Shkunov offered me guidance in device fabrication and characterization. Many other people at Merck contributed with helpful advice and I want to specially thank my industrial supervisor Iain McCulloch and LC expert Christopher Dunn.

Also in the lab in Cambridge I received lots of help and advice from many. Steve, your advice was invaluable and your fresh ideas gave new inspiration many times when I got stuck. I thank Andy and Ron, who spent precious time on synthesizing silane initiator for the lab. Andy you're synthetic knowledge is incredible! Waldo, thank you for your helpful advice in the field of conjugated

polymers. Saghar, Madeleine and Sarah are thanked for their small but essential experimental contributions. Ron, Adam Moughton, Luis, Dan, Saghar and Waldo are thanked for proof reading this thesis.

Just as essential for good working conditions is a good atmosphere in the lab. The regular pub-visits, barbecues, punting trips and dinner parties formed a good change from the daily lab work. I want to thank Andy, Dan, Jean, Luis, Maaike, Madeleine, Manuela, Marijn, Neelam, Omar, Patrick, Ron, Saghar, Steve, Tijs, Waldo and Yang for their warm friendship and all the good fun in and out of the lab.

I thank all my Cambridge friends — in Caius college, in the orchestras I was involved in, my house mates and all the others — for making me feel at home during those three years in England. I specially thank Nick for the happy times we spent together.

During the three years in England, I still could count on my friends at home in the Netherlands whenever I came back. I want to thank Marjan, Ralf, Koen and Wouter for their enduring friendship and the warm welcome home. I am proud to have such great friends!

I thank my parents, my brother Carlo and his wife Cora for their care, love and support.

It is impossible to mention all the people by name who supported, helped and adviced me during the years of my PhD. I want to thank everyone who contributed in any possible way, I had a great time working with you! Good luck to everyone!

Paul